Cooperative platoon maneuvering using Artificial Potential Fields

K. Elferink

DC 2016.084

Department:	Mechanical Engineering
Research group:	Dynamics & Control
Student:	K.Elferink
Identity number:	0716494
TU/e supervisor:	prof. dr. H. Nijmeijer
TNO supervisors:	dr. ir. E. Semsar-Kazerooni
	dr. ir. J. Ploeg

Date: September 28, 2016

Abstract

Nowadays, traffic congestion on highways is a major problem. Hence, there is an increasing societal demand for smart solutions which can increase the throughput, comfort and safety of driving on a road. This has raised interest in the development of automated systems, up to the level of fully autonomous driving. A recent development has been vehicle platooning, i.e. the guidance of a group of vehicles at small inter-vehicular distances. This technology is realized by the use of vehicle-to-vehicle (V2V) communication, which enables vehicles to share their intended actions. By having V2V communication in place, the minimal inter-vehicular distance can be reduced significantly, whereas safety is increased. Additionally, sharing the vehicle intentions might enable multi-vehicle maneuvers to be cooperatively executed. As a result, a significant increase in road throughput can be realized. However, further development is still required to enable large scale implementation of cooperative autonomous driving. The development of cooperative autonomous driving can introduce an improvement in comfort, safety and the reduction of traffic congestion.

In this thesis, a longitudinal control strategy is developed to safely incorporate platooning and maneuvering functionality for cooperative driving. The objective herein is to combine platooning, gap closing, obstacle avoidance and platoon merging functionality into a single control design, ensuring comfort and safety. To this end, multiple controller designs are developed, based on the concept of Artificial Potential Fields. The designs are evaluated by means of simulation and analysis, and additionally compared to a linear controller. As a result, a control strategy is selected and further elaborated. Next, by means of a theoretical analysis, the safety conditions for nominal operation are derived and verified. Consequently, a set of states is derived wherein safety can be guaranteed by only the nominal controller, within the bounds of normal operation. An additional collision avoidance controller is defined for other scenarios.

In addition, the merging of platoons or vehicles into a neighboring lane is considered. Herein, a control strategy, using the concept of artificial potential fields, is implemented such that a relatively smooth longitudinal acceleration profile can be guaranteed during a transition to a new platoon configuration. The resulting controller should therefore be able to platoon and maneuver safely for nominal operation.

Hence, an approach is presented to include platooning, gap closing, obstacle avoidance, and merge maneuvering functionality into an elegant control design. This functionality is analyzed and verified by means simulations and experiments, using the fleet of Priuses from TNO. The developed controller has shown to provide a significant improvement in performance and safety with respect to the currently implemented linear controller.

Nomenclature

Acronyms

ACC	Adaptive Cruise Control
AP	Attractive Potential
APF	Artificial Potential Field
APF-ACC	Artificial Potential Field Adaptive Cruise Control
APF-CACC	Artificial Potential Field Cooperative Adaptive Cruise Control
CA	Collision Avoidance
CACC	Cooperative Adaptive Cruise Control
CC	Cruise Control
GCDC	Grand Cooperative Driving Challenge
ISE	Integral Square error norm (signal l_2 norm)
MIO	Most Important Object
MR	Merge Request
OA	Obstacle Avoidance
PD	Linear controller, Proportional gain and Damper
RP	Repulsive Potential
STOM	Safe to Merge

Symbols

α	Ratio for safe distance for STOM	$-$
$\bar{u}_i$	Compensated acceleration input for vehicle i	ms^{-2}
β	Ratio for difference desired headway	$-$
Δv_i	Relative velocity vehicle i with respect to preceding vehicle	ms^{-1}
$\Delta_t s_i(t)$	Covered distance during an emergency braking maneuver	m
$\hat{a}_1$	Estimated feedforward signal using gracefull degradation of CACC	ms^{-2}
$\mathbf{e}_i$	Set of errors states $(e_{1,i}, e_{2,i}, e_{3,i})$ from vehicle i	$-$
$\mathbf{x}_i$	Set of errors states $(x_{1,i}, x_{2,i}, x_{3,i})$ from vehicle i	$-$
Ψ	Potential function	$-$
τ	Time constant for vehicle dynamics	s^{-1}
A	System matrix for description of state dynamics	$-$
a_i	Acceleration vehicle i	ms^{-2}
B	Input matrix for system dynamics	$-$
c	Parameter for ratio $e_{1,i}, e_{2,i}$ in $x_{1,i}$	$-$
D	Position dependent damping coefficient	
d_i	Distance between vehicle i and its preceding vehicle	m
$d_{r,i}$	Desired distance for vehicle i with respect to the preceding vehicle	$-$
$e_{1,i}$	Position error vehicle i with respect to preceding vehicle	m
$e_{2,i}, x_{2,i}$	Time derivative of error $e_{1,i}$ or $x_{1,i}$ respectively	ms^{-1}
$e_{3,i}, x_{3,i}$	Second time derivative of error $e_{1,i}$ or $x_{1,i}$ respectively	ms^{-2}
f_1, f_2	Parameters for position dependent damping coefficient	m
h	Velocity dependent time headway	s
i, k, l	arbitrary vehicle	$-$
j	from lane or lane position	$-$
K	Set of controller tuning parameters $K = [k_1, k_2, k_3, k_4, k_5]$ for APF	$-$
k_p, k_d	Proportional gain and damper for linear PD controller	$-$
L_i	Length of vehicle i	m
m	Amount of vehicles taken into consideration	$-$
$M\#$	Number of vehicle from merging triplet $(M1, M2, M3)$	$-$
P	arbitrary point $P = [d_i(t_0), v_i(t_0), \Delta v_i(t_0), a_i(t_0), a_{i-1}(t_0)]^T \in \mathcal{Y}_1$	$-$

Q	Performance criteria	$\begin{bmatrix} - \end{bmatrix}$
r	Standstill headway distance	$\begin{bmatrix} m \end{bmatrix}$
S	arbitrary point $S = [e_{1,i}(t_0), e_{2,i}(t_0), e_{3,i}(t_0), v_i(t_0), a_{i-1}(t_0)]^T \in \mathcal{Y}_2$	$\begin{bmatrix} - \end{bmatrix}$
s_i	Longitudinal position vehicle i	$\begin{bmatrix} m \end{bmatrix}$
u_i	Acceleration input for vehicle i	$\begin{bmatrix} ms^{-2} \end{bmatrix}$
V	Lyapunov function	$\begin{bmatrix} - \end{bmatrix}$
v_i	Velocity vehicle i	$\begin{bmatrix} ms^{-1} \end{bmatrix}$
$v_{1,CC}$	lead vehicle cruise speed	$\begin{bmatrix} ms^{-1} \end{bmatrix}$
$x_{1,i}$	Alternative error notation with respect to $e_{1,i}$ for vehicle i	$\begin{bmatrix} - \end{bmatrix}$
$z_i(t)$	Scaled distance for CA controller	$\begin{bmatrix} m \end{bmatrix}$

Subscripts, superscripts and annotation

$*$	Special set of original
A	with respect to MIO_A
$APF1$	Position error dependent APF
$APF2$	Dual state APF alternative
$APF3$	Position error dependent APF and damping
$APFx$	Combined state APF
c	Comfort limit
ca	collision avoidance
$crit$	Critical
iA	MIO_A from point of view of vehicle i
iL	MIO_L from point of view of vehicle i
iR	MIO_R from point of view of vehicle i
k	Discrete time interval
$lead$	Lead vehicle
max	maximum
min	minimum, within comfort restrictions
MR	merge request
PD	Linear PD controller
$RPsat$	Saturated Repulsive potential
$STOM$	Safe to Merge
$stop$	Stopped
tol	tolerance

Domain and space descriptions

$\hat{D}_m^*$	Selection of critical region of operation D_m^* where $v_i(t_0) \geq v_{min}$
$\mathcal{Y}_1$	State space of all possible $P = [d_i(t_0), v_i(t_0), \Delta v_i(t_0), a_i(t_0), a_{i-1}(t_0)]^T \in \mathcal{Y}_1 \subset \mathbb{R}^5$
$\mathcal{Y}_2$	State space of all possible $S = [e_{1,i}(t_0), e_{2,i}(t_0), e_{3,i}(t_0), v_i(t_0), a_{i-1}(t_0)]^T \in \mathcal{Y}_2 \subset \mathbb{R}^5$
C	Continuously differentiable
D_c	Region with guaranteed collision
D_d	Region of potentially dangerous operation
D_m	Critical region of operation: $D_m \subset \mathcal{Y}_2 \subset \mathbb{R}^5$
D_m^*	Critical region of operation in error domain description: $D_m^* \subset \mathcal{Y}_1 \subset \mathbb{R}^5$
D_s	Region of safe operation

Contents

1: Introduction

In modern society, road transportation and traffic intensity have been increasing significantly [1], which can result in severe traffic jams. This traffic intensity causes problems for the vehicle throughput and safety on the roads. Additionally, in order to save the environment, the pressure for reducing the emissions (CO_2, NO_x and other particulate matter) has been growing. To alleviate congestion, the classic idea of extending existing infrastructure can be implemented. However, such adaptations are expensive, neither does it alleviate emissions. Another promising solution is automated vehicle technology, which can increase safety, moreover reduce congestion and emissions. The goal of this project is to create a controller for the longitudinal behavior of an autonomous vehicle, while ensuring safety and comfort on the road.

1.1 Motivation for automatic driving

By means of automation, vehicles can be (partially) controlled by an automatic system instead of a driver. Since the human factor (higher response time, lower control accuracy) is eliminated, a vehicle response can be faster and more predictable. This can increase safety significantly. Additionally, vehicles are enabled to drive at smaller inter-vehicular distances, with respect to normal driving [2]. As a result, more vehicles can drive safely, at desirable velocity, on the same stretch of road. Thereby, congestion is reduced and the maximum throughput of a road is increased. The automation also enables platoons to be created, which are groups of automated vehicles driving at small inter-vehicular distance. The effects of platooning on the road throughput and safety are further evaluated in the work of Shladover [3]. According to Shladover, vehicle automation can promise a significant increase in both road throughput and safety. For platoons of large vehicles in particular, such as trucks, the shorter inter-vehicular distance significantly reduces the air drag effect [4–6]. Therefore, platooning can reduce the fuel consumption, reducing both costs and emissions. Hence, a significant motivation for automatic driving can be found.

Current technologies are mainly driver assistance systems such as Cruise Control (CC) or Adaptive Cruise Control (ACC). The ACC technology not only adapts the velocity towards a certain set-point as in a CC, it can also automatically adapt the velocity using a minimal distance set-point with respect to the preceding vehicle. However, the ACC technology still requires a relatively large time headway of over 1 second [7, 8], which is insufficient to reach a significant increase in vehicle throughput. Since most vehicles only use radar and/or vision systems, the available information on the predecessor is rather limited. Most systems can only measure a relative distance, although a doppler radar can also measure the relative velocity. Although these measurements can be used to accurately determine the relative velocity or acceleration, it requires multiple measurements and therefore results in a delay.

In order to decrease the needed time headway, the available information must be as reliable and real-time as possible. To this end, Cooperative ACC (CACC) is introduced [5–7]. By applying wireless communication, more real-time information is available. The

communication additionally enables cooperative driving, since vehicles can share their intentions with vehicles nearby, intentions such as the acceleration and maneuvering objectives. With this useful set of extra information, vehicles can anticipate on some of the actions in their surroundings that have not occurred yet. Hence, as opposed to ACC systems, CACC allows vehicles to respond to its surroundings with a significantly reduced delay and increased precision. Using this technology, vehicles can drive with smaller inter-vehicular distances, which improves the road throughput.

Figure 1.1: Platoon of CACC-equiped vehicles [7]

Figure 1.1 shows a platoon formation from the test fleet used by TNO Automotive [7]. This test fleet is used for experiments on cooperative driving. Although extensive research is ongoing, a comprehensive method to enable cooperative driving has not been fully developed.

1.2 Research goals

As mentioned in the previous section, smaller inter-vehicular distances have multiple advantages. However while doing so, the safety and traffic flow cannot be compromised. Since human drivers cannot ensure safety in these conditions, the ability to automatically perform maneuvers is also desirable. For instance, the capability to create platoons and thereby close a large gap between two vehicles is required. Similarly, autonomous vehicles should ensure their safety; requiring the ability to prevent collisions and smoothly increase the inter-vehicular distances when required. For highway maneuvering, it should additionally be noted that the road throughput is mainly determined by the bottleneck of the network. These bottlenecks mainly consist of merging lanes and other comparable situations, and often require several complex maneuvers. Therefore, it is desirable that these complex maneuvers can cooperatively be executed. The objective of this assignment is to design a longitudinal controller which can achieve the following objectives:

1. Vehicle following with guaranteed safety
2. Gap closing
3. Merge maneuvering

while ensuring comfortable and smooth behavior. Therefore, multiple aspects will have to be further investigated. To indicate this the structure of the report, the outline will be presented next.

1.3 Outline

In this report, longitudinal vehicle and platoon maneuvering is of interest, using an Artificial Potential Field control approach. The preceding research will first be elaborated in Chapter 2, such that the problem description and research question can be stated. Next, the dynamics and the control suggestions are elaborated and compared for platooning, gap closing and obstacle avoidance in Chapter 3. Hereafter, longitudinal safety is investigated in Chapter 4, by dividing the state space into multiple safety classifications. An approach for safe and smooth platoon maneuvering is introduced in Chapter 5. Additional tests have been performed using three test vehicles from TNO, the result of these experiments are analyzed in Chapter 6. Finally, Chapter 7 will present the conclusions and recommendations for future work.

2: Literature review

2.1 Platooning control strategies

Currently, research is still ongoing to find and extend the control strategies to enable platooning and other vehicle automation aspects. One example for platooning control is presented in the work of Ploeg et al. [7], which presents a design approach and evaluation scheme for a CACC mechanism. For a homogeneous string of vehicles using a velocity dependent spacing policy, the vehicle and error dynamics are derived. In [7], the authors use a linear control action on the error and its first two derivatives. A set of requirements on the control parameters have been derived to guarantee stability; for cases without communication or sensor delay. Since delay is unavoidable in practice, the authors continue with an analysis in the presence of a delay. Since a delay introduces a phase delay in the frequency domain, the headway time needs to be adjusted accordingly [7–9]. The string stability is addressed as well as the system input-output stability. String stability entails that the error in a string should never increase towards the back or tail of the platoon. String stability is additionally improved in case of a velocity dependent spacing policy [7, 9]. In addition however, [10] introduces a nonlinear spacing policy that can further improve string stability. Although these works are very interesting in the field of platooning, additional functionality is desirable. For instance, the possibility to make a gap or to perform a merging maneuver can be mentioned. Hence, vehicle automation is desired to be able to handle many other situations, such as merging one or more vehicles into a platoon, or closing a gap.

2.2 Technical implications

Next to developing an appropriate control strategy, the implementation aspects are of importance as well. For instance, full vehicle automation will require a sufficient level of awareness of the vehicle state and environment. This system should be safe and reliable, since the system cannot rely on the driver to ensure safety. Hence, an autonomous vehicle needs to be equipped with the appropriate sensors. The vehicle will firstly need to know its acceleration, velocity and position on the road using appropriate vehicle sensors. The vehicle position can be determined using GPS, although the accuracy and update rate of a traditional GPS is limited. To this end, RTK-GPS and other technologies [11] are applied to improve the accuracy, although these systems are still too expensive to be installed on passenger cars or even trucks.

The velocity and acceleration can be determined using on-board vehicle sensors and state estimators. By sending and receiving the appropriate information through wireless communication, a vehicle can partially perceive the environment. However, the reliability and precision of this type of perception is dependent on the perception of other vehicles. Additionally, the wireless communication is subject to delay and (temporary) failure caused by packet loss, although methods have been suggested to decrease communication problems and delay [12], the communication channel may not be reliable. In case of communication or

positioning failure, the safety still has to be guaranteed. Therefore, sensors like radar, lidar and possibly camera can be used. Combined use and analysis of the available information should enable the vehicle to respond accordingly. In order to be able to anticipate the actions of other vehicles and reduce the effects of delay, the vehicle intentions can be communicated [7, 8, 13]. By sending the vehicle intention, the effect of delay on the platooning dynamics can be reduced.

Since each measurement is of limited precision, errors can occur, and time delay is unavoidable, margins have to be applied to guarantee safety [14]. Especially failure of certain vehicle elements can result in unknown or unexpected behavior. For instance, the communication channel can be unable to send and/or receive information, or an onboard sensor like the radar can have an error. Additionally, in many cases homogeneity is assumed for theoretical analysis, which is often not the case. In fact, neighboring vehicles can be controlled differently. Therefore, it is important to be able to cooperate in all of these situations while additionally guaranteeing safety. The development and testing of all these aspects has been one of the main objectives of the Grand Cooperative Driving Challenge (GCDC) [15,16], which has taken place in May 2016. Combining these aspects in hardware and software is a complex challenge and requires a controller which accounts for these aspect in order to guarantee safety.

2.3 Artificial Potential Fields

In the previous sections, vehicle following technologies based on a linear controller design have been considered. Linear (PD) controllers are often useful for tracking problems, where relatively small changes in magnitude of the tracking error are present. However, for platooning and longitudinal maneuvering, the position error can vary significantly in magnitude. Consequently, a linear PD controller will respond either too weak or too strong, for various magnitudes of the error. Hence, the desired control action is nonlinear:

- A negative position error denotes that the inter-vehicular distance is too small. A significant negative distance error compromises safety, whereas a a positive position error does not; Hence, the control action for negative errors must be larger than for positive errors of equal magnitude, thus yielding a nonlinear control objective.

In order to resolve this issue, different controllers are often applied for the varying situations. A platooning controller can be implemented next to controllers for collision avoidance, obstacle avoidance and gap closing, where each controller is active only in a separate stage and/or range of operation. However, this can cause non-smooth behavior, since the controller switches according to each situation. Such transient behavior can be undesirable, for the sake of comfort and performance.

More complex control problems can be found in the field of robotics [17–21], where problems can have multiple objectives and/or a large difference in magnitude of the error. There, the Artificial Potential Field (APF) control strategy is often used to control individual robots. The suggested APF control strategy might provide a solution to incorporate multiple

control objectives into one controller, and to accomodate the nonlinear properties of the platooning control problem. When using APF control instead of a linear (PD) controller, the control action can be tuned accordingly in cases of large and small inter-vehicular distances. The APF control strategy is therefore similarly suggested in previous work of the author [22], to control the assembly of platoons of trucks. Additionally, the APF control strategy is considered in various other control problems [17, 18, 23], often also applied in the field of robotics. The APF control approach can similarly be compared to having nonlinear control laws, where the control input is determined by the derivative of the designed potential field function. In [17], a theoretical framework is presented for flocking of multi-agent systems using APF. In [22], the potential function has to comply to a number of criteria, to be able to reach the desired behavior. Herein, the main objective is to save fuel by creating platoons of trucks. The platoon merging times and total energy consumption are evaluated for the longitudinal merging maneuver of one or multiple trucks for evaluation.

One of the more common applications of APF is incorporation of obstacle avoidance functionality [15, 17, 18, 22, 24–26]. For instance, in [26], APF is used to assist the driver, by application of automatic lanekeeping and obstacle avoidance functionality in case the driver is not responding. Similarly, obstacle avoidance and/or motion planning with APF is often used in the field of robotics [17–21]. For these applications, APF can be used to prevent collisions with the environment or penalize approaching the physical limit of an actuator. Similarly, [23] suggests an alternative APF function design, in an attempt to combine platooning, gap closing and obstacle avoidance functionality. However, this approach will have to be further elaborated. The APF approach has also proven to be useful when it is used to combine multiple objectives, possibly in dynamic environments and/or realtime applications [25, 27]. For comfort, this acceleration profile should be very smooth. Since safety is very important, the physical bounds on the acceleration can become a crucial issue. Therefore, these acceleration bounds ought to be taken into account in a safety and stability analysis. Especially for an emergency braking situation, safety needs to be guaranteed. For an advanced stability analysis, actuator saturation is accounted for in [19–21, 28], for single or multiple unicycle robots. These saturation functions enable a more elaborate asymptotic stability and tracking analysis, taking actuator and/or state limits into account. Hence, much research has already been conducted using APF, mainly also in the field of robotics. Also at TNO, research is ongoing to extend the control capabilities of CACC using APF [23].

2.4 Collision Avoidance

Although the APF approach is also often applied for collision avoidance purposes, it is important to evaluate if collision can be avoided in all cases. In the work of Alam [29], the safe set of states are calculated within the longitudinal domain, using a pursuit-evasion game approach. With this analysis, all safe states can be derived using a vehicle model. These safe states will consist of all possible combinations of initial conditions for the

pursuit-evasion game on which a collision can be avoided. One should note that Alam did not bound the velocity to the positive domain, this condition can however easily be added. The advantage of the analysis of Alam is that it can be implemented using any valid vehicle model. An elaborate analysis on collision avoidance control is presented in the work of Koudijs [30]. Although his work is more on the control aspect, the relevance of both studies to this thesis is similar, that is to know in which state space domain additional collision avoidance need not be initiated.

2.5 Maneuvering

Most of the existing literature is focused on single-lane platooning, without taking vehicles on other lanes into account. However, in practice, traffic jams etc. are mostly created at the locations where special maneuvers are taking place, such as the situation in which two lanes change into a single lane. In such a case, a vehicle needs to be able to join a platoon, at any convenient location in the platoon. This not only requires a platooning vehicle to create a gap, but also requires communication between the merging vehicles.

Different aspects of this communication are explained in the i-GAME project document [15]. In this document, a framework is presented for the interaction protocol between various vehicles equipped with automated driving and wireless communication capabilities. The document is linked to the Grand Cooperative Driving Challenge (GCDC) [31]. The goal of this Challenge is to enable various contributors to design and test an advanced framework, in which several cooperative driving challenges should be completed. The vehicles can vary highly in their configurations, however they should cooperatively be able to complete the challenges. In short, these challenges are designed to enable the merging of two platoons from two lanes into one lane, to cooperatively navigate a junction without traffic lights, and to make room for an emergency vehicle. The i-GAME document [15] poses various optional configurations and a number of requirements for each vehicle. Additionally, some aspects are predetermined, such as a merging communication protocol for various use-cases. For two merging platoons, this protocol is designed to limit the deceleration levels towards the tail of the platoons, and thereby prevent or limit full stops or unsafe situations during the maneuver. The i-GAME document [16] presents suggestions for the general control architecture in order to combine the various control objectives. For instance, an obstacle avoidance approach is suggested, with much resemblance to an repulsive APF. By combining multiple potential fields, for instance with addition, the functionality can be extended. These controllers are then switched on or off by the supervisory controller, which is the decision layer for an automated vehicle. This supervisory controller uses the available data for enabling various controllers needed in each situation. In the field of autonomous driving, the APF control approach might be an important element to enable the advanced capabilities that cooperative driving can promise.

2.6 Problem formulation and research question

As noted in the introduction, the use of communication in automatic driving enables numerous other capabilities to be incorporated in smart vehicles. However, this requires a more advanced control strategy. This project will restrict itself to longitudinal control of vehicle platoons, only. Next to platooning itself, a vehicle should be able to make a merging maneuver from any point of entry in the platoon. Additionally, a gap should be created or closed, in case another vehicle wishes to join or leave, using adjacent lanes. Hence, a vehicle should be able to cooperatively join or split a platoon, and close or open a gap. Hence, use-cases as suggested in [15] should be safely conducted. During all these maneuvers, collisions should be avoided at all cost. Therefore, safety and stability of the system subject to the control strategy is paramount. Additionally, comfort and performance is of importance. These functions should all be incorporated in a multi-objective control scheme such as an APF based controller. Therefore, the objective of this project is to apply an Artificial Potential Field approach (APF) in a coherent solution to longitudinally control a vehicle. The approach should safely and smoothly control the vehicle during platooning and maneuvering situations, as for instance described in [15].

3: Control design for platooning

In this chapter, the design approach for platooning and CACC will be discussed. Firstly, a vehicle model will be introduced, along with the notation for the vehicle and platoon dynamics. Following this, the suggested artificial potential field (APF) control approach will be introduced and further investigated in Section 3.3. Herein, three options for APF design will be introduced, related to different possibilities for introducing a damping term in the controller, along with a linear *PD* controller for comparison. Subsequently, the design objectives will be evaluated for each choice of APF controller design in Section 3.4, so that the final design choice can be further motivated and elaborated upon.

3.1 Dynamics

In this chapter, the dynamics of a string of m vehicles is derived. Only the longitudinal dynamics are considered, and all vehicles are assumed to have equal dynamics. The longitudinal dynamics of the i^{th} vehicle are approximated using a third-order model, as presented in the work of Ploeg et al. [7]. The position, velocity, and acceleration of vehicle i are denoted with s_i, v_i, and a_i, respectively. Consequently, the dynamics can be written as:

$$\begin{pmatrix} \dot{s}_i(t) \\ \dot{v}_i(t) \\ \dot{a}_i(t) \end{pmatrix} = \begin{pmatrix} v_i(t) \\ a_i(t) \\ \frac{1}{\tau}(u_i(t) - a_i(t)) \end{pmatrix}, \quad 1 \leq i \leq m, \tag{3.1}$$

where $u_i(t)$ denotes the desired acceleration of vehicle i, and parameter τ is a time constant representing the engine and brake system dynamics. In this thesis, it is assumed that all vehicles have equal dynamic properties, therefore $\tau = 0.1$ is assumed for all vehicles. For a homogeneous string of m vehicles, $d_{r,i}(t)$ is the desired distance for vehicle i with respect to its predecessor $i-1$. This desired distance is constructed using a standstill distance r and a time gap h in seconds. Thereby, the desired inter-vehicular distance is dependent on velocity $v_i(t)$, as is also the case in normal driving. This spacing policy, defined as

$$d_{r,i}(t) = r + hv_i(t), \quad 2 \leq i \leq m, \tag{3.2}$$

is known to improve string stability [32]. The actual inter-vehicular distance is equal to

$$d_i(t) = s_{i-1}(t) - s_i(t) - L_i, \tag{3.3}$$

with L_i denoting the vehicle length. Using (3.1)–(3.3), the dynamics of vehicle i in a platoon can be formulated as:

$$\begin{pmatrix} \dot{d}_i \\ \dot{v}_i \\ \dot{a}_i \end{pmatrix} = \begin{pmatrix} v_{i-1}(t) - v_i(t) \\ a_i(t) \\ -\frac{1}{\tau}a_i(t) + \frac{1}{\tau}u_i(t) \end{pmatrix}, \quad 2 \leq i \leq m. \tag{3.4}$$

Equation (3.4) can be used to model the dynamics for a vehicle driving in a platoon. The next section will introduce the error dynamics to be used for control and the subsequent analysis.

3.2 Error dynamics

In this section, the error dynamics of the vehicle motion will be derived. This notation is adopted from the work of Ploeg [7]. For a platooning problem, the position error for vehicle i with respect to its predecessor can be described by:

$$e_{1,i}(t) = d_i(t) - d_{r,i}(t), \quad 2 \leq i \leq m. \tag{3.5}$$

Using (3.5), the time derivatives of the position error can be determined. For readability, the time dependency is discarded in future notation. Using (3.2)–(3.5), the position error and its derivatives can be written as:

$$\mathbf{e}_i = \begin{pmatrix} e_{1,i} \\ e_{2,i} \\ e_{3,i} \end{pmatrix} = \begin{pmatrix} e_i \\ \dot{e}_i \\ \ddot{e}_i \end{pmatrix} = \begin{pmatrix} s_{i-1} - s_i - L_i - r - hv_i \\ v_{i-1} - v_i - ha_i \\ a_{i-1} + (\frac{h}{\tau} - 1)a_i - \frac{h}{\tau}u_i \end{pmatrix}, \quad 2 \leq i \leq m. \tag{3.6}$$

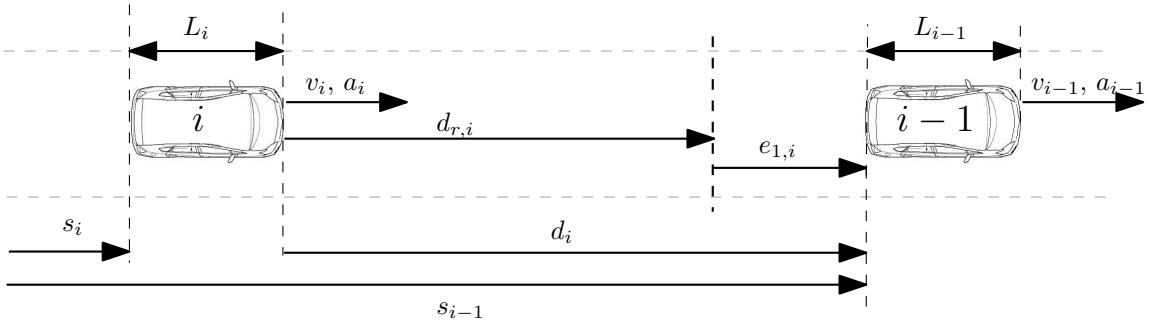

Figure 3.1: Top view of vehicle i and $i-1$ in a platoon

Figure 3.1 illustrates vehicle i in a platoon. In this illustration, the error $e_{1,i}(t)$ is positive, therefore vehicle i should try to decrease the error such that $d_i \to d_{r,i}$. The dynamics of the error can be obtained by differentiation and rewriting of (3.6). Using (3.4), this results in

$$\dot{\mathbf{e}}_i = \begin{pmatrix} \dot{e}_{1,i} \\ \dot{e}_{2,i} \\ \dot{e}_{3,i} \end{pmatrix} = \underbrace{\begin{pmatrix} 0 & 1 & 0 \\ 0 & 0 & 1 \\ 0 & 0 & -\frac{1}{\tau} \end{pmatrix}}_{A} \begin{pmatrix} e_{1,i} \\ e_{2,i} \\ e_{3,i} \end{pmatrix} + \underbrace{\begin{pmatrix} 0 \\ 0 \\ \frac{1}{\tau} \end{pmatrix}}_{B} (u_{i-1} - u_i - h\dot{u}_i), \quad 2 \leq i \leq m. \tag{3.7}$$

By introducing a new input $\bar{u}_i$ as

$$\bar{u}_i = u_i + h\dot{u}_i, \quad 2 \leq i \leq m, \tag{3.8}$$

the dynamics in (3.7) can be rewritten to

$$\dot{\mathbf{e}}_i = A\mathbf{e}_i + B(u_{i-1} - \bar{u}_i), \quad 2 \leq i \leq m. \tag{3.9}$$

Equation (3.9) shows a general expression for the error dynamics, with control input $\bar{u}_i$ as defined in (3.8). Note that u_i can always be calculated from a set-point $\bar{u}_i$, since

rewriting (3.8) yields an equivalent lowpass filter. In this project, an Artificial Potential Field (APF) approach is used to derive the control input $\bar{u}_i$. However, different design options are possible. These will be further elaborated in the following section.

3.3 APF-based control

In this section, the controller design will be discussed. Therefore, various APF architectures and the subsequent design choices will be elaborated upon in this section. Subsection 3.3.1 motivates the initial APF design, which has been adapted from linear control, in order to achieve the objectives as discussed in Chapter 2. Consequently, alternative APF approaches are suggested to allow further improvements in Subsection 3.3.2. For simplification of the controller design, an alternative state description will be suggested in Subsection 3.3.3. Consequently, the controllers can be compared in the next section.

3.3.1 Linear PD and APF control

For controlling a system as presented in (3.9), a linear control approach is often applied, as for example the error state feedback law in [7]. Since full state information is often unavailable or unreliable, the *PD* controller is common practice. Therefore, the *PD* control approach will used for comparison, as can be defined by

$$PD: \qquad \bar{u}_{i,PD} = k_p e_{1,i} + k_d e_{2,i} + u_{i-1}, \quad 2 \leq i \leq m, \tag{3.10}$$

where the proportional gain k_p and damping gain k_d determine the action of the controller, in combination with the feedforward term u_{i-1}. When using an APF control design, an artificial potential field function Ψ_A assigns a value to each operation state. Generally, the smooth positive definite APF function Ψ_A has a single point minimum. The APF control objective is to minimize this function value, using the partial derivative of Ψ_A. For introduction, a position dependent potential function will be used in combination with linear damping. This results in the first APF design, which can be described by

$$APF1: \qquad \bar{u}_{i,APF1} = \frac{\partial \Psi_A(e_{1,i})}{\partial e_{1,i}} + k_d e_{2,i} + u_{i-1}, \quad 2 \leq i \leq m. \tag{3.11}$$

In order to translate (3.10) into (3.11), the minimal requirements for function Ψ_A can be considered. In order to reach the state $e_{1,i} = 0$, it can be concluded from (3.7)–(3.9) that the position dependent APF component in (3.11) cannot oppose the sign of $e_{1,i}$. Note, this is similarly the case for the first component of (3.10). This results in the minimal requirement:

$$\Psi_A(e_{1,i} = 0) = 0, \tag{3.12}$$

$$\begin{cases} \frac{\partial \Psi_A(e_{1,i})}{\partial e_{1,i}} \leq 0 & e_{1,i} < 0, \qquad i \in m, \\ \frac{\partial \Psi_A(e_{1,i})}{\partial e_{1,i}} \geq 0 & e_{1,i} > 0, \end{cases} \tag{3.13}$$

where $sign\left(\frac{\partial \Psi_A(e_{1,i})}{\partial e_{1,i}}\right) = sign(e_{1,i})$ must hold for the domain of $e_{1,i}$ where platooning or gap closing is of interest. Condition (3.12) ensures the potential is zero on the desired platooning distance, and (3.13) ensures the platooning distance is the minimum of the APF. When substituting Ψ_A for

$$\Psi_{PD}(e_{1,i}) = \frac{1}{2} k_p e_{1,i}^2, \quad 2 \leq i \leq m, \tag{3.14}$$

the linear controller (3.10) can be obtained. A linear controller is very useful for linear systems and/or systems with relatively small changes in magnitude of the error. However, when combining platooning, gap closing and gap-making scenarios, one should note that the position error $e_{1,i}$ can vary significantly in magnitude. Therefore, it is desirable to consider the desired position-dependent behavior when following a preceding vehicle, thereby designing an Artificial Potential Field Cooperative Cruise Adaptive Cruise Control (APF-CACC). Herein, the distinction between a Repulsive Potential (RP) and an Attractive Potential (AP) is made, resulting in a deceleration or acceleration term respectively, such that the total platooning potential can be defined by:

$$\Psi_A(e_{1,i}) = \Psi_{RP}(e_{1,i}) + \Psi_{AP}(e_{1,i}), \quad 2 \leq i \leq m. \tag{3.15}$$

For illustration, the desired repulsive and attractive potential fields (Ψ_{RP}, Ψ_{AP}) can be sketched, with an equivalent linear control potential Ψ_{PD} as in (3.14) for comparison.

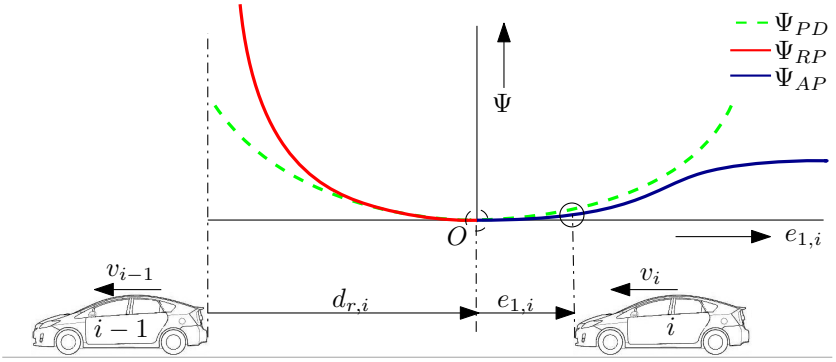

Figure 3.2: The desired repulsive and attractive potential (Ψ_{RP}, Ψ_{AP}), in comparison with a quadratic potential (Ψ_{PD})

Figure 3.2 illustrates the shape of a desirable potential function. In case $e_{1,i} \ll 0$, collision has to be avoided, therefore the repulsive potential increases rapidly along the red line. For a small magnitude of the error, damped and subtle behavior is desirable, therefore the potential changes only slightly. In case the gap is very large, gap closing might be no longer of interest. Therefore, $\Psi_A(e_{1,i})$ should be approximately constant for $e_{1,i} \gg 0$, creating a fade-off at large inter-vehicular distances. During gap closing however, a balance between performance, comfort, safety, and fuel consumption will be desirable. A controller will use the partial derivative of such a function to control the potential towards zero. In a

previous research at TNO, an APF function has already been suggested [23]. Although the AP function will be kept in similar shape as in [23], an alternative RP will be chosen for this project in order to have a significant design freedom. The resulting APF components are described by:

$$\Psi_{RP}(e_{1,i}) = \begin{cases} k_1 e_{1,i}^4 - k_2 e_{1,i}^3 + k_3 e_{1,i}^2 & e_{1,i} \leq 0, \\ 0 & e_{1,i} > 0, \quad 2 \leq i \leq m, \end{cases} \tag{3.16}$$

$$\Psi_{AP}(e_{1,i}) = \begin{cases} 0 & e_{1,i} < 0, \\ k_4(1 - e^{-k_5 e_{1,i}})^2 & e_{1,i} \geq 0, \quad 2 \leq i \leq m. \end{cases} \tag{3.17}$$

Using a polynomial for the RP, the platooning segment can be tuned separately, while additional parameters remain available for tuning the OA functionality. Parameter k_3 can be chosen as $k_3 = k_4 k_5^2$, such that $\Psi(e_{1,i}) \in C^2$. As a result, the controller will approximate a linear controller with $k_p = 2k_3$ for small magnitudes of the error, which can be desirable for analysis and comparison. Equally, the balance of RP and AP is of importance for the average tracking error; in case a negative error always results in a larger response then a positive error of equal magnitude, a random noise disturbance will result in a positive average position error in infinite time. The shape of the APF components (3.16) and (3.17) can be tuned using multiple parameters, such that the response can be designed for each segment while satisfying requirement (3.13). The equation itself guarantees $\Psi_A(0) = 0$, which should be the only minimum of a suitable platooning potential function. Hence, $k_1, k_2, k_3, k_4 > 0$ should hold.

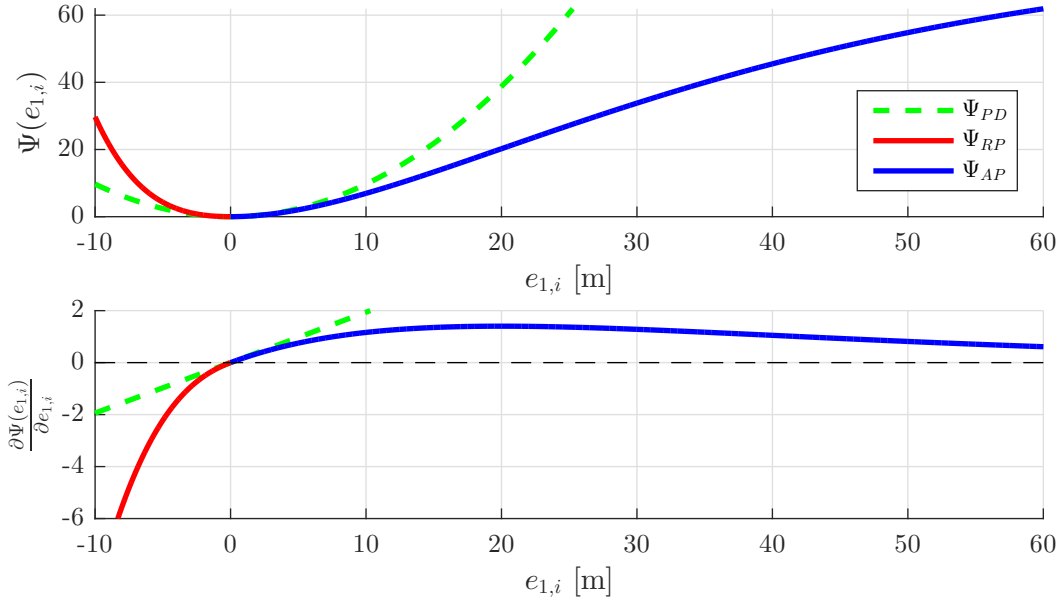

Figure 3.3: APF-CACC potential function in comparison to a linear controller

Figure 3.3 shows a plot of the potential function (3.15)–(3.17) and its derivative, with again the linear controller potential field Ψ_{PD} as defined in (3.14) for comparison. Note, both controllers depicted in Figure 3.3 have the same linear spring stiffness near the equilibrium, with $k_p = 0.194$, which is realized by selecting the APF parameters as $K = [k_1\ k_2\ k_3\ k_4\ k_5] = [0.001\ 0.01\ 0.097\ 80.79\ 0.0347]$. Using any suitable set of parameters for (3.15)–(3.17), the control action $\bar{u}_i$ can be calculated using the potential field derivative. The derivative, as shown in Figure 3.3, shows that the linear controller responds insufficient for significant negative errors, yet too fierce for large errors. Therefore, APF is preferred over linear control to determine the input $\bar{u}_i$ for combining platooning, gap closing and obstacle avoidance into one controller. In other words, although the system to be controlled is linear, the control objectives are not. When regarding controller *APF1* as in (3.11), it can be noted that the damping is linear. However, when regarding gap closing or platooning, the range of permitted velocity differences change significantly. Therefore, other APF alternatives will be introduced to introduce nonlinear damping, which will additionally be discussed and compared. Consequently, the preferred final APF controller will be selected and further reviewed for string stability.

3.3.2 Introducing nonlinear damping

In the previous section, (3.11) was introduced, which introduces a position-dependent potential field, either (3.14) or (3.15), in combination with linear damping. However, in this section, two alternative choices for control law will be introduced where a nonlinear damping is used. Both controllers will introduce a nonlinear damping term, which had been linear up till now. The first alternative is to create an additional damping APF such that:

$$\textit{APF2:} \qquad \bar{u}_{i,APF2} = \frac{\partial \Psi_A(e_{1,i})}{\partial e_{1,i}} + \frac{\partial \Psi_d(e_{2,i})}{\partial e_{2,i}} + u_{i-1}, \quad 2 \leq i \leq m. \tag{3.18}$$

However, one should note that this does not create the desirable design freedom, since the tolerance on the velocity difference is mainly dependent on position: At large inter-vehicular distance, a reduced damping can be desirable to allow significant velocity differences for gap closing performance. During platooning however, a significant level of damping is required to limit the inter-vehicular velocity for safety purposes. With design (3.18), it is impossible to tune the damping for platooning and gap closing separately. Therefore, *APF2* as in (3.18) will not be further applied or investigated. Instead, a damping factor is introduced which can distinguish between the platooning and gap closing state, by having a position error dependency:

$$\textit{APF3:} \qquad \bar{u}_{i,APF3} = \frac{\partial \Psi_A(e_{1,i})}{\partial e_{1,i}} + D(e_{1,i})e_{2,i} + u_{i-1}, \quad 2 \leq i \leq m, \tag{3.19}$$

where the damping coefficient is determined by:

$$D(e_{1,i}) = \begin{cases} k_{d1}, & \text{if } e_{1,i} \leq f_1, \\ k_{d2}, & \text{if } e_{1,i} \geq f_2, \\ k_{d2} + \frac{k_{d1}-k_{d2}}{2}(1 + cos(\pi \frac{e_{1,i}-f_1}{f_2-f_1})), & \text{otherwise.} \end{cases} \tag{3.20}$$

With the nonlinear damping (3.20) determined using $f_2 \geq f_1$ and typically $f_1 > 0$. The parameters f_1, f_2 determine the positions at which the damping changes between level k_{d1} and k_{d2} respectively, with $k_{d1}, k_{d2} \geq 0$.

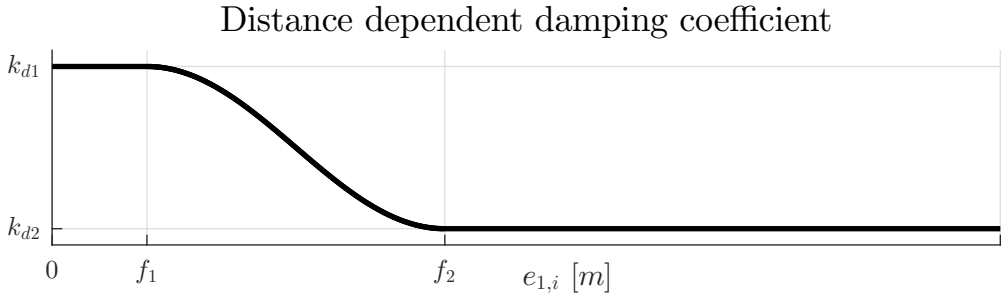

Figure 3.4: Damping coefficient as a function of position error $e_{1,i}$

Figure 3.4 illustrates the suggested position dependent damping. When $e_{1,i} \leq f_1$, the vehicle state is typically close to the platooning state, requiring sufficient damping. Therefore, $k_{d1} = k_d = 0.7$ is chosen as the platooning damping coefficient. As $e_{1,i}$ increases, a reduced damping is desired, allowing higher velocity differences and potentially increasing the gap closing performance. Therefore, the damping coefficient is reduced to k_{d2} using a transient function for the domain $f_1 < e_{1,i} < f_2$, with $f_1 = 3\ m$ and $f_2 = 20\ m$. Finally, only a reduced damping ratio $k_{d2} = \frac{k_{d1}}{4}$ will be used for $e_{1,i} \geq f_2$. A possible issue with controller (3.19) is the varying ratio in influence, between the position APF and the damping term during gap closing. This can result is undesirable behavior during gap closing. In an attempt to overcome this issue by design, an alternative design will be suggested in the next section.

3.3.3 Control using a linear combination of the errors

Since the previous choices use two control components to determine $\bar{u}_i$, another APF approach will be introduced. This method has been previously suggested in an internal research at TNO [33]. The idea is to include damping in the distance dependent APF, and to reduce complexity of designing two potential functions. This is achieved using an error description which includes the position error and its derivative into the same potential function for platooning. Therefore, the error $\mathbf{x}_i$ is introduced as:

$$\mathbf{x}_i = \begin{pmatrix} x_{1,i} \\ x_{2,i} \\ x_{3,i} \end{pmatrix} = \begin{pmatrix} e_{1,i} + ce_{2,i} \\ e_{2,i} \\ e_{3,i} \end{pmatrix}, \quad 2 \leq i \leq m, \tag{3.21}$$

where the constant c determines the weight of $e_{2,i}$ with respect to $e_{1,i}$. Using (3.7), the dynamics corresponding to (3.21) can be described by:

$$\dot{\mathbf{x}}_i = \begin{pmatrix} \dot{x}_{1,i} \\ \dot{x}_{2,i} \\ \dot{x}_{3,i} \end{pmatrix} = \underbrace{\begin{pmatrix} 0 & 1 & c \\ 0 & 0 & 1 \\ 0 & 0 & -\frac{1}{\tau} \end{pmatrix}}_{A_x} \begin{pmatrix} x_{1,i} \\ x_{2,i} \\ x_{3,i} \end{pmatrix} + \underbrace{\begin{pmatrix} 0 \\ 0 \\ \frac{1}{\tau} \end{pmatrix}}_{B} (u_{i-1} - \bar{u}_i), \quad 2 \leq i \leq m. \tag{3.22}$$

Since the error (3.21) includes the position and velocity error in the first term, the fourth option for $\bar{u}_i$ can be written as:

$$APFx: \qquad \bar{u}_{i,APFx} = \frac{\partial \Psi_A(x_{1,i})}{\partial x_{1,i}} + u_{i-1}, \quad 2 \leq i \leq m. \tag{3.23}$$

In (3.23), the required damping is included using $x_{1,i}$ into the potential function. In (3.21), parameter c determines the ratio for damping. Hence, the isocline $\bar{u}_{i,APFx} = 0$ is described by $x_{1,i} = 0 \rightarrow e_{2,i} = -\frac{1}{c} e_{1,i}$. For the linear PD controller, this isocline is described by $e_{1,i} = -\frac{k_p}{k_d} e_{2,i}$. Since the controller $APFx$ is much different in design with repect to the PD controller, it is important to analyze the stability of this system. Therefore, a more elaborate analysis is performed in Appendix C on the equilibrium and asymptotic stability of system (3.22) in combination with (3.23). There, asymptotic stability has been proven for a system using the proposed controller $APFx$ as in (3.23). Since multiple control structures have now been introduced, the controllers will be compared and evaluated in the next section.

3.4 Comparison of APF controllers

In this section, the APF controllers will be compared using simulation. To this end, a set of performance criteria will first be derived for platooning and gap closing. Next, the gap closing and the platooning scenario will be further evaluated, after which the final choice of controller can be motivated.

3.4.1 Scenarios and performance criteria

For simulation and evaluation, we consider a discrete time-span of K equal segments of length Δt_k, the time span defined by $t \in [t_0, t_K]$. For both platooning as well as gap closing scenarios, vehicle i is considered to be driving directly behind the lead vehicle. In both scenarios, the initial lead vehicle velocity is set to $v_{lead}(t_0) = 20\ m/s = 72\ km/h$. Vehicle i will have an equal initial velocity. The headway settings are $r = 2\ m$ and $h = 0.5\ s$, resulting in $d_{r,i}(v_i(t_0)) = 12\ m$. Since the feedback controller response is mainly of interest, it is assumed that there is no feedforward from the lead vehicle. Hence, this scenario is evaluated using ACC. For the platooning scenario, the vehicles start in a perfect platooning configuration at constant speed. During the test, the lead vehicle will start a slight braking maneuver, with $u_{lead}(t) = -1\ m/s^2$, for $t \in [5\ 10]s$. For safe

and efficient platooning, disturbance attenuation and smooth behavior, while minimizing the magnitude of the position error, is very important. Because of the desire to minimize changes in acceleration for fuel consumption and comfort purposes, the acceleration profile will be evaluated using an integral square error (ISE) criterion [34], also known as the l_2 signal norm:

$$Q_{1,i} = ||a_i(t)||_2 = \sqrt{\sum_{k=1}^{K} a_i(t_k)^2 \Delta t_k}, \quad t \in [t_0, t_K]. \tag{3.24}$$

Equation (3.24) calculates the ISE of the acceleration profile in time span $t \in [t_0, t_K]$. As discussed in Chapter 2, limiting the changes in acceleration level is desirable for both comfort and fuel consumption. Since safety and tracking are additionally of importance, the controller should not allow the position error to become too large. Therefore, the position error is evaluated using the infinity norm:

$$Q_{2,i} = ||e_{1,i}(t)||_\infty = max(|e_{1,i}(t)|), \quad t \in [t_0, t_K]. \tag{3.25}$$

Using both (3.24) and (3.25), the performance of the platooning control mechanism be quantified.

The second scenario in evaluation is the gap closing scenario. In this scenario, the lead vehicle velocity and measured velocity will remain constant, hence $v_{lead}(t) = v_{lead}(t_0)$. Herein, vehicle i has to close the gap, starting from initial conditions $e_{1,i}(t) = 30\ m$, $a_i(t_0) = 0\ m/s^2$ and $v_i(t_0) = v_{lead}(t_0)$. Since the initial position error is rather large and likely to decrease, criteria (3.25) cannot be applied for the gap closing scenario. For this scenario however, it is important to quantify the corresponding time required to reduce the gap. Therefore, the absolute position error is integrated in time:

$$Q_{3,i} = \sum_{k=1}^{K} |e_{1,i}(t_k)| \Delta t_k, \quad t \in [t_0, t_K]. \tag{3.26}$$

In addition to (3.24), (3.26) can be used to quantify the controller performance for the gap closing scenario. Using these two scenarios, with the given three performance criteria, the controller choice will be elaborated.

3.4.2 Performance evaluation of platooning controller

In this section, the platooning performance is analyzed for all suggested control structures. Herein, various controllers are evaluated while driving behind the same simulated lead vehicle. This lead vehicle provides no feedforward, and will brake lightly for five seconds. Note, in the platooning case, controller (3.19) is equal to the one in (3.11), since (3.20) equals k_d for $e_{1,i} < f_1$ and typically $f_1 >> 0$. Therefore, the controller in (3.19) will not be shown in the platooning performance evaluation. However, the performance of the other controllers can be evaluated. Herein, $k_p = 0.2$, $k_d = k_{d1} = 0.7$, and $c = 5$ have been selected along with the APF parameters equal as in Figure 3.3.

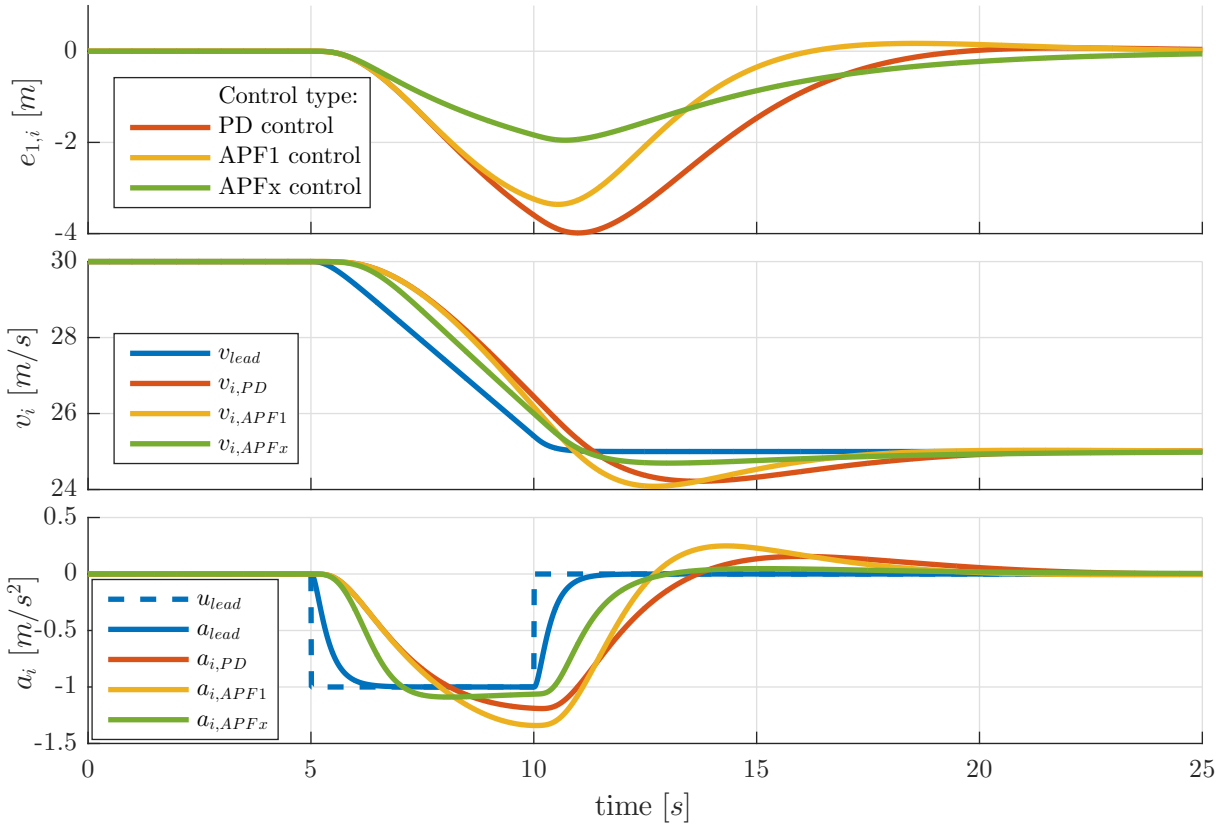

Figure 3.5: Platooning test for three different control architectures

Figure 3.5 shows the behavior of the various controllers for the platooning scenario. The performance of the system subject to *PD* controller (3.10) is depicted with the red line. As expected, Figure 3.5 shows that the *PD* controller allows a significant negative position error. Although controller *APF1* performs better in this respect, controller *APFx* performs best by having the smallest peak deceleration level. This can similarly be concluded when evaluating performance criteria (3.24) and (3.25) as is shown in Table 3.1.

Table 3.1: Performance evaluation in platooning scenario for three controllers

Vehicle	$Q_1(a_i(t_k))$	$Q_2(e_{1,i}(t_k))$ $[m]$
Lead vehicle	2.1622	-
PD control (3.10)	2.3412	3.9860
APF1/APF3 control, (3.11) and (3.19)	2.5264	3.3596
APFx control (3.23)	2.2365	1.9516

Table 3.1 shows the performance of the controllers for the platooning scenario for $t_k \in [0\ 25]$ s. For all vehicles, the ISE acceleration norm exceeds the corresponding lead

vehicle norm. Although this is undesirable, it remains reasonable due to the absence of feedforward in combination with the small headway. With respect to the position error, the combined APF controller (3.23) performs much better in this scenario than the other control algorithms. This is similarly visible in the velocity plot of Figure 3.5, where there is little velocity overshoot at approximately $t = 12\ s$ with respect to the other controllers. Consequently, it is important to review the gap closing capabilities for further comparison.

3.4.3 Gap closing performance

For the gap closing scenario, the vehicles will start at a 30 m gap from their desired setpoint, as further described in Subsection 3.4.1. For gap closing, it is important to know how each controller will perform. An extensive analysis of the response of each controller can be found in Appendix A. In reality, a feasible domain for the acceleration is $a_i(t) \in [-6\ 3]\ m/s^2$. Hence for a realistic comparison, the accelerations are saturated within the bounds $u_i(t) \in [-6\ 3]\ m/s^2$, thereby limiting the actual acceleration and rate of change of the acceleration to a realistic level.

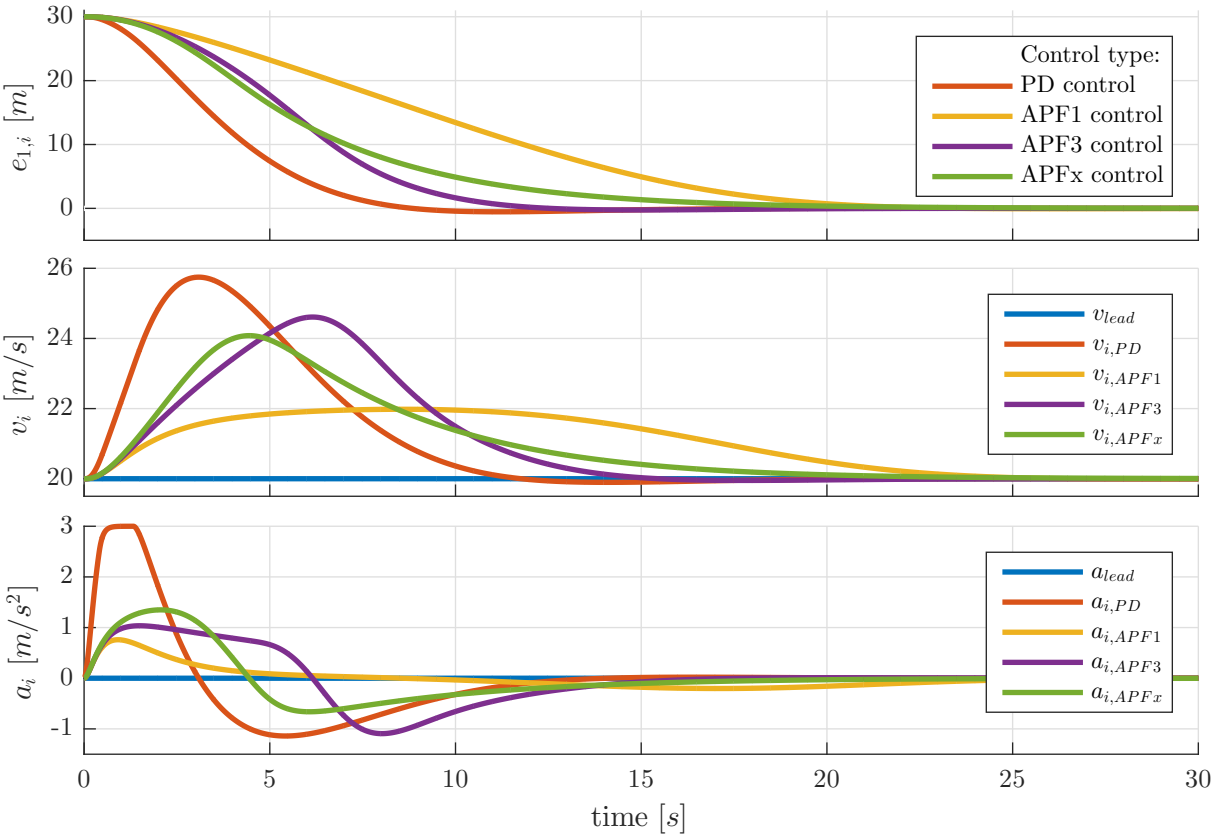

Figure 3.6: Gap closing test for four different control strategies

Figure 3.6 shows the simulated results for a gap closing scenario using controllers (3.10), (3.11), (3.19) and (3.23), referred to as *PD*, *APF1*, *APF3*, and *APFx*, respectively. Herein, the *PD* controller reaches the physical saturation on acceleration at around $t = 1\ s$, which is highly undesirable for fuel consumption and comfort. The other acceleration levels remain reasonable. However, in this respect the braking level should remain low. This is best achieved by controller (3.11) depicted with an orange line, however it is rather slow in converging. The performance can also be quantified using criteria (3.24) and (3.26).

Table 3.2: Performance evaluation in gap closing scenario for the controllers

Vehicle	$Q_1(a_i(t_k))$	$Q_3(e_{1,i}(t_k))$ $[ms]$
Lead vehicle	0	-
PD control (3.10)	4.3501	106.8886
APF1 control (3.11)	1.1164	286.0787
APF3 control (3.19)	2.6978	168.9997
APFx control (3.23)	2.4825	191.9660

To this end, Table 3.2 quantifies the performance of the controllers for the gap closing scenario. As expected, the *PD* controller has the largest Q_1 norm since it saturates the acceleration. The controller (3.11) performs best in minimizing accelerations, however, it closes the gap very slowly with a maximum approach velocity of 2 m/s in this scenario. Although this can be improved by gain selection, the options are very limited since changing the damping can compromise the platooning performance. Controllers *APF3* and *APFx*, (3.19) and (3.23), respectively depicted in purple and green, are more reasonably balanced between limiting the gap closing time and the acceleration levels, and are rated best in Table 3.2. In Figure 3.6 it can be seen that controller *APFx* requires a less substantial peak deceleration, yet a slightly higher peak acceleration. Initially, controller *APFx* is slightly faster than *APF3* in approach, only the final part of the approach is a little slower. However, controller *APFx* performs best in the platooning test, and as one of the best options in gap closing. Additionally, this control strategy has been proven to be asymptotically stable in Appendix C. Therefore, the control method *APFx* will be further elaborated in this thesis.

3.5 String stability review

In this thesis, a controller is designed to control vehicles longitudinally in a platoon, to guarantee a verhicle following objective. One of the aspects of platooning is to increase the traffic throughput, reduce unnecessary accelerations, and increase safety. Therefore, it is important that a platoon is string stable [7, 8]. In the work of Ploeg [7], string stability is analyzed for a platoon of vehicles subject to a linear controller. The notion of string stability is there introduced as the attenuation of disturbances towards the back of the string. Hence, an acceleration, velocity, or position error oscillation should be reduced in magnitude along the string. Ploeg analyses string stability for a linear controller

using a transformation to the frequency domain. However, since the control design $APFx$ is nonlinear, proving theoretical string stability can be difficult, or perhaps impossible. Therefore, string stability will not be theoretically investigated in this thesis. However, it is very important to investigate if string stability is a plausible property, therefore this aspect is investigated by means of simulation. To this end, the TNO CACC simulation model is used, since it additionally incorporates sensor and communication delays, object tracking and fusion algorithms, and a discrete time implementation of controller and the sensor information [8]. A platoon of 10 vehicles is simulated, starting at a perfect platooning configuration with equal constant initial velocity of $v_i(t_0) = 10\ m/s$. For the spacing policy, $r = 2\ m,\ h = 0.5\ s$ is used, throughout this chapter. Also, the first vehicle follows an oscillatory velocity profile, the frequency content is can be depicted.

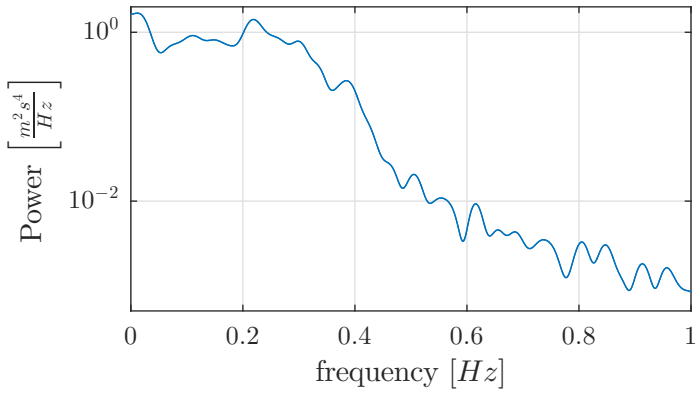

Figure 3.7: Power spectral density of the platoon acceleration excitation signal

The Power Spectral Density of the acceleration of the virtual lead vehicle is plotted in Figure 3.7, which shows that the frequency band is appropriate to test the longitudinal behavior of the platoon, since the typical longitudinal dynamics of a platoon are below frequencies of $\omega = 2\ rad/s \approx 0.32\ Hz$, as can be concluded from [7]. Since a string of 10 vehicles is used, the attenuation of acceleration and velocity changes should be clearly visible. In order to provide a quantitative measure of this aspect, an additional ISE norm is introduced to analyze the velocity difference with respect to the predecessor:

$$Q_{4,i} = ||\Delta v_i(t)||_2 = \sqrt{\sum_{k=1}^{K} (\Delta v_i(t_k))^2 \Delta t_k}, \quad t \in [t_0, t_K], \qquad 2 \leq i \leq m., \tag{3.27}$$

Consequently, the simulation can be evaluated. Since the control strategy is nonlinear, multiple criteria will have to be evaluated. By evaluating the performance criteria $Q_{1,i}$, $Q_{3,i}$ and $Q_{4,i}$ as in (3.24), (3.26) and (3.27), the disturbance attenuation in the string can be investigated for acceleration, accumulative tracking error, and the inter-vehicular velocity difference respectively.

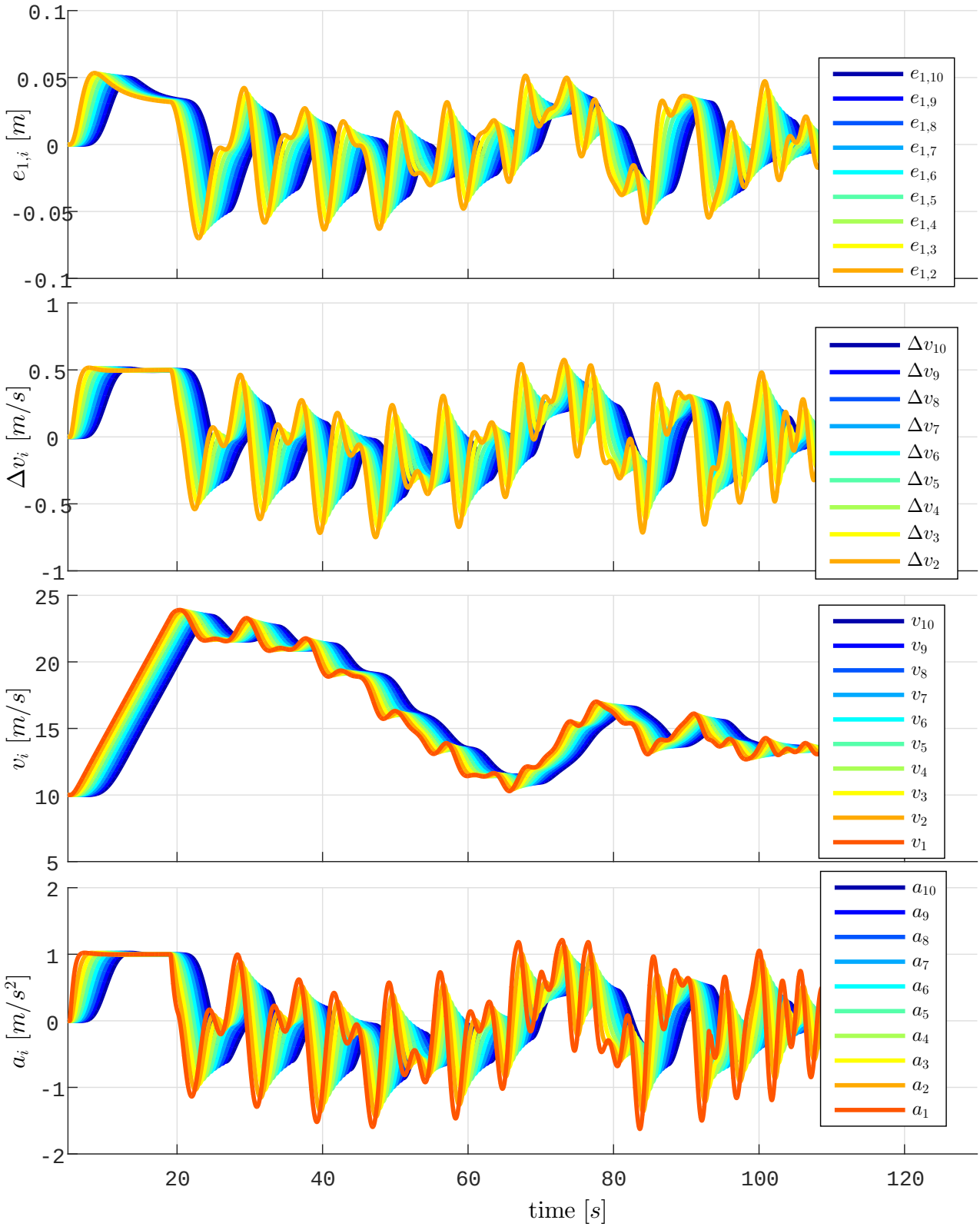

Figure 3.8: Response plot for a platoon of 10 vehicles

Figure 3.8 shows a plot of the simulation, the corresponding performance evaluation can be found in Table 3.3:

Table 3.3: *APFx* performance evaluation for string of ten vehicles

Vehicle	$Q_1(a_i(t_k))$	$Q_3(e_{1,i}(t_k))$	$Q_3(\Delta v_i(t_k))$
Lead vehicle	7.5555	-	-
$i = 2$	6.7715	0.2074	3.5095
$i = 3$	6.2686	0.1642	3.2233
$i = 4$	5.9266	0.1418	3.0294
$i = 5$	5.6810	0.1294	2.8910
$i = 6$	5.4964	0.1220	2.7876
$i = 7$	5.3522	0.1174	2.7074
$i = 8$	5.2359	0.1142	2.6432
$i = 9$	5.1396	0.1119	2.5904
$i = 10$	5.0580	0.1102	2.5460

The performance results are shown in Table 3.3. It can be seen that magnitude of the acceleration, maximal position error and the relative velocity decrease towards the end of the string. This is similarly visible in Figure 3.8, where the first vehicle is clearly oscillating extensively, whereas the last vehicle has a relatively smooth velocity profile. Although this analysis obviously does not prove string stability, the analysis does confirm plausibility of string stability. As a result, this controller can further be analyzed in the next chapters.

3.6 Summary

In this chapter, multiple controllers have been introduced and compared. For the quantification of performance, multiple performance criteria have been determined in Subsection 3.4.1. For sake of comparison, a platooning scenario and a gap closing scenario have been simulated and evaluated. As a result, the *APFx* controller of (3.23) has been chosen as the preferred controller. In an attempt to further investigate the platooning potential of this controller, a string stability review has been conducted in Section 3.5. In evaluation, the *APFx* controller has shown to be promising for gap closing and platooning. In the upcoming chapters, controller (3.23) will be further elaborated and investigated. To this end, Chapter 4 will provide a longitudinal safety analysis. Afterwards, Chapter 5 will provide a strategy to allow safe and smooth platoon maneuvering on the road.

4: Safety and Collision Avoidance

In this chapter, the longitudinal safety with respect to the preceding vehicle is investigated for a vehicle controlled using APF-CACC. For autonomous cooperative driving, it is important to ensure that the vehicle can always avoid collisions, even in case the preceding vehicle makes an unexpected emergency braking action. To this end, various regions in the state space will be defined, indicating the level of safety assurance. Depending on this level, the expected control action can be indicated. Additionally, while in a safe state, the intended acceleration will remain within certain bounds for comfort purposes. The set of states where full braking is required will be derived in Section 4.2, such that a Collision Avoidance (CA) controller can be defined in Section 4.3.

When regarding the nominal controller, it is desirable to ensure a significant intended braking set-point from the nominal controller before the CA controller intervenes. Therefore, the limits of the nominal controller with respect to safety will be investigated in Section 4.4. The first step towards the above mentioned objectives, is to define safety regions as denoted in the next section.

4.1 Safety regions

In order to elaborate on safety, four operation regions will be defined in the state space $\mathcal{Y}_1 \subset \mathbb{R}^5$, indicating the longitudinal safety status of a vehicle with respect to its preceding vehicle at a time t_0. Herein, $\mathcal{Y}_1$ consists of all feasible combination of states for $P = [d_i(t_0), v_i(t_0), \Delta v_i(t_0), a_i(t_0), a_{i-1}(t_0)]^T \in \mathcal{Y}_1$. These operation regions are denoted with $D_x \subset \mathbb{R}^5$, where x can be s, d, m, or c, as defined in Table 4.1.

Table 4.1: Safety regions of operation

Symbol	**Regions of operation**	**description**	**action**
D_s	Safe region	normal operation	$u_i \in [u_{min}, u_{max}]$
D_d	Potentially dangerous	proper braking action required	$u_i \in [u_{ca}, 0]$
D_m	Critical region	full braking required	$u_i = u_{ca}$
D_c	Collision region	full braking required	$u_i = u_{ca}$

The acceleration limits u_{min}, u_{max} and u_{ca}, denote the lower and upper acceleration comfort limits, and the full braking limit, respectively. Therefore, it should be noted that $u_{ca} \leq u_{min} < 0 < u_{max}$. As a result of this analysis, the safety status of a point $P = [d_i(t_0), v_i(t_0), \Delta v_i(t_0), a_i(t_0), a_{i-1}(t_0)]^T \in \mathcal{Y}_1$ can be evaluated. Since the operation domains $D_x \subset \mathbb{R}^5$ are rather complex, the number of parameters will need to be reduced for visualization. Assuming all other states in $\mathcal{Y}_1$ are given and known, the operation domains can be illustrated as a function of d_i and $\Delta v_i = v_{i-1} - v_i$ as in Figure 4.1.

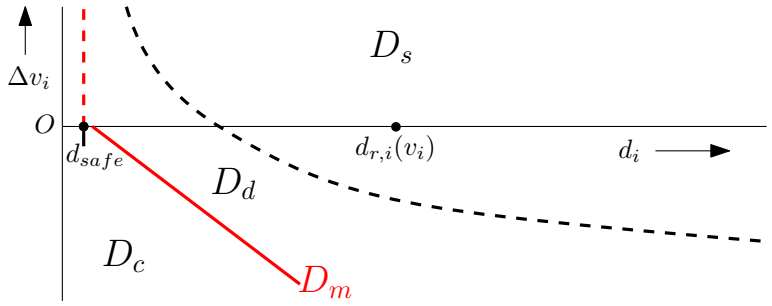

Figure 4.1: Schematic drawing of regions of safety as a function of d_i and Δv_i

Figure 4.1 shows the safety regions of operation D_x, as denoted in Table 4.1. Distance d_{safe} is the minimal inter-vehicular distance, hence a small positive distance assuring that the vehicles do not collide. In case $d_i < d_{safe}$ and $\Delta v_i \leq 0$, it is assumed that collision occurs. Region D_c indicates all states where collision cannot be avoided by vehicle i for a worst case scenario. Since vehicle $i-1$ is not in our control, vehicle i should be able to guarantee longitudinal safety. Hence, vehicle i should apply full braking in D_c, to limit the impact speed and/or reduce the chance of collision. In the critical region D_m, vehicle i will only be able to prevent a collision for a worst-case scenario if full braking is applied. In Figure 4.1, the upper part of the red line is dashed since $\Delta v_i > 0$ there, hence a collision has previously occurred or a cut-in maneuver has been performed.

The next region of interest is the safe region D_s, where nominal operation is active and emphasis can be placed on comfortable driving for platooning or maneuvering. Between D_s and D_m, the potentially dangerous region D_d can be found. In this region, safety cannot be warranted by the nominal controller, which is limited to the comfort bounds. There, hard braking is desired in order to prevent or limit the need of full braking.

Each region of operation indicates a level of danger, and has a corresponding acceleration range as indicated in Table 4.1. An approximately similar division for the acceptable acceleration range is introduced for automated vehicle testing in the GCDC [13]. However, there in addition two modes of operations are considered, namely an automated and manual mode of operation. For normal automated operation, the acceleration of vehicle i is bounded by $a_i \in [-2, 2]$ m/s^2. For potentially dangerous situations, $a_i \geq -4$ m/s^2 is considered for automated driving, or $a_i \geq -8$ m/s^2 for manual braking in a car.

In this report, the safety analysis will be limited to automatic control. In this case, vehicles are limited to a lower bound acceleration $u_{ca} = -6$ m/s^2. Using the given acceleration limits, the region D_m will be determined in Section 4.2. In practice, reaching D_m will only be tolerated for extreme use-cases, and region D_c should be prevented at all cost. The region D_m will therefore be further elaborated in the next section. Consequently, region D_s will be discussed. Note, region D_c will simply follow from D_m, since it consists of all states where collision avoidance cannot be guaranteed. When knowing region D_m, D_c and D_s, region D_d simply consists of all states between D_m and D_s, which are not covered in the other three regions. Hence, the analysis can be limited to regions D_m and D_s.

4.2 Region of critical safety

In this section, the critical set D_m will be derived, by determining all feasible critical states $P = [d_i(t_0), v_i(t_0), \Delta v_i(t_0), a_i(t_0), a_{i-1}(t_0)]^T \in D_m$. Additionally, this region will be denoted by another notation for further analysis. The objective is to find a minimal set of states wherein collision avoidance can only be guaranteed by a full braking maneuver. Similar to the pursuit-evasion game approach of [29], the most extreme use-case will be evaluated, under the assumption that both vehicles drive the same path and direction. Hence, an emergency braking maneuver from the preceding vehicle $i-1$ is evaluated, as a consequence of which vehicle i should evade collision. It has been stated in the pursuit-evasion game approach that if collision can be avoided in this scenario, it can similarly be avoided for other, easier, scenarios. Although this approach is rather conservative, it should be noted that the occurrence of an emergency braking action cannot simply be excluded.

To examine the emergency braking scenario, the longitudinal acceleration, velocity and distance profile of a vehicle will first be evaluated for $u_i = u_{ca}$. Next, this analysis can be used to investigate the behavior of two vehicles in an emergency braking maneuver in Subsection 4.2.2. Herein, the limits on the initial conditions are examined to determine $D_m \subset \mathbb{R}^5$. For the analysis of safety with respect to nominal controller, the critical region D_m will additionally be described in the error domain in Subsection 4.2.3. As a result of this section, a CA controller is developed in Section 4.3, and the safety of the nominal controller is evaluated in Section 4.4.

4.2.1 Emergency braking maneuver

In this subsection, the acceleration, velocity, and distance profile will be examined while performing an emergency braking maneuver. Herein, the vehicle dynamics of (3.4) will be assumed for vehicle i, starting the maneuver at time $t_{i,0}$ and reaching a standstill at $t_{i,stop}$. For vehicle i performing this maneuver, the following acceleration profile can be acquired:

$$a_i(t) = a_i(t_{i,0}) + (u_{ca} - a_i(t_{i,0}))(1 - e^{\frac{-(t-t_{i,0})}{\tau}}), \qquad t \in [t_{i,0}, t_{i,stop}]. \tag{4.1}$$

By integration of (4.1), the velocity profile can be denoted as:

$$v_i(t) = v_i(t_{i,0}) + \int_{t_{i,0}}^{t} a_i(t)dt = v_i(t_{i,0}) + u_{ca}(t - t_{i,0}) + (u_{ca} - a_i(t_{i,0}))\tau(e^{\frac{-(t-t_{i,0})}{\tau}} - 1). \tag{4.2}$$

Using (4.2), the stopping time can be derived using the boundary condition $v_i(t_{i,stop}) = 0$. Similarly, by means of integration of (4.2), the traveled distance during the maneuver, within time span $t \in [t_{i,0}, t_{i,stop}]$, can be described by:

$$\begin{aligned} \Delta_t s_i(t) = s_i(t) - s_i(t_{i,0}) &= \int_{t_{i,0}}^{t} v_i(t)dt \\ &= v_i(t_{i,0})t + \frac{1}{2}u_{ca}(t - t_{i,0})^2 - (u_{ca} - a_i(t_0))\tau(t - t_{i,0} + \tau e^{\frac{-(t-t_{i,0})}{\tau}} - \tau). \end{aligned} \tag{4.3}$$

Equations (4.2) and (4.3) describe the velocity and position profile for a vehicle which

starts emergency braking at $t_{i,0}$ until the moment of standstill $t_{i,stop}$. Of main interest for safety however, is an emergency braking maneuver from both the host and the preceding vehicle. For simplicity, the effects of sensor and communication delay are neglected, hence both vehicles initiate an emergency braking maneuver at $t_0 = t_{i-1,0} = t_{i,0}$. Note that an analysis with delay can be found in Appendix B.1. Both vehicles will be assumed to have equal characteristics, hence equal dynamics parameter τ and an equal lower bound acceleration $u_{ca} = -6\ m/s^2$. As a result, the final stopping distance for a two-vehicle emergency braking maneuver can be described by:

$$d_{i,stop} = \Delta_t s_{i-1}(t_{i-1,stop}) - \Delta_t s_i(t_{i,stop}) + d_i(t_0). \tag{4.4}$$

Equation (4.4) describes the final inter-vehicular distance after a two-vehicle emergency braking maneuver. Since equal dynamics are considered for both vehicles, $d_{i,stop}$ will coincide with the maneuver's smallest inter-vehicular distance in case $t_{i,stop} \geq t_{i-1,stop}$. In case $t_{i,stop} < t_{i-1,stop}$, then $v_{i-1}(t) > v_i(t)$ holds throughout the maneuver, making collision impossible since $s_{i-1}(t_0) > s_i(t_0)$. Using this analysis, the pursuit-evasion game approach will be considered to determine the states which describe D_m.

4.2.2 Two-vehicle pursuit-evasion game

In order to determine the critical region $D_m \subset \mathbb{R}^5$, the pursuit-evasion approach of [29] will be applied to evaluate the states $P = [d_i(t_0), v_i(t_0), \Delta v_i(t_0), a_i(t_0), a_{i-1}(t_0)]^T \in \mathcal{Y}_1$. This approach describes a problem with an evader, i.e. the host, and a pursuer, i.e. the preceding vehicle. From multiple combinations of initial conditions, the pursuer will attempt to cause an accident. Hence, this creates a worst-case scenario where the host should avoid collision. In case the host can prevent collision in this scenario, the host can also do this for more favorable scenarios.

Therefore, the objective is to determine if state $P = [d_i(t_0), v_i(t_0), \Delta v_i(t_0), a_i(t_0), a_{i-1}(t_0)]^T$ is safe. In order to limit the complexity of the resulting critical region D_m, only three of the states are varied and the rest of variables are fixed. Hence, D_m will be determined for constant $a_i(t_0)$ and $a_{i-1}(t_0)$. For this analysis, we evaluate the domain of $v_{i-1}, v_i \in [v_{min}, v_{max}]$, with $v_{min} = 0$ as the lower bound velocity and v_{max} the maximal velocity for automated operation. Note, these bounds will result in a less conservative set for D_m. It is assumed that the initial accelerations remain within the bounds of D_s, hence $a_i(t_0), a_{i-1}(t_0) \in [a_{min}, a_{max}]$. Hence in order to reduce complexity, $a_{i-1}(t_0) = a_{min}$ and $a_i(t_0) = a_{max}$ will be selected to follow the pursuit-evasion game approach. These initial conditions will be applied in evaluation of a grid of possible combinations for $v_i(t_0)$ and $\Delta v_i(t_0)$. Subsequently, D_m can be determined as a function of $d_i(t_0)$, $v_i(t_0)$ and $\Delta v_i(t_0)$, with $a_{i-1}(t_0) = a_{min}$, $a_i(t_0) = a_{max}$ and $u_{i-1} = u_i = u_{ca}$.

Table 4.2: Algorithm to determine the critical region D_m for given $a_i(t_0)$ and $a_{i-1}(t_0)$

Algorithm to determine all points $P = [d_i(t_0), v_i(t_0), \Delta v_i(t_0), a_{max}, a_{min}]^T \in D_m$
Input: parameters $u_{i-1} = u_i = u_{ca}$, a_{min}, a_{max}, d_{safe}, v_{min}, v_{max}
1. Set a grid of $v_i(t_0) \in [v_{min}, v_{max}]$
2. Set a grid of $\Delta v_i(t_0) = v_{i-1}(t_0) - v_i(t_0)$ and calculate corresponding $v_{i-1}(t_0)$ Remove all entries with $v_{i-1}(t_0) \notin [v_{min}, v_{max}]$
3. For each entry in the remaining 2D grid:
a. Set worst-case initial accelerations; $a_i(t_0) = a_{max}$, $a_{i-1}(t_0) = a_{min}$
b. Determine $t_{i-1,stop}$ and $t_{i,stop}$ using (4.2) and $v_{i-1}(t_{i-1,stop}) = v_i(t_{i,stop}) = 0$
c. Region D_m corresponds with a final stopping distance of $d_{i,stop} = d_{safe}$. Consequently, the initial distance can be calculated by rewriting (4.4): $d_i(t_0) = \Delta_t s_i(t_{i,stop}) - \Delta_t s_{i-1}(t_{i-1,stop}) + d_{safe}$
4. Remove the non-relevant entries for D_m, with $t_{i,stop} < t_{i-1,stop}$ and/or $d_i(t_0) < d_{safe}$
5. D_m is described by the resulting set of $v_i(t_0)$, $d_i(t_0)$ and $\Delta v_i(t_0)$

Table 4.2 shows an algorithm to determine D_m as a function of $d_i(t_0)$, $\Delta v_i(t_0)$, $v_i(t_0)$ domain for constant and given $a_i(t_0)$ and $a_{i-1}(t_0)$, assuming delay can be neglected. Consequently, using the algorithm of Table 4.2, D_m can be shown as a function of $d_i(t_0)$, $v_i(t_0)$ and $\Delta v_i(t_0)$, using colored lines in Figure 4.2.

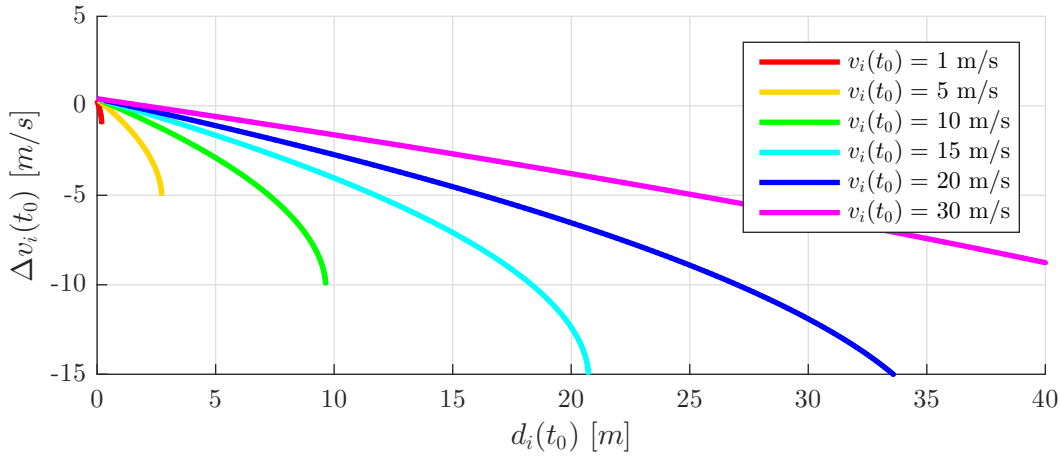

Figure 4.2: Critical region D_m for $a_i(t_0) = a_{max}$ and $a_{i-1}(t_0) = a_{min}$

Figure 4.2 shows the critical region D_m in the $(d_i(t_0), \Delta v_i(t_0))$ plane for various $v_i(t_0)$, given that $a_i(t_0) = a_{max} = 2\ m/s^2$ and $a_{i-1}(t_0) = a_{min} = -2\ m/s^2$. Additionally, $d_{safe} = 0\ m$ and $u_{ca} = -6\ m/s^2$ have been selected. Due to the selected values for $a_i(t_0)$ and $a_{i-1}(t_0)$, a small positive velocity difference is required to prevent collision at $d_i(t_0) = d_{safe} = 0$. The bottom ends of the colored lines coincide with $v_{i-1} = 0$, and therefore show the needed stopping distance for vehicle i. Regarding the required initial inter-vehicular distance $d_i(t_0)$, it can be seen that it reduces for smaller host vehicle velocities, and a reduced velocity

difference $\Delta v_i(t_0)$. Moving along one particular curve: for a given $v_i(t_0)$, it appears that for smaller $d_i(t_0)$, $\Delta v_i(t_0)$ needs to be smaller to (just) avoid a collision. Similarly for a higher $v_i(t_0)$, the initial conditions $d_i(t_0)$ or $\Delta v_i(t_0)$ will need to be more favorable. Hence, the required initial distance is highly dependent on the relative velocity $\Delta v_i(t_0)$ and the vehicle velocity $v_i(t_0)$.

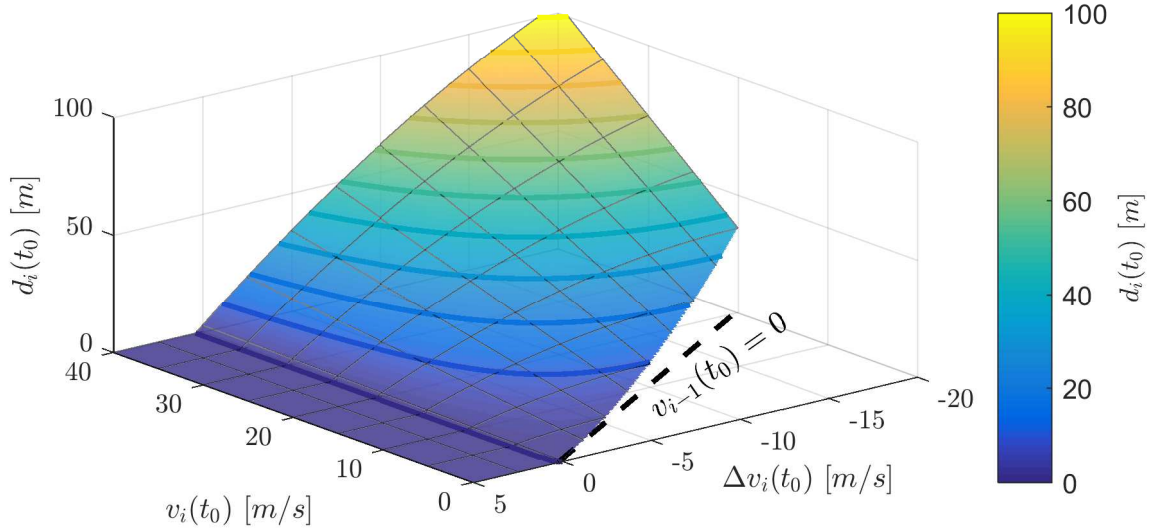

Figure 4.3: 3D plot of $D_m \subset \mathbb{R}^5$, for constant and given $a_i(t_0)$ and $a_{i-1}(t_0)$

Figure 4.3 shows the critical region D_m as a plane in the three dimensional space of $d_i(t_0)$, $v_i(t_0)$, $\Delta v_i(t_0)$, assuming $a_i(t_0) = a_{max}$ and $a_{i-1}(t_0) = a_{min}$. Note that the lines in Figure 4.2 describe the surface given in Figure 4.3. The colored horizontal lines are isoclines where an equal $d_i(t_0)$ is required. Figure 4.3 shows that the minimal inter-vehicular distance is mainly dependent on $\Delta v_i(t_0)$ although it additionally increases when combined with large $v_i(t_0)$. The area above the depicted plane, with larger $d_i(t_0)$, is the combined region of D_s and D_d. Below the plane, D_c is located, where collision avoidance cannot be guaranteed. Using this set D_m, a CA controller can be determined to ensure safety. For comparison however, the critical domain will first be described in the error domain, such that D_m can be related to the nominal controller.

4.2.3 Critical domain in an error description

In this subsection, the critical region $D_m \subset \mathcal{Y}_1$ of Subsection 4.2.2 will be transformed to an error domain description. Hence, next to the state space $\mathcal{Y}_1$, an additional state space $\mathcal{Y}_2$ will be defined, where both $\mathcal{Y}_1, \mathcal{Y}_2 \subset \mathbb{R}^5$. The states for $\mathcal{Y}_2$ are $e_{1,i}(t_0), e_{2,i}(t_0)$, $e_{3,i}(t_0)$ and two additional states. As a result, safety can be directly linked to states in the tracking error, which will enable the analysis of safety for the presented controllers of Section 3.3. By rewriting the error definition of (3.5) to $d_i(t_0) = d_{r,i}(t_0) + e_{1,i}(t_0)$, the stopping distance as in (4.4) can be rewritten:

$$d_{i,stop} = \Delta_t s_{i-1}(t_{i-1,stop}) - \Delta_t s_i(t_{i,stop}) + d_{r,i}(t_0) + e_{1,i}(t_0) \tag{4.5}$$

Equation (4.5) shows the inter-vehicular stopping distance as a function of $e_{1,i}(t_0)$. The objective is to find a description of D_m in $(e_{1,i}(t_0), e_{2,i}(t_0), e_{3,i}(t_0))$, using the pursuit-evasion game approach as in Section 4.2. Since $\mathcal{Y}_1 \subset \mathbb{R}^5$, two additional states are required. Due to the strong velocity dependency, the host velocity $v_i(t_0)$ will be considered. Similar to the previous analysis, a_{i-1} is proposed as the fifth state, resulting in the state space $\mathcal{Y}_2 \subset \mathbb{R}^5$, where $S = [e_{1,i}(t_0), e_{2,i}(t_0), e_{3,i}(t_0), v_i(t_0), a_{i-1}(t_0)]^T \in \mathcal{Y}_2$. Hence, a description should be found to describe $\mathcal{Y}_2$ as a function of $\mathcal{Y}_1$. When again selecting $u_{i-1}(t), u_i(t) = u_{ca}$ for the scenario in $t > t_0$, and assuming $u_i(t_0) = a_i(t_0)$ and $a_{i-1}(t_0) = a_{min}$, the error states of (3.6) can be rewritten to:

$$\begin{pmatrix} e_{1,i}(t_0) \\ e_{2,i}(t_0) \\ e_{3,i}(t_0) \end{pmatrix} = \begin{pmatrix} d_i(t_0) - d_{r,i}(t_0) \\ v_{i-1}(t_0) - v_i(t_0) - h a_i(t_0) \\ a_{i-1}(t_0) + \frac{h-\tau}{\tau} a_i(t_0) - \frac{h}{\tau} u_i(t_0) \end{pmatrix} \approx \begin{pmatrix} d_i(t_0) - r - h v_i(t_0) \\ \Delta v_i(t_0) - h a_i(t_0) \\ a_{min} - a_i(t_0) \end{pmatrix}, \tag{4.6}$$

where $2 \leq i \leq m$. Using (4.6) and assuming that the set of possible $d_i(t_0)$, $v_i(t_0)$, $\Delta v_i(t_0)$, $a_i(t_0)$ is known, we can determine $e_{1,i}(t_0), e_{2,i}(t_0)$, and $e_{3,i}(t_0)$. The initial state $a_{i-1}(t_0) = a_{min}$ is assumed in order to obtain the worst-case initial condition, as stated before. However, contrary to Section 4.2, the actual $a_i(t_0)$ needs to be included in the analysis. Additionally, the dependence of the error states on the headway parameters r and h for (3.2) can be noted. Therefore, the resulting critical region $D_m^* \subset \mathcal{Y}_2$, is unequal to $D_m \subset \mathcal{Y}_1$, and will be denoted with an extra superscript. Using (4.6), an algorithm can be derived to determine $D_m^* \subset \mathcal{Y}_2$, where $S = [e_{1,i}(t_0), e_{2,i}(t_0), e_{3,i}(t_0), v_i(t_0), a_{i-1}(t_0)]^T \in \mathcal{Y}_2$:

Table 4.3: Algorithm to determine the critical region $D_m^* \subset \mathcal{Y}_2$ for given $a_{i-1}(t_0)$

Algorithm to determine all points $S = [e_{1,i}(t_0), e_{2,i}(t_0), e_{3,i}(t_0), v_i(t_0), a_{min}]^T \in D_m^*$
Input: parameters u_{ca}, a_{min}, a_{max}, d_{safe}, v_{min}, v_{max} , h, r
1. Set a grid of $v_i(t_0) \in [v_{min}, v_{max}]$
2. Set a grid of $a_i(t_0) \in [a_{min}, a_{max}]$, set $a_{i-1}(t_0) = a_{min}$ and $u_i(t_0) = a_i(t_0)$ Determine corresponding grid $e_{3,i}(t_0)$
3. Set a grid of $\Delta v_i(t_0) = v_{i-1}(t_0) - v_i(t_0)$ and calculate the corresponding $v_{i-1}(t_0)$
a. Remove all entries with $v_{i-1}(t_0) \notin [v_{min}, v_{max}]$
b. Determine corresponding grid $e_{2,i}(t_0)$
4. For each entry in the remaining $v_i(t_0)$, $e_{3,i}(t_0)$, $e_{2,i}(t_0)$ grid:
a. Set $u_{i-1}(t), u_i(t) = u_{ca}$ for $t > t_0$, and determine $t_{i-1,stop}$ and $t_{i,stop}$ using (4.2), knowing that $v_{i-1}(t_{i-1,stop}) = v_i(t_{i,stop}) = 0$
b. Calculate the corresponding initial distance if $d_{i,stop} = d_{safe}$, using (4.4): $d_i(t_0) = \Delta_t s_i(t_{i,stop}) - \Delta_t s_{i-1}(t_{i-1,stop}) + d_{safe}$
5. Remove all non-relevant entries with $t_{i,stop} < t_{i-1,stop}$ or $d_i(t_0) < d_{safe}$
6. Determine corresponding minimal initial position errors: $e_{1,i}(t_0) = d_i(t_0) - r_i - h v_i(t_0)$
7. D_m^* is described by the resulting set of $v_i(t_0)$, $e_{1,i}(t_0), e_{2,i}(t_0)$, $e_{3,i}(t_0)$ and $a_{i-1}(t_0)$

The algorithm of Table 4.3 results in a plane in the $e_{1,i}(t_0), e_{2,i}(t_0)$, and $v_i(t_0)$ space for every $e_{3,i}(t_0)$, assuming $a_{i-1}(t_0) = a_{min} = u_{min}$. The resulting $D_m^* \subset \mathcal{Y}_2$ can be visualized in the $(e_{1,i}(t_0), e_{2,i}(t_0)$ plane for various $v_i(t_0)$ and $e_{3,i}(t_0))$, and given $a_{i-1}(t_0)$:

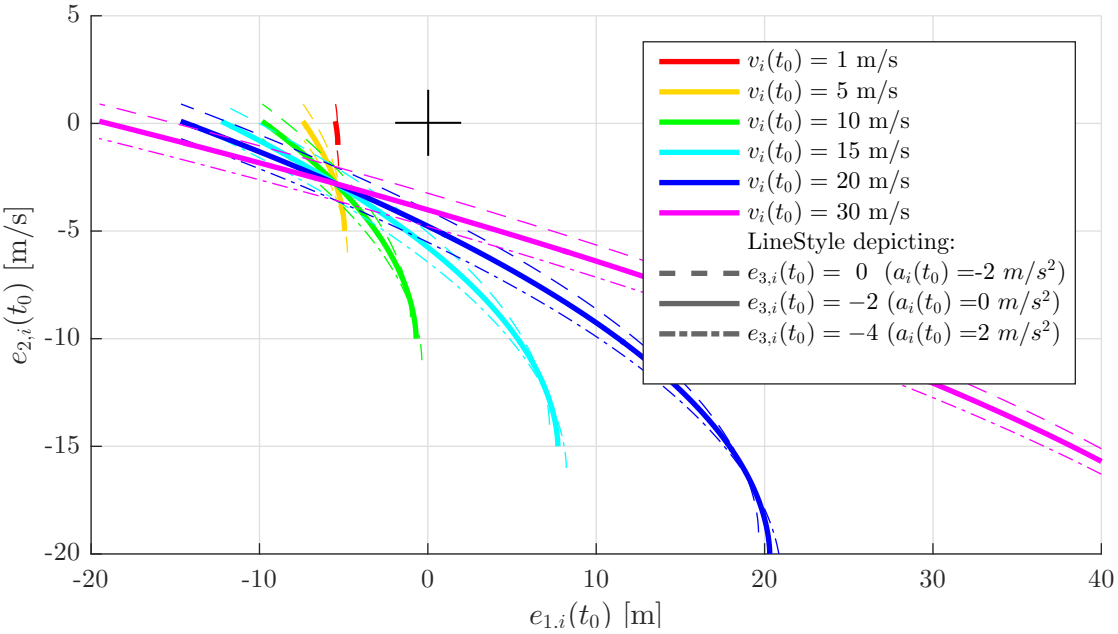

Figure 4.4: Critical region $D_m^* \subset \mathcal{Y}_2$ for $d_{safe} = 0\ m$, $r = 5\ m$ and $h = 0.5\ s$

Figure 4.4 shows the critical region $D_m^* \subset \mathcal{Y}_2$ for $a_{i-1}(t_0) = a_{min}$, determined by application of the algorithm in Table 4.3. Herein the headway parameters $r = 5\ m$ and $h = 0.5\ s$ have been chosen. When reviewing Figure 4.4 using (3.2) and (3.5), it can be noted that the left tops of the colored lines coincide with $e_{1,i}(t_0) = -d_{r,i}(t_0) + d_{safe}$ and hence $d_i(t_0) = 0$. It can be additionally noted that the lines in Figure 4.2 are comparable to the dash-dotted lines for $a_i(t_0) = 2\ m/s^2$ in Figure 4.4. Herein, the lines for each $v_i(t_0)$ have equal initial condition in Figure 4.2 as the dash-dotted lines in Figure 4.4. However, in Figure 4.4 the lines are shifted to the left by $d_{r,i}$ since $e_{1,i} = d_i - d_{r,i}$. Similarly, since $e_{2,i} = \Delta v_i - h a_i$, the lines are shifted up with $-h a_i$. Due to this effect, it is important to evaluate the full set of possible initial accelerations for vehicle i in order to determine $D_m^* \subset \mathcal{Y}_2$.

In Figure 4.4, nearly all the lines have a common cross point, which shifts as a function of $e_{3,i}(t_0)$. For constant $a_{i-1}(t_0)$, there exists a unique collection of $(e_{1,i}(t_0), e_{2,i}(t_0), e_{3,i}(t_0))$ which can be found in D_m^* for any $v_i(t_0) > 0$, with

$$e_{1,i}(t_0) = d_i(t_0) - d_{r,i}(t_0) = \Delta_t s_{i-1}(t_{i-1,stop}) - \Delta_t s_i(t_{i,stop}) + d_{safe} - r - h v_i(t_0), \quad (4.7)$$

$$e_{2,i}(t_0) = \Delta v_i(t_0) - h a_i(t_0). \quad (4.8)$$

In order to examine this cross point, an analysis will be conducted by neglecting the acceleration dynamics, using a constant acceleration. Hence for both vehicles, $a_i(t) = u_{ca}$ for $t \in (t_0, t_{i,stop}]$ is assumed. Application of this assumption in (4.2) and rewriting yields:

$$t_{i,stop} - t_0 \approx \frac{v_i(t_0)}{u_{ca}}. \tag{4.9}$$

As an additional result of this assumption, the relative velocity will be constant during the maneuver: $\Delta v_i(t) = \Delta v_i(t_0)$ for time $t \in [t_0, t_{i-1,stop}]$. When considering (4.8), it can be noted that $\Delta v_i(t_0)$ is equal for all lines of a certain $a_i(t_0)$. Using (4.3), the term $\Delta_t s_{i-1}(t_{i-1,stop}) - \Delta_t s_i(t_{i,stop})$ in (4.7) can be rewritten as:

$$\begin{aligned} \Delta_t s_{i-1}(t_{i-1,stop}) - \Delta_t s_i(t_{i,stop}) &= \int_{t_{i,0}}^{t_{i-1,stop}} v_{i-1}(t)dt - \int_{t_{i,0}}^{t_{i,stop}} v_i(t)dt, \\ &\approx \Delta v_i(t_0)(t_{i-1,stop} - t_0) + \frac{1}{2}\Delta v_i(t_0)(t_{i,stop} - t_{i-1,stop}). \end{aligned} \tag{4.10}$$

Substitution and rewriting of (4.9) in (4.10), for i and $i-1$, results in

$$\Delta_t s_{i-1}(t_{i-1,stop}) - \Delta_t s_i(t_{i,stop}) \approx \Delta v_i(t_0)\left(\frac{v_i(t_0)}{u_{ca}} + \frac{v_{i-1}(t_0) - v_i(t_0)}{2u_{ca}}\right), \tag{4.11}$$

such that substitution and rewriting of (4.11) into (4.7) yields:

$$e_{1,i}(t_0) \approx v_i(t_0)\left(\frac{\Delta v_i(t_0)}{u_{ca}} - h\right) + \frac{\Delta v_i(t_0)^2}{2u_{ca}} + d_{safe} - r, \tag{4.12}$$

Since the cross point is not velocity dependent, the first term between brackets in (4.12) is zero, hence $\Delta v_i(t_0) = h u_{ca}$. As a result, the coinciding points of D_m^* as visualized in Figure 4.4 can be approximated by:

$$e_{1,i}(t_0) \approx d_{safe} - r + \frac{1}{2}h^2 u_{ca}, \tag{4.13}$$

$$e_{2,i}(t_0) \approx h\left(u_{ca} - a_i(t_0)\right), \tag{4.14}$$

which shows that for any initial velocity $v_i(t_0)$, there exists a unique collection of $\{e_{1,i}(t_0), e_{2,i}(t_0), e_{3,i}(t_0)\}$ for a selected $a_{i-1}(t_0)$; in other words, all curves for equal $e_{3,i}(t_0)$ in Figure 4.4 have a common intersection point assuming an equal $a_{i-1}(t_0)$. For the settings as used in Figure 4.4, this will result in a cross point at $(e_{1,i}, e_{2,i}) = (-5.75, -3)$ for $a_i(t_0) = 0 \rightarrow e_{3,i}(t_0) = -2m/s^2$, which is approximately correct. Note however, due to the constant acceleration assumption, the results of this analysis are not exact. In conclusion, the critical domain D_m^* has now been extensively described and elaborated. When regarding safety however, it is important to have a controller that ensures collision avoidance. Therefore, a CA controller will be introduced in the next section.

4.3 Collision avoidance controller

In this section a collision avoidance controller will be developed using the critical domain as found in Section 4.2. This CA controller will operate in addition to the platooning controller, and should only be activated in case of emergencies. Hence, the suggested controller can operate separately from the nominal controller. Therefore, the result of Section 4.2 can be used to determine a stopping distance tolerance using $D_m \subset \mathcal{Y}_1$. Next,

a CA controller will be introduced which applies a certain braking level depending on the estimated stopping distance.

For this analysis, it is assumed that all states for $P = [d_i(t_0), v_i(t_0), \Delta v_i(t_0), a_i(t_0), a_{i-1}(t_0)]^T \in \mathcal{Y}_1$ are known, measurement errors are assumed negligible. Using this state information, the stopping distance can be calculated for a two-vehicle emergency braking maneuver initiated at time t, using (4.4). The stopping distance tolerance $d_{i,tol}(t)$ is now defined by:

$$d_{i,tol}(t) := d_{i,stop}\Big(d_i(t), v_i(t), a_i(t), v_{i-1}(t), a_{i-1}(t)\Big) - d_{safe}. \tag{4.15}$$

Using (4.15), it can easily be derived that a collision can be avoided for all initial states with $d_{i,tol}(t) \geq 0$. Since full braking is only desired when really necessary, the CA controller will only be activated when $d_{i,tol}(t) \leq d_{ca}$, with $d_{ca} > 0$ typically a small positive distance. For collision avoidance controller design, an APF is introduced by:

$$\Psi_{ca}(z_i(t)) = \begin{cases} 0 & z_i(t) \geq 0, \\ \frac{1}{3} z_i(t)^3 u_{ca} & z_i(t) < 0, \end{cases} \tag{4.16}$$

With:

$$z_i(t) = \frac{d_{i,tol}(t) - d_{ca}}{d_{ca}}. \tag{4.17}$$

Note, the CA controller should not be subject to the spacing policy correction as stated in (3.8). As a result, the CA control input can be introduced by:

$$u^*_{ca}(t) = \frac{\partial \Psi_{ca}(z_i(t))}{\partial z_i} \tag{4.18}$$

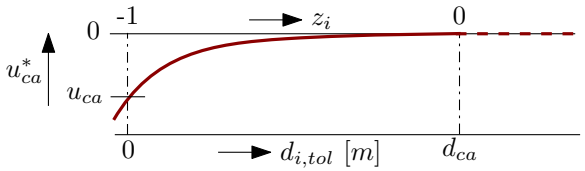

Figure 4.5: CA functionality using stopping distance estimate

Next, the CA functionality can be combined with the nominal controller (3.8) by:

$$u^*_i(t) = \begin{cases} u_i(x_{1,i}(t), u_{i-1}(t)) & d_{i,tol}(t) > d_{ca}, \\ min(u^*_{ca}(t), u_i(x_{1,i}(t), u_{i-1}(t))) & d_{i,tol}(t) \leq d_{ca}, \end{cases} \tag{4.19}$$

with $u^*_i(t)$ the control input with included CA functionality. In the domain of $d_{i,tol} \leq d_{ca}$, the CA controller (4.19) will only be selected in case it requires a lower acceleration than the nominal controller. This strategy is selected since it is desired to limit the chance and severity of an intervention from CA. Although the collision avoidance controller uses the full state information, all suggested controllers only operate as a function of $(e_{1,i}, e_{2,i})$. Therefore, the influence of the CA controller within the $(e_{1,i}, e_{2,i})$ plane will be evaluated in the next section.

4.4 Limits of nominal operation

In the previous sections, the critical region $D_m^* \subset \mathcal{Y}_2$ has been elaborated and a CA controller has been determined. However, the performance of the nominal controller with respect to safety has not been investigated. In this section, safety and comfort aspects of the nominal controller will be investigated, for a range of r and h for headway (3.2).

Next, a saturated controller is introduced for purposes of analysis, to ensure the assumption of $a_i \in [a_{min}, a_{max}]$ can be validated when assuming zero feedforward. Using Lyapunov's theorem [35], global asymptotic stability can be proven for a $APFx$ controlled vehicle. Using this theorem and the critical region D_m^*, the safe operation region D_s can be determined. For region D_s, safety and convexity will be proven for when $a_{i-1}(t) \in [a_{min}, a_{max}]$. Herein, the comfort acceleration limits for D_s, $u_i \in [u_{min}, u_{max}]$ will be taken into account, assuming zero feedforward. As a result, safe and smooth behavior can be guaranteed for the nominal controller when in region D_s.

4.4.1 Transition to the critical domain

In this section the critical domain will be related to the nominal controller. For analysis purposes, no feedforward control is assumed. Next, consider the case where the nominal controller already implements the desired CA setpoint when necessary. Hence, when

$$\bar{u}_i(e_{1,i}(t_0), e_{2,i}(t_0)) \leq u_{ca} \quad \forall \quad S \in D_m^* \cup D_c \subset \mathbb{R}^5, \tag{4.20}$$

with $S = [e_{1,i}(t_0), e_{2,i}(t_0), e_{3,i}(t_0), v_i(t_0), a_{i_1}(t_0)]^T$. As a result, CA functionality can be guaranteed by the nominal controller when assuming $u_i \approx \bar{u}_i$, thereby neglecting the influence of the inverse spacing policy dynamics of (3.8). A suitable combination of settings to satisfy (4.20) is for instance $r = 15\ m$ and $h = 0.5\ s$ for (3.2), with $c = 5$ for controller (3.23) and Ψ_A such that $\bar{u}_i(x_{1,i} = -10) = u_{ca}$. The resulting effect of requirement (4.20) is visualized in Figure 4.6.

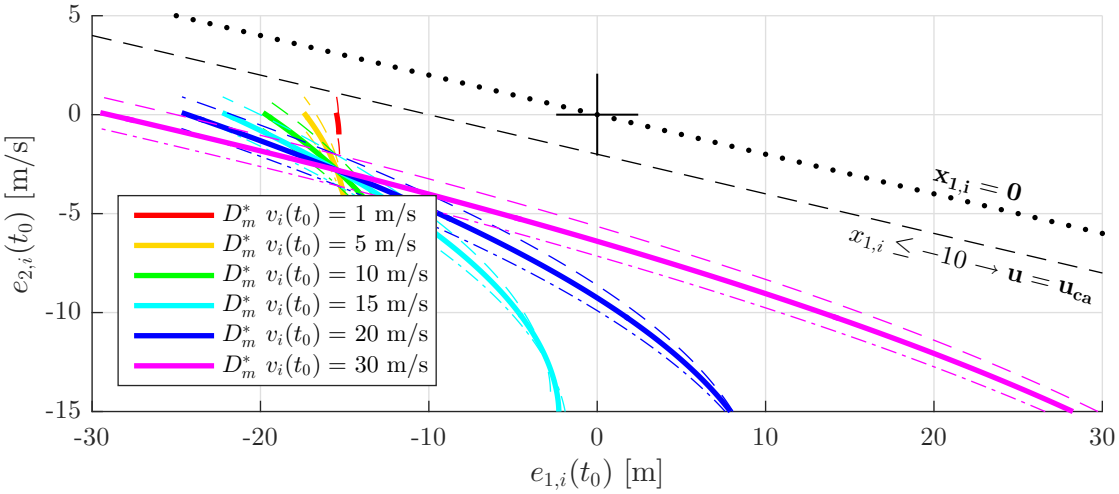

Figure 4.6: CA using the nominal controller, for $d_{safe} = 0\ m$, $r = 15\ m$ and $h = 0.5\ s$

From this figure it can be concluded that collision will be avoided, since $\bar{u}_i \leq u_{ca}$ for $x_{1,i}(t_0) \leq -10$, and all other states with $x_{1,i}(t_0) = e_{1,i}(t_0) + ce_{2,i}(t_0) > -10$ are not included in $S = [e_{1,i}(t_0), e_{2,i}(t_0), *, *, *]^T \in D_m^*$. However, with $r = 15\ m$, this is a rather undesirable solution. In case r is reduced, D_m^* will come closer to the line $x_{1,i} = 0$, such that the CA controller will be required to ensure safety. As can be seen in Figure 4.6, the lower host velocities are mainly critical, since these coincide with the smallest magnitude of $x_{1,i}$. Therefore, two notions are introduced, thereafter further elaborated, with the objective to enable smaller $d_{r,i}$ without compromising comfort when in nominal operation:

1. For any intervention from the CA controller (4.18), $\bar{u}_i \leq u_{min}$ must hold for the nominal controller (3.23). It is assumed there exists a $x_c \in \mathbb{R}$ such that $\bar{u}_i(x_{1,i} = x_c, u_{i-1} = 0) = u_{min}$ for controller (3.23).
2. A minimal velocity $v_i(t) > v_{min}$ can be assumed for nominal operation, limiting the evaluated critical domain D_m^*.

When regarding point 1, it can be derived that with controller (3.23) as depicted in Figure 3.3, that $x_c \approx -4.7$ for $u_{min} = a_{min} = -2\ m/s^2$. In case $\bar{u}_i \leq u_{min}$ can be warranted before intervention of CA, the nominal controller will always implement a reasonable braking level in an attempt to prevent intervention of CA. For point 2, a derivation has been performed in Appendix B.2 to quantify the critical states of D_m^*. By assuming $a_i(t) \approx u_i(t) \approx u_{min}$ and $\Delta v_i(t) \leq 0$, a minimal velocity can be calculated to ensure $\bar{u}_i \leq u_{min}$ before intervention of CA:

$$v_i \geq v_{min} = -cu_{min} + \frac{1}{h}\left(d_{safe} - r - x_c + c\Delta v_i\right), \tag{4.21}$$

as derived in Appendix B.2. Application of (4.21) results in $v_i \geq v_{min} = 11.4\ m/s$, derived using parameters $c = 5$, $r = 5\ m$, $h = 0.5\ s$, $d_{safe} = 1\ m$, and $x_c = -4.71\ m$. For instance when considering $h = 0.3\ s$, then $v_{min} = 12.4\ m/s$ will be found as a result. By combining the two points, a new critical domain can be introduced as:

$$\hat{D}_m^* = \{ \quad S = [e_{1,i}(t_0), e_{2,i}(t_0), e_{3,i}(t_0), v_i(t_0), a_{i_1}(t_0)]^T \in D_m^* \quad | \quad v_i(t_0) \geq v_{min} \quad \}. \tag{4.22}$$

When assuming a minimal velocity $v_i(t) \geq v_{min}$ for normal operation, only $\hat{D}_m^*$ has to be considered and $\bar{u}_i \leq u_{min}$ can be ensured before intervention of CA. In case $v_i(t_0) < v_{min}$, $\bar{u}_i \leq u_{min}$ cannot be guaranteed before activation of CA, and an additional controller may be required to ensure a smooth and safe deceleration profile. Note however, $v_i(t_0) \geq 12.4\ m/s$ is a reasonable assumption for highway maneuvering at the small inter-vehicular distance of $r = 5\ m$ and $h = 0.3\ s$.

4.4.2 Saturation for comfort purposes

In this subsection, the acceleration limitation for the safe nominal operation domain is considered. For purposes of analysis, a saturated controller will be developed to investigate the safe operation region. When in this region D_s, as mentioned in Section 4.1, it is desired not to exceed the acceleration comfort bounds, realized by limiting $u_i \in [u_{min}, u_{max}]$. When reviewing (4.21) and Figure 4.4, one should note that $a_i(t_0)$ and u_{min} cannot be too low

since this shifts D_m^*. Hence to ensure $a_i(t_0), u_i(t_0) \geq u_{min}$, a saturated version of the *APFx* controller (3.23) is introduced, described by:

$$\bar{u}_i = \begin{cases} u_{min} & x_{1,i} \leq x_c, \\ \frac{\partial \Psi(x_{1,i})}{\partial x_{1,i}} & x_{1,i} > x_c, \end{cases} \qquad 2 \leq i \leq m, \tag{4.23}$$

with $x_c \leq 0$ and assuming zero feedforward. Note, in order to achieve this, the repulsive potential (3.16) can easily be adapted to ensure saturation:

$$\Psi_{RPsat}(x_{1,i}) = \begin{cases} k_1 x_c^4 - k_2 x_c^3 + k_3 x_c^2 + u_{min}(x_{1,i} - x_c) & x_{1,i} < x_c, \\ k_1 x_{1,i}^4 - k_2 x_{1,i}^3 + k_3 x_{1,i}^2 & x_c \leq x_{1,i} \leq 0, \\ 0 & x_{1,i} > 0, \quad 2 \leq i \leq m. \end{cases} \tag{4.24}$$

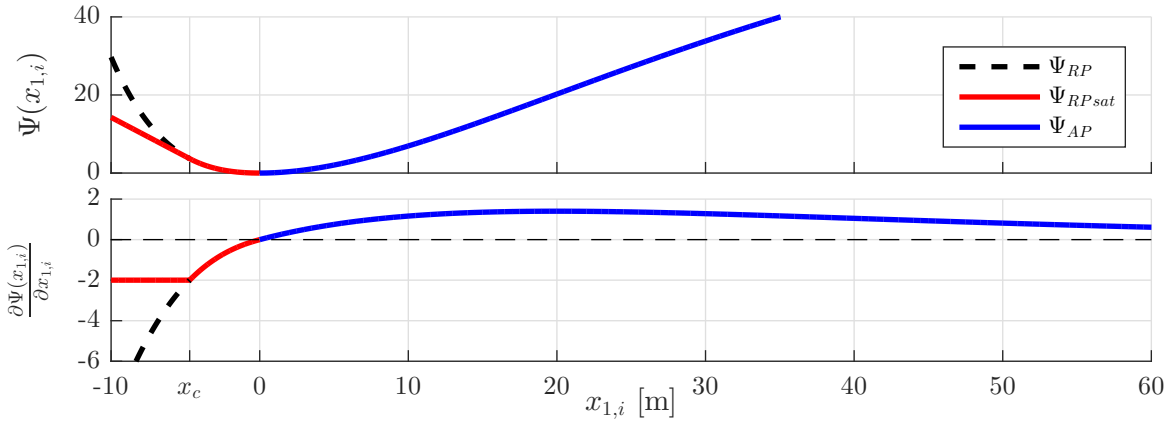

Figure 4.7: Controller (4.23) in comparison to unsaturated controller (3.23)

The resulting APF using (4.24) is shown in Figure 4.7. Since it is assumed that the attractive potential function (3.17) is designed such that $\bar{u}_i(t) \leq u_{max}$, only the saturation on braking has to be considered. As a result, the *APFx* controller (3.23) can be saturated using APF design

$$\Psi_{Asat} = \Psi_{RPsat} + \Psi_{AP}, \tag{4.25}$$

instead of (3.15). Using controller (3.23) with APF (4.25), the assumption of $u_i \in [u_{min}, u_{max}]$ is validated when assuming zero feedforward. Next, region D_s can be derived, when additionally accounting for actuator saturation.

4.4.3 Region of safe operation

In this section, Lyapunov's theorem [35] is used to derive the safe nominal operation region D_s. In this analysis, the saturated input function as defined in (4.23) will be used, hence using $\Psi_{Asat}(x_{1,i})$ such that $\bar{u}_i(t) \in [u_{min}, u_{max}] = [a_{min}, a_{max}]$. In Appendix C, a global asymptotic stability analysis has been conducted. There, the Lyapunov function has been introduced as:

$$V(\mathbf{x}_i) = \Psi(x_{1,i}) + \begin{bmatrix} x_{2,i} & x_{3,i} \end{bmatrix} \begin{bmatrix} b_1 & b_2 \\ b_3 & b_4 \end{bmatrix} \begin{bmatrix} x_{2,i} \\ x_{3,i} \end{bmatrix}, \tag{4.26}$$

using error notation (3.21). For (4.26), the time derivative $\dot{V} \leq 0$ can be proven for $c > \tau$ in combination with a valid APF function. For a valid APF function, hence a continuously differentiable potential function satisfying criteria (3.12), (3.13) and (C.1), global asymptotic stability is proven in Appendix C.

In [35], a theory is introduced to determine a set of initial conditions from which the system will converge to its equilibrium. The first condition of this theorem is $\dot{V}(\mathbf{x}_i) \leq 0 \; \forall \; \mathbf{x}_i \in \Omega$, with Ω as all possible combinations of $\mathbf{x}_i$. Using (3.21), it can be derived that $\mathbf{e}_i = [e_{1,i}, e_{2,i}, e_{3,i}]^T = [x_{1,i} - cx_{2,i}, x_{2,i}, x_{3,i}]^T$. Therefore this first condition can be rewritten to:

$$\dot{V}(\mathbf{x}_i) \leq 0 \; \forall \; S = [e_{1,i}, e_{2,i}, e_{3,i}, *, *]^T \in \mathcal{Y}_2 \subset \mathbb{R}^5. \tag{4.27}$$

Where the $'*'$ can be any arbitrary value. Due to (4.27), the Lyapunov function value cannot increase in time. Therefore, if the Lyapunov function value is lower than the minimal value on the edge of D_s, the solution is guaranteed not to escape set D_s. As a result, $D_s \subset \mathbb{R}^5$ can be described by:

$$D_s = \{ \quad V(\mathbf{x}_i(t_0)) < V_{crit} \quad | \quad S = [e_{1,i}(t_0), e_{2,i}(t_0), e_{3,i}(t_0), *, *]^T \in \mathcal{Y}_2 \subset \mathbb{R}^5 \quad \}, \tag{4.28}$$

valid for all $v_i(t_0) > v_{min}$ and assuming $a_{i-1}(t_0) = a_{min}$. In (4.28), V_{crit} is a critical Lyapunov function value that should not be exceeded. In order to derive V_{crit}, consider the desired properties of D_s with respect to the other domains of operation. Although D_s neighbors D_d, the safe area should preferably be as large as possible. Therefore, this region will be limited by a single intersection with $\hat{D}_m^*$. Hence, V_{crit} can be obtained by:

$$V_{crit} = min\left(V(\mathbf{x}_i)\right), \quad \forall \quad S = [e_{1,i}(t_0), e_{2,i}(t_0), e_{3,i}(t_0), *, *]^T \in \hat{D}_m^* \subset \mathbb{R}^5. \tag{4.29}$$

using (3.21) to determine $\mathbf{x}_i$. As a result of (4.28) and (4.29), the region D_s can be determined. Herein, acceleration saturation can be accounted for by using (4.25) and (3.23), which limits $\bar{u}_i \in [u_{min}, u_{max}]$ when assuming no feedforward. As a result, the control input will therefore not pass the acceleration saturation limit required for D_s. Hence, in case $V(x_i(t_0)) < V_{crit}$, $a_{i-1}(t) \in [a_{min}, a_{max}]$ and $v_i(t) > v_{min}$, the solution will remain in D_s. Therefore, point $\mathbf{x}_i(t_0)$ is a safe initial situation.

Using (4.28), a set of initial conditions and range of parameters can be derived, for which safety can be guaranteed without the need of a CA controller. However, this domain is dependent on multiple parameters and not easily determined. Therefore, a set of safe states will be derived for a conservative set of parameters, using the following algorithm:

Table 4.4: Algorithm to determine safe set D_s

Algorithm: Determine safe set D_s
Input: parameters u_{ca}, d_{safe}
Input: limits for $h \in (h_{min}, h_{max})$, $c \in (c_{min}, c_{max})$, and limits r_{min} and v_{max}

1. Choose and optimize other parameters:
- Limits for $a_i \in (a_{min}, a_{max}) = (u_{min}, u_{max})$
- Design $\Psi(x_{1,i})$, determine x_c
- set $h = h_{min}$ if $d_{safe} - r_{min} - x_c \geq 0$, else $h = h_{max}$ (see Appendix B.2)
- Determine v_{min} using (4.21):
  $v_{min} = -c_{max} u_{min} + \frac{1}{h}(d_{safe} - r_{min} - x_c)$
- Check suitability of parameter set v_{min}, $x_c < 0$ and h, otherwise adapt settings and repeat previous steps

2. Determine Critical region $\hat{D}_m^*$ using the algorithm as found in Table 4.3, for r_{min}, v_{min}, h, c_{max} and $a_{i-1}(t_0) = u_{min}$, etc.

3. Determine V_{crit} using (4.29)

4. Verify steps 2, 3 separately for c_{min}, possibly adapt the following settings: increase c_{min}, r_{min}, u_{min}, u_{ca} and/or h_{min}, or decrease v_{max} and/or d_{safe}

5. Determine set D_s using (4.28)

Table 4.4 shows an algorithm to determine the safe set with respect to the initial parameters. Note that determining D_s is not arbitrary, since one should account for the full range of parameters. Additionally, note that the safe region D_s can increase significantly in size when assuming higher velocities for nominal operation. However, the result can be used to create a look-up table or likewise for implementation. The resulting safe set can also be visualized in the error domain as shown in Figure 4.8.

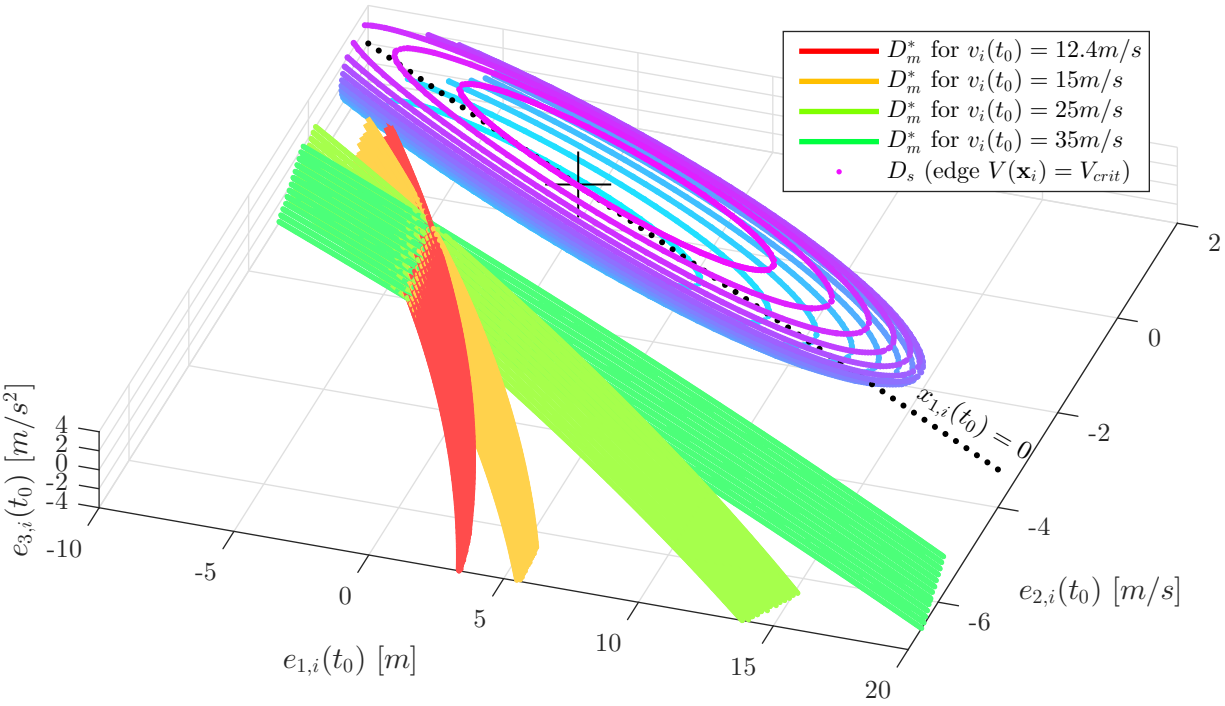

Figure 4.8: Regions $\hat{D}_m^*$ and D_s for $v_{min} = 12.4\,m/s$, $r = 5\,m$, $h = 0.3\,s$ and $a_{i-1}(t_0) = a_{min}$

Figure 4.8 shows the edges of D_s as determined by (4.28), and the critical region $\hat{D}_m^* \subset \mathcal{Y}_2$ for various velocities and $a_{i-1}(t_0) = a_{min}$. The safe region D_s is situated within the blue to purple ovals, for settings $u_{min} = 2\ m/s^2$, $h_{min} = 0.3\ s$, $r_{min} = 5\ m$, $d_{safe} = 1\ m$, and $c = 5$. The red surface depicts $\hat{D}_m^*$ for $v_{min} = 12.4\ m/s$. As expected and desirable, the domains D_s and D_m^* do not cross each other. They only intersect at one point, as determined by (4.29). Note that region D_d is situated between D_s and D_m^*, although this region will not be further elaborated.

Figure 4.8 shows a reasonably large domain for D_s, wherein the system can operate with guaranteed safety. Additionally however, it should be noted that this domain is highly dependent on the design parameters, since region D_s increases in size for higher velocities, and decreases for lower u_{min}. In Figure 4.8, it can additionally be noted that the resulting region D_s can be considered slightly conservative. Consider for example the state $(e_{1,i}(t_0), e_{2,i}(t_0)) = (12, 0)$, situated at the right top section of Figure 4.8. Since this initial state is more favorable for safety than most other points in D_s, and the subsequent path is highly likely to intersect D_s, this state is probably also safe. However, a theoretical analysis may be required to support this statement. When considering the safe region D_s for the chosen parameters, the region D_s covers a reasonable region for maneuvering. Therefore, this controller can safely be used for highway maneuvering.

4.5 Simulation and verification

In this section, the results of the previous sections will be verified in simulation, in the absence of feedforward and delay. Hence, the CA controller (4.19) will be evaluated, which should ensure safety using a smooth acceleration set point. Additionally of interest, is the set point of the nominal controller at CA activation. In Subsection 4.2.3, the desire has been stated that $u = u_{min}$ should be ensured by the nominal controller, previous to activation of CA.

For the simulation analysis, a model has been implemented in Matlab Simulink. The CA controller (4.18) is combined with the nominal $APFx$ controller using (4.19). The $APFx$ controller is saturated for purposes of analysis, using (4.23) and u_{min}, u_{max} as -2 and $2\ m/s^2$ respectively. The parameters $d_{safe} = 0.25\ m$ and $d_{ca} = 3\ m$ have been selected for (4.18) and $h = 0.3\ s$, $r = 5\ m$ and $c = 5$ for (3.2) and (3.21).

Since $a_{i-1}(t)$ is not known real-time, the worst case initial acceleration $a_{i-1}(t_0) = u_{ca} = -6\ m/s^2$ will be considered for $D_m^* \subset \mathcal{Y}_2$. Since the host acceleration can be accurately determined, the actual acceleration $a_i(t_0) = a_i(t)$ will be used to determine the error (3.6) for $\mathcal{Y}_2(t_0) = (e_{1,i}(t_0), e_{2,i}(t_0), e_{3,i}(t_0), v_i(t_0), a_{i-1}(t_0))$. However, one should note that due to the stricter initial condition $a_{i-1}(t_0) = u_{ca}$, and due to $d_{ca} = 3\ m$, the CA controller will intervene slightly faster than with $a_{i-1}(t_0) = u_{min}$. For the presented parameters, an emergency braking maneuver is shown for a platoon of six vehicles in Figure 4.9.

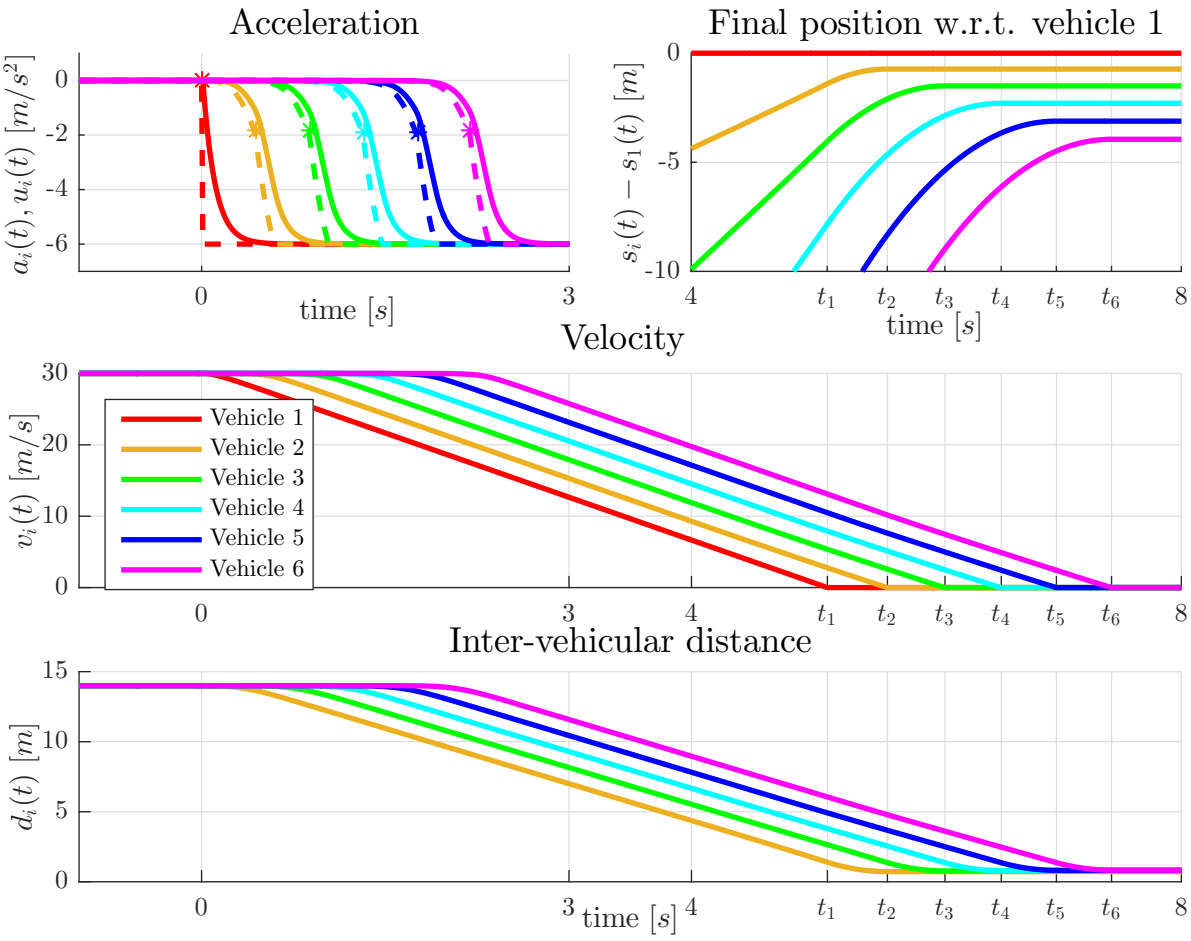

Figure 4.9: Time simulations of a platoon emergency braking maneuver

In Figure 4.9, the intended acceleration levels are shown with dashed lines, with an asterisk indicating the last point at which the nominal controller is still in control, for each vehicle. Vehicle 1 starts braking at $t = 0$, and has reached a full stop at $t_1 = 5.11\ s$. The stopping times t_i for vehicles $i = 2, 3, .., 6$ are indicated on the time axis.

Initially, all vehicles are platooning at a steady 30 m/s. As vehicle 1 decelerates, vehicle 2 initially starts slowing down gradually. After only 0.44 s, with $a_2(t) = -1.10\ m/s^2$, $u_2(t) = -1.83\ m/^s$, $d_2(t) = 13.65\ m$, $\Delta v_i(t) = -1.88\ m/s$, and $v_i = 29.9\ m/s$, the CA from vehicle 2 intervenes with $u_2(t) = -2.05\ m/s^2$. The CA control action quickly increases, up to full braking at $t = 0.6\ s$, resulting in a final stopping distance of $d_2(t_2) = 0.725\ m > d_{safe}$.

The CA controller has provided smooth collision avoidance for vehicle 2. Although the nominal controller had provided $\bar{u}_i(t) = -2\ m/s^2$ for each vehicle previous to activation of CA, the effect of the spacing policy correction (3.8) has limited the intended acceleration to $u_2(t) = -1.83\ m/s^2$. This has been expected due to the limitation of $\bar{u}_i(t) \geq -2\ m/s^2$, which will not be implemented in practice.

During full braking, $\Delta v_i(t) = v_{i-1}(t) - v_i(t) \approx -2.61\ m/s^2$ for all vehicles. The CA controller of vehicle 3 intervenes at $t = 0.88\ s$, with $a_3(t) = -1.14\ m/s^2$, resulting in $d_3(t_3) = 0.77\ m$. The acceleration profile of vehicle 3 is slightly smoother than for vehicle 2, which is due to the slightly more gradual acceleration profile of vehicle 2, with respect to vehicle 1. The normal controller and the velocity dependent headway $d_{r,i}(t)$ provide the damping effect herein. With all inter-vehicular stopping distances between $0.725 \leq d_i(t_i) \leq 0.83\ m$ and $d_{safe} = 0.25\ m$, the CA controller has provided safety. The final inter-vehicular distances are slightly higher than d_{safe}, which is probably due to the numerical implementation using a look-up table, along with the more strict assumption $a_{i-1}(t_0) = u_{ca}$ for initialization of CA.

4.6 Summary

In this chapter, longitudinal safety has been examined, by dividing the state space for operation into multiple domains. The emphasis has been placed on the critical region and the safe region, where the critical region requires an emergency braking action to ensure safety, whereas the safety is ensured in the safe region by the nominal controller. The critical region has been determined using a pursuit-evasion game approach in Subsection 4.2.2, evaluating safety for the most severe use-case scenario.

In order to asses the safety properties of the nominal controller, which is a function of the distance error and its first derivative, the critical region has additionally been rewritten as a function of $e_{1,i}(t_0), e_{2,i}(t_0), e_{3,i}(t_0), v_i(t_0)$ and $a_{i-1}(t_0)$ in Subsection 4.2.3. As a result, the critical region has been linked to the nominal controller. Analysis of the critical region in Subsection 4.4.1 has shown that safety can only be guaranteed by the nominal controller for relatively large time headway settings.

A further reduction of the inter-vehicular distance is enabled by introduction of a CA controller in Section 4.3. Using simulations, Section 4.5 has shown that safety can be warranted in combination with a smooth intended acceleration profile. For purposes of analysis, a saturated controller is introduced in Subsection 4.4.2. Preceding to the intervention of CA, a minimal deceleration set-point can be promised; $\bar{u}_i(t_0) \leq -2\ m/s^2$, when assuming a minimal velocity $v_i(t_0) \geq v_{min}$. Note, when not saturating the nominal controller, the CA controller can intervene even later, or not at all.

In Section 4.4, the safe domain has been determined using Lyapunov's theorem and the saturated *APFx* controller as determined by (3.23) and (4.25). The nominal controller, with the possible addition of a CA controller, has shown that comfortable and safe maneuvering can be warranted for a large set of initial conditions. Hence, the longitudinal safety has been evaluated for platooning and maneuvering purposes. Using this analysis, the next chapter will introduce an approach for safe maneuvering with respect to vehicles on a neighboring lane.

5: Cooperative merging

In this chapter, the longitudinal control for performing a cooperative merging maneuver will be considered, hence involving vehicles on a neighboring lane. As discussed in Section 2.5, an autonomous vehicle should be able to perform cooperative merging maneuvers on a public road. In Subsection 5.1.1, the relevant vehicles surrounding a vehicle on the highway will be classified. Hereafter, the interaction protocol will be introduced, including an approach to handle merging maneuvers for two platoons. Individually, a vehicle should therefore be able to merge into another lane and to make a gap for another vehicle. In Subsection 5.2.1, an APF-based method will be introduced to handle multiple objectives without compromising safety. Hereafter, an approach is introduced to adapt the controller according to each stage of the maneuver, while additionally ensuring smooth and safe maneuvering. At the end of this chapter, simulations will be presented for purposes of illustration.

5.1 Environment perception and interaction

In this section, the interaction requirements for maneuvering will be introduced. Assuming each autonomous vehicle has advanced object tracking capabilities, the required vehicle classification system will be introduced first. Next, the interaction protocol will be stated for the cooperative merging of two platoons. Hereafter, the individual tasks and requirements for each vehicle can be stated using this interaction protocol. Hence, this section will present the interaction requirements for vehicles in a merging maneuver.

5.1.1 Vehicle classification

In order to be able to perceive the environment, a vehicle can be equipped with multiple sensors. For cooperative driving, the wireless communication is required to share the vehicle intentions. However, it cannot be assumed that all vehicles are always able to communicate. By using additional on-board sensors, a vehicle should be able to reliably perceive and track all relevant objects in its surroundings. In this project, an object tracking mechanism is considered where each vehicle can track up to six objects, referred to as "Most Important Objects (MIO's)."

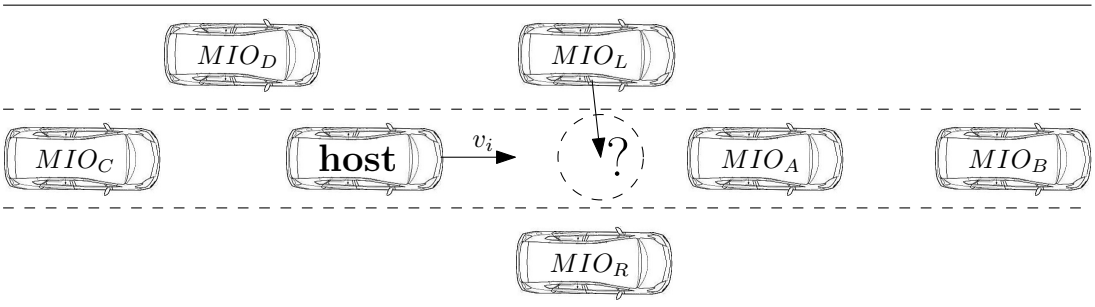

Figure 5.1: Most Important Objects (MIO) detected and tracked on a multi-lane road

Figure 5.1 illustrates the possible MIO's with respect to the host vehicle. The MIO's are longitudinally either in front of or behind the host vehicle, classified using the position of the rear axle. These MIO's are defined as MIO_A: closest vehicle in front on the same lane, MIO_B: second closest vehicle in front on the same lane, MIO_C: first vehicle behind the host on the same lane, MIO_L: first vehicle in front on the left adjacent lane, MIO_R: first vehicle in front on the right adjacent lane and MIO_D: first and most relevant vehicle in back on either of the adjacent lanes. Note, for MIO_L, MIO_R and MIO_D, the vehicles are only tracked in case they are longitudinally situated between MIO_A and MIO_C. The relevance of MIO_D is mainly determined by proximity, in combination with anticipated maneuvers such as merging or splitting. In case a vehicle is situated before MIO_A or behind MIO_C, this vehicle is not of direct interest for maneuvering. Next, an interaction protocol will be introduced for the merging of two platoons.

5.1.2 Merging interaction protocol

In this section, the required interaction for a merging scenario will be further elaborated. Since a merging scenario can involve a large number of vehicles, the general approach will first be introduced, thereafter the scenario will be broken down in sets of three vehicles. For a general merging scenario, the interaction protocol as defined in [15] is considered. In general, a Merge Request (MR) can be issued by each vehicle that wishes to merge in a platoon. Hereafter, a gap needs to be created for each vehicle requesting to merge. Each merge request should eventually be followed by a Safe To Merge (STOM) message from the gap making vehicle, indicating it is safe to complete the maneuver. This procedure, also in case of merging of two platoons, is explained in [15] and will be further discussed in this section. Consider a merging scenario of two platoons, where the platoon on lane $j+1$ wishes to merge with the platoon on the neighboring lane j. Such a platoon merging scenario can be summarized in four stages, as shown in Figure 5.2.

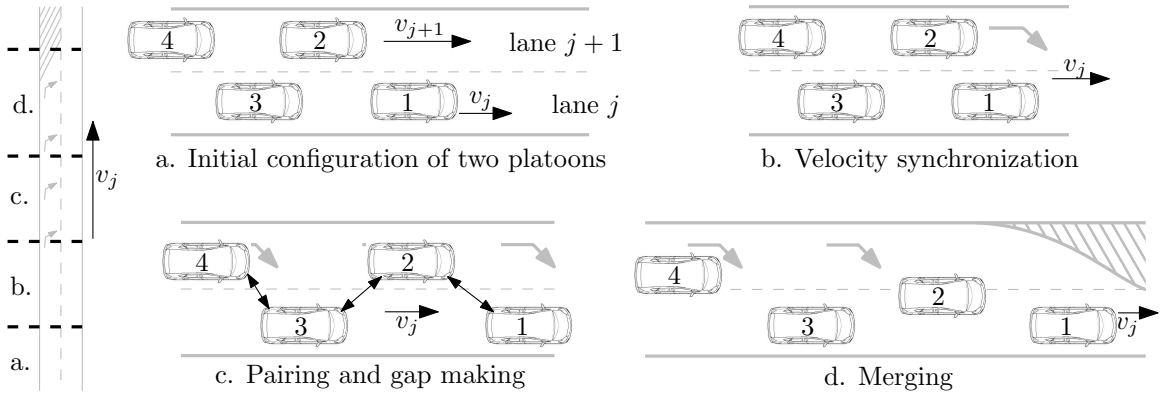

Figure 5.2: Execution stages for merging of two platoons

This figure illustrates a merging scenario for four vehicles. Herein, two platoons are driving next to each other, where only the right lane remains available further ahead. Hence, the

platoon on the closed lane, i.e. the left lane, has to merge into the platoon on the right lane. In accordance with the protocol in [15], the velocity has to be synchronized between the two platoons, illustrated by Figure 5.2.b. Subsequently, the merging pairs are determined, where a vehicle can have a forward and/or a backward pair. These pairs determine the following order of the vehicles in the final platoon, and allow the appropriate gaps to be created in step c. In Figure 5.2, vehicle 2 will have vehicle 1 as forward pair, and have vehicle 3 as backward pair. The next step is gap making, which is preferably initiated in a gradual sequence from the front to the back of the vehicle string, such that the braking level at the back of the platoons can be limited to some extent [15].

When regarding a two-platoon merging scenario, the scenario can be broken down in triplets, as for example the triplet of vehicles $1, 2, 3$ in Figure 5.2. For simplicity, the vehicles in a triplet will be indicated by $M1, M2, M3$. Hence, a general triplet consist of the lead vehicle $M1$, the merging vehicle $M2$, and the gap making vehicle $M3$, which need to be determined in accordance with the established pairing.

In addition, some vehicles might have shared roles in different triplets, for instance vehicle $M3$ might have a forward pair in one triplet, and an additional backward pair in another one. For an additional simplification of the triplets, vehicle $M2$ will always be merging from the neighboring left lane $j + 1$. Note that this can easily be mirrored for application on other scenarios. As a result, a general triplet can be described by:

vehicle $M1$	Vehicle on lane j, i.e. the rightmost lane,
vehicle $M2$	Vehicle on lane $(j + 1)$, sends a MR to enter lane j between $M1$ and $M3$,
vehicle $M3$	Vehicle on lane j, drives directly behind $M1$, responsible for generating STOM,

hence with $M1, M2, M3$ as the order of the newly created platoon. When reviewing Figure 5.2, the triplet $(1, 2, 3)$ will have priority in merging before any consecutive triplets. During the maneuver, vehicle 2 will have vehicle 1 as forward pair, and vehicle 3 as backward pair. Here, vehicle 3 should make an appropriate gap with respect to vehicle 1, allowing the forward pair, vehicle 2, to merge. For simplicity, assume $(M1, M2, M3)$ can be denoted as vehicles $(1, 2, 3)$. For this set of three appropriately determined vehicles, the longitudinal position errors for platooning are denoted as:

$$e_{1,21} = d_{21} - d_{r,2} = s_1 - s_2 - L_2 - d_{r,2}, \tag{5.1}$$

$$e_{1,32} = d_{32} - d_{r,3} = s_2 - s_3 - L_3 - d_{r,3}, \tag{5.2}$$

$$e_{1,31} = d_{31} - d_{r,3} = s_1 - s_3 - L_3 - d_{r,3}. \tag{5.3}$$

In (5.1)–(5.3), the last number in the subscripts of the errors denote the target vehicle instead of assuming a comparison with the predecessor as in (3.6). Hence, note that for $(i, k) = (2, 1), (3, 2), (3, 1)$ individually, the error dynamics of $\mathbf{e}_{ik} = [e_{1,ik}\ e_{2,ik}\ e_{3,ik}]^T$ can be denoted by (3.9). Equivalently, $\mathbf{x}_{ik}$ can be determined using $\mathbf{e}_{ik}$ and (3.21).

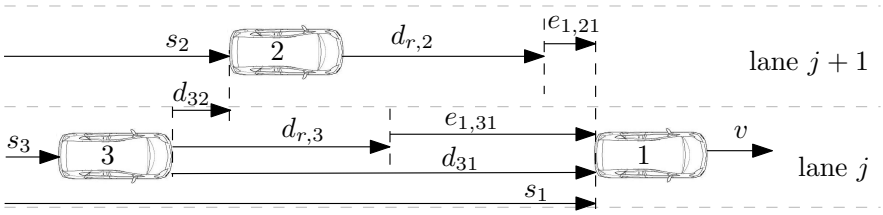

Figure 5.3: General triplet for a merging scenario where vehicle 2 issues a MR

Figure 5.3 shows the triplet $(1, 2, 3)$, with position errors and inter-vehicular distances. With platoon $(1, 2, 3)$ as the final objective, it can be noted that $e_{1,21}, e_{1,32} \to 0$ is desired. For vehicle 3, $e_{1,31} \geq 0$ will be desirable for safety. Regarding a triplet, it can easily be derived that the pairing is correct in case:

$$s_3 \leq s_2 \leq s_1, \tag{5.4}$$

when assuming the velocity is appropriately synchronized. Otherwise, vehicle 2 will be part of a different triplet. After the MR from vehicle 2, the pairing is therefore confirms the intended maneuver and participants. Next, vehicle 3 should start making a gap, allowing vehicle 2 to merge. The triplet should thereby create an appropriate longitudinal formation, such that the merge can be completed as soon as both vehicles 3 and 2 have a sufficient longitudinal headway with respect to their forward pairs:

$$d_{21}(t) \geq \alpha d_{r,2}(t), \tag{5.5}$$
$$d_{32}(t) \geq \alpha d_{r,3}(t). \tag{5.6}$$

with $\alpha \in [0\ 1)$ as a scaling factor. Rewriting equations (5.5) and (5.6) using (5.1) and (5.2), results in the error requirement

$$e_{1,21}(t) \geq (\alpha - 1) d_{r,2}(t) = e_{1,2STOM}(t), \tag{5.7}$$
$$e_{1,32}(t) \geq (\alpha - 1) d_{r,3}(t) = e_{1,3STOM}(t), \tag{5.8}$$

with $e_{1,2STOM}(t), e_{1,3STOM}(t) < 0$ as the lower bound position errors, indicating when it is considered safe to merge. When assuming the velocity differences are appropriately small, α should be chosen such that safe and smooth maneuvering can be ensured, without blocking or delaying a merge for reasonable scenarios. The minimal value for α should be derived from the safety analysis in Chapter 4. Using the safe domain D_s as in (4.28), a lateral merge can only be safely executed in case longitudinal safety can be warranted for vehicles 2 and 3 with respect to the forward pair:

$$[e_{1,32}, e_{2,32}, e_{3,32}, v_3, a_2]^T, [e_{1,21}, e_{2,21}, e_{3,21}, v_2, a_1]^T \in D_s. \tag{5.9}$$

For simplicity, it is assumed that parameter α is appropriately determined, such that (5.9) is satisfied for all use cases. Since vehicle 3 cannot check condition (5.7) directly, an additional criterion is used for the purpose of redundancy with respect to the perception of vehicle 2. Hence before sending a STOM, vehicle 3 will additionally check if

$$d_{31} \geq \alpha \left(d_{r,3} + d_{r,2} \right) + L_2, \tag{5.10}$$

as follows from (5.5) and (5.6). Since vehicle 3 can send the STOM whenever appropriate, vehicle 3 can warrant smooth and comfortable driving as vehicle 2 changes lane. After completion of the merging maneuver, the vehicles switch to platooning in the new formation. Using this protocol, a vehicle controller can be introduced to incorporate safe and smooth gap making and merging functionality.

When considering Figure 5.2, it can be noted that triplets can still be found where either vehicle $M1$ or $M3$ is absent, as is the case for the set $(M1, M2, M3) = (3, 4, -)$. Since the gap making vehicle is missing in this example, a MR is not required, the gap is already present, and a STOM cannot be received. As a result, all actions or criteria linked to vehicle $M3$ can be discarded in this analysis, resulting in a simplified interaction protocol.

5.2 Control design for maneuvering

In the previous section, a general protocol for merging has been introduced and broken down for a simplified analysis of sets of three vehicles. In this section, a longitudinal control approach for merging will be considered from a vehicle perspective. As has become clear from the previous section, a gap making vehicle, $M3$, needs to maneuver with respect to MIO_L while ensuring safety with respect to MIO_A. Similarly, the merging vehicle $M2$ needs to maneuver with respect to its MIO_R while ensuring safety with a MIO_A, if available. Therefore, the scenario for $M2$ and $M3$ is comparable. As a result, the control design for the gap making vehicle, i.e. $M3$, will be further described. Similar analysis applies to vehicles being in the $M2$ position.

5.2.1 A multi-objective problem formulation

In this subsection, a general approach will be introduced to combine multiple objectives into a final control design using APF theory. When having various objectives, multiple artificial potential functions can be determined to ensure each objective, as discussed in Section 2.3. With respect to both control objectives, APF functions are designed in accordance with the general APF requirements (3.13) and (3.12), to ensure each maneuvering objective. Hence, the objectives for vehicle $M3$ with respect to $M1$ and $M2$ are a function of (5.2) and (5.3) respectively. These objectives can be combined to a final APF using addition:

$$\Psi_3(e_{1,32}, e_{1,31}) = \Psi_{32}(e_{1,32}) + \Psi_{31}(e_{1,31}). \tag{5.11}$$

However, in case multiple potential functions are active, there should always be one unique final objective. Hence, the combined potential function controlling the host, i.e. $\Psi_3(e_{1,32}, e_{1,31})$ for vehicle $M3$, should be convex with a minimum coinciding with a final objective. Preferably, this minimum can be determined by choice, such that it is independent of parameters. Note that this requirement is not specifically necessary, for instance gap making has been investigated without such a requirement [24]. However, as can also be concluded from [24], a dependency of the equilibrium on initial settings

can cause non-smooth behavior. Since the resulting desired inter-vehicular distance becomes dependent on parameters, safety can also be compromised. Therefore, the individual objectives cannot inherently be guaranteed, resulting in complex and undesirable requirements on the APF functions.

Therefore, the combined APF function $\Psi_3(e_{1,32}, e_{1,31})$ must satisfy equivalent requirements as in (3.13) and (3.12). Hence, there can only be a single point minimum of a convex APF function, such that the desired equilibrium is attractive. Hence for both comfort, safety and simplicity, the various active APF functions should never contradict each other, guaranteeing a combined single minimum without compromising the individual objectives. Therefore, the repulsive and attractive components can be decoupled, as can already be found in Ψ_A of (3.15). The attractive and repulsive APF components should then be selectively activated or deactivated to ensure $\Psi_3(e_{1,32}, e_{1,31})$ satisfies requirements (3.13) and (3.12) as a function of a combined input $(e_{1,32}, e_{1,31})$. To ensure all individual APF functions do not contradict, all simultaneously active APF components should have a partial derivative of the same sign. Consider vehicle i, having n_i APF components. For any two component APF functions, with respect to objects $k, l \in n_i$, the following criterion has to hold:

$$\begin{aligned} &sign\left(\frac{\partial \Psi_{ik}(e_{1,ik}(t))}{\partial e_{1,ik}(t)}\right) = sign\left(\frac{\partial \Psi_{il}(e_{1,il}(t))}{\partial e_{1,il}(t)}\right) \\ \forall \quad &\frac{\partial \Psi_{ik}(e_{1,ik}(t))}{\partial e_{1,ik}(t)}, \frac{\partial \Psi_{il}(e_{1,il}(t))}{\partial e_{1,il}(t)} \neq 0, \qquad k, l \in n_i, \quad i \in m, \end{aligned} \tag{5.12}$$

with for the gap making example $i = 3$, $k = 1$, $l = 2$ and $n_i = 2$. Requirement (5.12) describes that all nonzero, active, state-dependent APF partial derivatives for vehicle i, need to have an equal sign. Since the sign of this function is directly related to an acceleration or deceleration request, (5.12) states that two potential functions $\Psi_k(e_{1,ik})$ and $\Psi_l(e_{1,il})$ cannot request an acceleration and a deceleration request at the same moment in time, requiring consensus for all active components. Requirement (5.12) must hold for all m hosts individually, and their n_i potential function components. Therefore, an advanced supervisory controller should be applied, which switches the active APF functions according to each situation.

For simplicity, the inputs of the APF functions will be denoted using the position error, although one should note that $e_{1,32}$ and $e_{1,21}$ can be substituted for $x_{1,32}$, $x_{1,21}$ respectively. To further elaborate on this concept, the merging scenario will be investigated. After the velocity synchronization and pairing steps, a gap making action should be performed. This is elaborated in the following subsection.

5.2.2 Gap making controller

For automated driving, gap making and merging is a desirable functionality. In either positions $M3$ or $M2$, the host must eventually maneuver towards a safe distance with respect to its forward pair, since this forward pair is expected to become the new MIO_A

as soon as the merging is completed. For simplicity, the scenario is described from the perspective of $M3$, although the result will be analogues for vehicle $M2$.

Assume the host is initially platooning with its current MIO_A, i.e. vehicle $M1$. When the host receives a MR from its MIO_L, i.e. vehicle $M2$, the host's longitudinal set-point changes. A new objective is thereby created; to maneuver towards a safe distance with respect to the MIO_L, i.e. vehicle $M2$, and additionally requiring safety with respect to the current MIO_A, i.e. vehicle $M1$. Hence, a new potential function Ψ_M should be created for merging, with $\Psi_M(e_{1,32} = 0) = 0$ as the only minimum point on a convex multi-objective potential function. In order to satisfy (5.12), the APF-CACC attractive potential (3.17) with respect to MIO_A needs to be turned off. Meanwhile, the repulsive potential (3.16) is still required to guarantee safety with respect to the MIO_A, i.e. vehicle $M1$. This results in the combined potential function:

$$\Psi_M(e_{1,31}, e_{1,32}) = \Psi_{RP}(e_{1,31}) + \Psi_L(e_{1,32}). \tag{5.13}$$

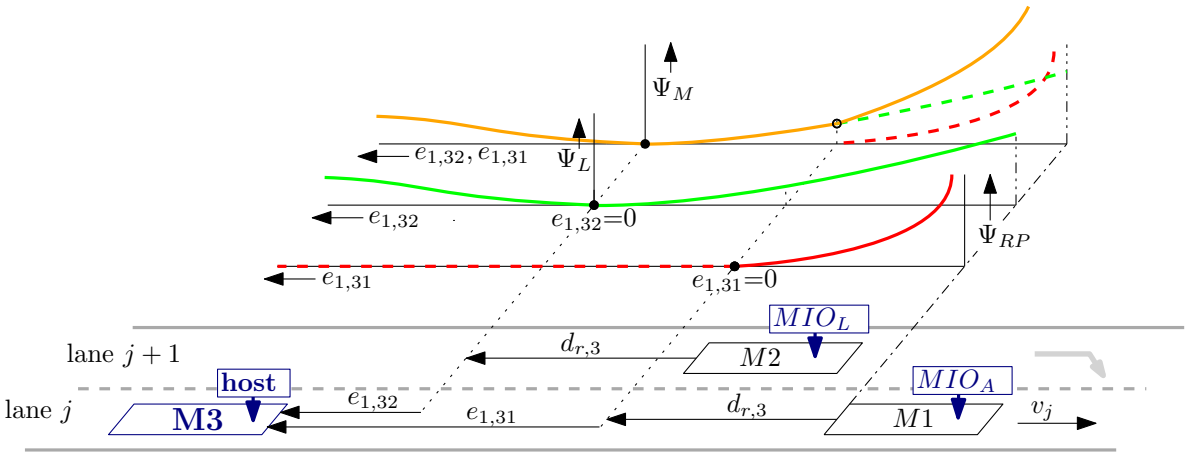

Figure 5.4: APF components determining Ψ_M (orange) during gap making

Figure 5.4 illustrates the potential functions with respect to both vehicles, during gap making. In the illustration, the longitudinal distance between $M3$ and $M2$ is already larger then required, which is generally not the case. In (5.13), $\Psi_L(e_{1,32})$ is dependent on the state of 2. This potential $\Psi_L(e_{1,32})$ can be chosen freely, with an emphasis on comfort and smooth behavior. However, Ψ_L should still meet requirement (3.13) with $\Psi_L(e_{1,32} = 0) = 0$. Meanwhile, the repulsive potential with respect to MIO_A, vehicle 1, must ensure collision and proximity avoidance, such that the safety analysis of Chapter 4 remains applicable. Since the two component potential functions have two different objectives, (5.12) should be verified for all feasible combinations of $e_{1,31}, e_{2,32} \in \mathbb{R}$. Application of criterion (5.12) to (5.13) results in the requirement that $e_{1,32} \leq 0$ should hold if $e_{1,31} < 0$. When rewriting requirement (5.4), it can be concluded that this requirement on $e_{1,32}$ is satisfied during gap making:

$$\begin{aligned} s_2 &\leq s_1, \\ e_{1,32} + s_3 + L_3 + d_{r,3} &\leq e_{1,31} + s_3 + L_{M3} + d_{r,3}, \\ e_{1,32} &\leq e_{1,31}. \end{aligned} \tag{5.14}$$

Since (5.14) is always satisfied, requirement (5.12) is satisfied for (5.13).

However, for this thesis, the controller *APFx* as in (3.23) will be applied, with the alternative error description $\mathbf{x}_{32}$ and $\mathbf{x}_{31}$ of (3.21). Hence, the control input for gap making will be determined using the APF:

$$\Psi_M(x_{1,31}, x_{1,32}) = \Psi_{RP}(x_{1,31}) + \Psi_L(x_{1,32}), \tag{5.15}$$

Hence, the resulting control input for gap making is determined by:

$$\bar{u}_3 = \frac{\partial \Psi_{RP}(x_{1,31})}{\partial x_{1,31}} + \frac{\partial \Psi_L(x_{1,32})}{\partial x_{1,32}} + u_{3ff}, \tag{5.16}$$

With u_{iff} for $i = 3$ as the feedforward signal, which will be assumed equal to zero for now. When using (5.15) and (5.16), requirement (5.12) should also be satisfied. Since the *APFx* controller includes a damping into the APF input, the requirement for a valid MR should be adapted to include the velocity, as an alternative or additional requirement to (5.4). Therefore, $s_3 + cv_3 \leq s_2 + cv_2 \leq s_1 + cv_1$ is suggested, which equals (5.4) in case all vehicle velocities are equal. Rewriting of this requirement yields:

$$\begin{aligned} s_2 + cv_2 &\leq s_1 + cv_1, \\ s_2 + c(v_2 - v_3 - ha_3) &\leq s_1 + c(v_1 - v_3 - ha_3), \\ e_{1,32} + ce_{2,32} &\leq e_{1,31} + ce_{2,31}, \\ x_{1,32} &\leq x_{1,31}, \end{aligned} \tag{5.17}$$

satisfying requirement (5.12). Although (5.17) is slightly more demanding, it is a logical requirement for use-case scenarios, since it includes the velocity difference into the requirement for a merge request. Since velocity synchronization is one of the first steps for merging, as noted in [15], the velocity differences will be rather small during these maneuvers. Therefore, (5.17) is a reasonable and highly comparable condition with respect to MR position requirement (5.4). The criteria for safe use of this gap making approach are within the use-case situations. A supervisory controller will be required to ensure meeting this criterion, or to abort or pause the gap making procedure otherwise.

5.2.3 Merge completion

The gap making procedure of Subsection 5.2.2 is initiated by a merge request from a vehicle intending to merge. In this subsection, the transition from gap making to APF-CACC will be discussed. Herein, a safe and smooth transition is desirable. For both the APF-CACC controller (3.23), as for the gap making controller (5.16), longitudinal safety with respect to the current MIO_A, i.e. $M1$, can be guaranteed within D_s. Hence, the switch from (3.23) to (5.16) can be smoothly introduced. However, for merge completion the MIO_A flag will switch, to a vehicle with a smaller inter-vehicular distance. After sending the STOM,

vehicle $M2$ can cut-in at any moment. As soon as this cut-in is detected, the MIO_A flag switches from vehicle $M1$ to vehicle $M2$, and the APF-CACC platooning mode should be reinstated.

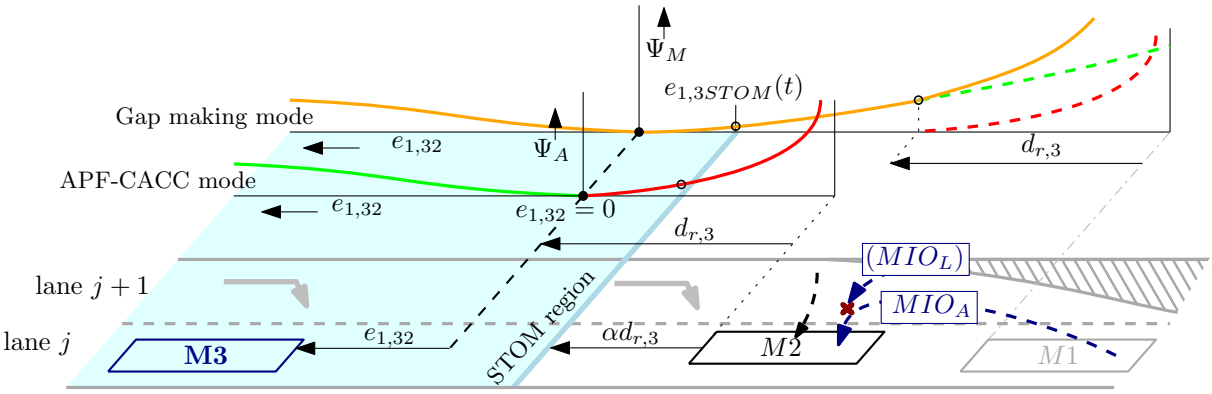

Figure 5.5: STOM situation and the artificial potential functions

Figure 5.5 illustrates the transition for 2 from MIO_L to MIO_A, and the resulting change in potential function for $M3$. Since $e_{1,31} \gg e_{1,32}$ at merging due to (5.10), a smooth transition in acceleration set-point can be achieved by adapting Ψ_L:

$$\Psi_L(e_{1,32}) \approx \Psi_A(e_{1,32}), \qquad e_{1,32} \geq e_{1,3STOM}. \tag{5.18}$$

However, one should note that this is not desirable for the full range of $e_{1,32}$. In case vehicle $M2$ is very close to $M3$, a large negative value for $e_{1,32}$ will be found. In case of platooning, hard braking is required for safety. For gap making however, this realistic scenario only requires subtle braking, since $M2$ is not on lane j. In order to improve comfort during gap making, the gap making APF component Ψ_L is adapted using (3.17) and (4.24) such that it cannot request an acceleration outside of the comfort bounds:

$$\Psi_L = \Psi_{AP} + \Psi_{RPsat}. \tag{5.19}$$

In Figure 5.4 and Figure 5.5, this effect is illustrated by the limited slope of the green and orange lines with respect to the slope of the red line. With controller (5.16) and using (4.24) and (5.19), requirement (5.18) can be satisfied by selecting $e_{1,3STOM}$ such that $x_{1,32}(t) \geq x_c$ when $e_{1,32}(t) \geq e_{1,3STOM}$ for all use-case scenarios. As a result, smooth behavior at a cut-in can be warranted, up to scenarios where $x_{1,32} \geq x_c$ for controller (5.16). In order to further elaborate this control approach, the performance will be analyzed using simulation.

5.3 Simulation analysis

In this section, the presented maneuvering controller of Section 5.2 will be tested in a simulation setup for merging of two platoons, as described in Subsection 5.1.2. Similar to 3.5, the TNO CACC simulation model will be used since it provides a realistic simulation environment. This model includes a realistic 2D world model, sensor, actuator and target tracking models, and MIO classification algorithms. Therefore, this simulation should provide a realistic result.

However, the position error will first be noted in a perception perspective, as defined in Subsection 5.1.1. Hence, the notation $e_{1,ik}$ will be applied for simulation, where i indicates number of the host, and k is either A, L or R, indicating the MIO_A, MIO_L or MIO_R status of the object with respect to the host. Hence, initially $e_{3A}(t_0) = e_{31}(t_0)$ and $e_{3L}(t_0) = e_{32}(t_0)$. However, as the merge is being completed, the MIO status of vehicle $M2$ can change, resulting in $e_{3A}(t) = e_{32}(t)$. As a result, this notation will allow an insight in the influence of perception on the performance of the controller.

In simulation, a merging scenario of four vehicles will be evaluated, as shown in Figure 5.2, with $v_1(t) = 60\ km/h$. The initial position $s_2(t_0) = s_3(t_0) + 0.4(s_1(t_0) - s_3(t_0))$ is selected, with $e_{1,2A}(t_0) = e_{1,4A}(t_0) = 0$, $v_i(t_0) = v_1(t_0)$ and $a_i(t_0) = 0$ for $i = 2, 3, 4$.

For the platooning controller (3.23), equal settings for K are selected for (3.15)–(3.17) throughout the report, as depicted in Figure 3.3. The spacing policy settings of $h = 0.5\ s$, $r = 5\ m$ and $c = 5$ are selected for (3.2) and (3.5). For gap making, (5.19) is selected with $u_{min} = -1.5\ m/s^2$. In the model, a blend function is applied at initialization of gap making in order to prevent a step in the longitudinal acceleration set-point.

Another important aspect for practical implementation is the feedforward signal, since a vehicle may have both a MIO_A as well as an MIO_L/MIO_R during gap making, resulting in two feedforward signals. In previous analysis, except for Appendix C and Section 3.5, the feedforward has been assumed zero. However, since feedforward is however very important for performance, it should be taken into account for analysis. Although selection of the feedforward and the effects on stability should be further investigated, $u_{iff} = min(u_{iA}, u_{iL})$ will be selected for (5.16) during gap making, with u_{iA}, u_{iL} as the feedforward from MIO_A and MIO_L respectively.

As a result, the control parameters are known, and the scenario can be evaluated by means of simulation. Using the presented initial setup of four vehicles, a MR is sent by vehicle 2 at $t_0 = 0\ s$. In accordance with the interaction protocol of Subsection 5.1.2, vehicle 4 will initiate the merging procedure as soon as a vehicle 2 starts merging, directly after STOM. The STOM is generated in accordance with (5.5) and (5.6), with $\alpha = 0.6$. As soon as the new MIO_A is identified, the platooning controller (3.23) is reinstated, finalizing the merge.

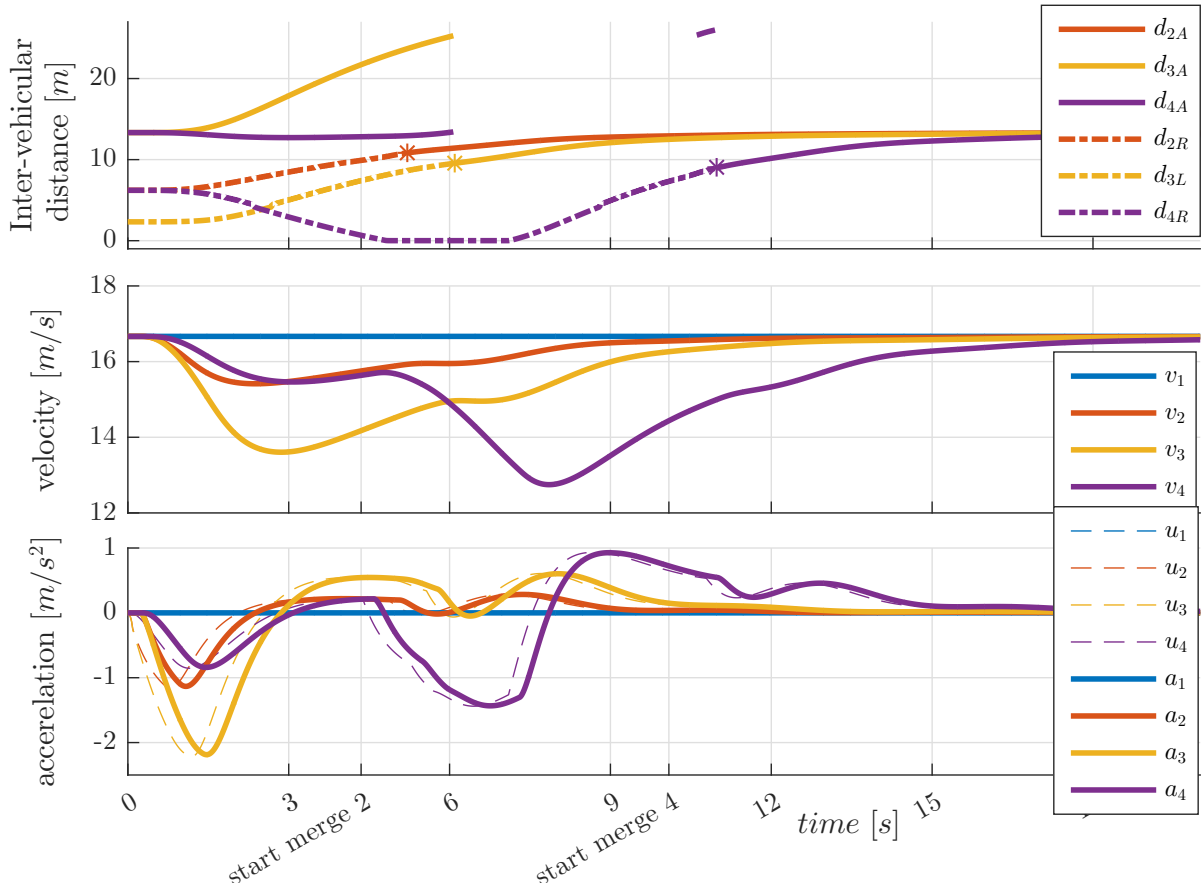

Figure 5.6: Simulation of merging of two platoons

Figure 5.6 shows the merging scenario for a set of four vehicles, where the MR is sent at $t_0 = 0$. Vehicles 2 and 4 are allowed to merge at $t = 4.38\ s$ and $t = 10.09\ s$, respectively. Directly after it is considered safe to start the merge, a vehicle initiates the lateral merge. At $t = 5.21\ s$, vehicle 2 identifies vehicle 1 as MIO_A instead of MIO_R, indicated with a red $'*'$. As vehicle 2 cuts-in directly in front of vehicle 3, vehicle 3 detects this at $t = 6.09\ s$, indicated by an orange $'*'$, where it changes the MIO status for both vehicles. Since vehicle 1 has become MIO_B for vehicle 3 and vehicle 2 has become MIO_A, vehicle 1 is no longer directly of interest for vehicle 3.

In the inter-vehicular distance plot of Figure 5.6, the fourth vehicle no longer detects a MIO_A as vehicle 2 has changed lane. Only after vehicle 2 has completed the merge, vehicle 4 is allowed to maneuver towards the merging position. Vehicle 4 initiates the merging at $t = 10.09\ s$. After an incorrect MIO_A detection, it finally identifies vehicle 3 as MIO_A at $t = 10.97\ s$. When regarding the behavior of vehicle 4, it can be noted that the presented interaction protocol can be further improved. In this simulation, vehicle 4 continues tracking its MIO_A until this vehicle merges. A more logical approach for this vehicle is to anticipate on the maneuvering objective before this event, since that can limit the required accelerations of vehicle 4.

When regarding the accelerations, no significant steps can be observed in the acceleration set-point as the platooning controller is reinstated. However, some unintended acceleration oscillations can be observed during the merging action of each vehicle. Since $x_{1,32}$ is positive at this moment, controllers (5.16) and (3.23) will result in an equal acceleration set-point, when neglecting feedforward.

The acceleration variation is caused by the sensor models which are included in the simulation. The sensors can introduce a step in the estimated state of a MIO, as a vehicles enters the field of view of camera or radar. This is additionally enlarged due to the assumption that the dynamics (3.4) for $i \in m$ are one dimensional, although the in-plane dynamics are apparent; the path from $M2$ is longer in reality due to the lateral maneuver. This has been further elaborated and verified in Appendix D.1. These vehicles are equipped with camera and radar for forward perception, and wireless communication for further perception. As the vehicle changes lane, it is more likely to enter the field of view of the radar and/or camera. Since radar is usually more reliable for longitudinal information than the wireless information, a step can occur in the perceived inter-vehicular distance and velocity. Since the relative velocity and distance are calculated with respect to the traveling direction of the host, the resulting estimated inter-vehicular velocity will be lower. As a result, $e_{2,i}$ reduces, which reduces $\bar{u}_i$, resulting in a lower acceleration for vehicles 2 and 3 as vehicle 2 performs the merge.

In order to quantify the performance of the APF control approach, performance criteria have been introduced in Subsection 3.4.1. Herein, the APF merging approach will be compared to the current merging controller from TNO. Since this scenario has a significant similarity with respect to gap closing, requirements (3.24) and (3.26) will be evaluated for the APF approach.

Table 5.1: Performance for APF merging in comparison to current TNO strategy

(a) Using APF merging method

Vehicle	$Q_1(a_i(t_k))$	$Q_3(e_{1,i\ i-1}(t_k))$
1	0	-
2	1.1232	30.7678
3	2.4890	49.6423
4	2.5374	70.9744

(b) Alternative merging method (TNO current)

Vehicle	$Q_1(a_i(t_k))$	$Q_3(e_{1,i\ i-1}(t_k))$
1	0	-
2	2.2380	119.7161
3	4.1521	70.3743
4	5.0096	47.6194

Table 5.1 compares the performance of the APF merging approach to the current merging controller from TNO, which is further elaborated in Appendix D.2. Criterion (3.24) herein penalizes the accelerations, whereas (3.26) integrates the position error with respect to the objective for maneuvering, vehicle $i-1$, thereby penalizing large errors and slow maneuvering. The maneuvering position error is evaluated in the time span starting with the moment where the coinciding triplet is allowed to maneuver. Hence, in evaluation of $Q_3(e_{1,i\ i-1}(t_k))$, vehicles $1, 2, 3$ are evaluated over time-span $t_k \in [0\ 20]$, and vehicle 4 over

time-span $t_k \in [4.38\ 20]$, for the APF method. The acceleration performance is evaluated for the full simulation time domain. When comparing Table 5.1.a with Table 5.1.b, it can be seen that the APF merging method performs much better that the current approach from TNO, for this scenario. The acceleration norms are significantly lower for all vehicles. This is, with the exception of vehicle 4, equally the case for criterion $Q_3(e_{1,i\ i-1}(t_k))$ as in (3.26). For the first triplet $(1, 2, 3)$, the APF controller has performed significantly better than the current TNO strategy. The fourth vehicle had been allowed to merge at $t = 10.09\ s$ for APF, and $t = 11.17\ s$ for the TNO approach. Hence, the required time and the acceleration norm are lower for the APF approach. Because of this, the APF merging algorithm is preferable. This is further elaborated in Appendix D.2, where simulation result of the TNO approach are presented. In conclusion, the merging approach can present a significant improvement in the ability to smoothly merge two platoons.

5.4 Summary

In this chapter, an APF approach for maneuvering on the highway has been presented, with the objective to guarantee longitudinal safety and a smooth acceleration profile. In Subsection 5.1.2, the interaction protocol has been presented for merging of vehicles and platoons. Next, a method has been presented in Subsection 5.2.1 to manage multiple objectives. Hereafter, the proposed multi-objective design approach has been implemented for gap making control in Subsection 5.2.2. Under the assumption of one-dimensional dynamics, a smooth acceleration transition has been obtained in Subsection 5.2.3. Using simulations, the effects and performance of the maneuvering controller has been further illustrated. As a result, the APF merging algorithm has shown to be a promising improvement with respect to the current merging method from TNO. In order to further validate the APF controller, experiments have been performed, which will be evaluated in the next chapter.

6: Experimental analysis

As part of the evaluation of the presented APF controller, experiments have been conducted at Lelystad using the test fleet of Priuses from TNO. In this chapter, these experiments will be further investigated to identify the capabilities, benefits, and performance of the APF controller for practical implementation. First, the functionality tests for platooning, gap closing and obstacle avoidance will be discussed, in the absence of wireless communication. Without wireless communication, these experiments have are equivalent to using an APF controller for ACC automation (APF-ACC).

In case the communicated intended acceleration is unavailable, an estimated feedforward acceleration is used as feedforward input for the controller (3.23). This estimated feedforward is derived using onboard sensor information for string stable gracefull degradation of CACC [8, 36]. In order to show the influence of this feedforward term for $\bar{u}_i$, this feedforward estimate will be shown as $\hat{a}_1$. In the figures, a_i, $\hat{a}_1$ and u_2 will be shown for accelerations. It should herein be noted that $u_i = \bar{u}_i - h\dot{u}_i$, as can be derived from (3.8). As a result, this causes phase delay.

After the platooning, gap closing and obstacle avoidance experiments, the last functionality test is cooperative merging, where wireless communication is required. The experiments have been conducted for a merging maneuver using two cooperative autonomous vehicles, and a CC-equipped lead vehicle. For all experiments, the controller settings have been equivalent to the settings as introduced in Section 5.3, although the selected time gap in (3.2) can vary per experiment. For comparison, additional experiments have been performed using the currently preferred set of controllers at TNO's disposal. As a result, the performance of the APF controller can be compared to TNO's current alternative. First, the platooning experiments will be presented in the next section.

6.1 Platooning

In this section, an experiment for APF-ACC will be investigated. Herein, two vehicles are driving behind each other, where the second vehicle is longitudinally controlled by the $APFx$ controller as presented in (3.23). Since use of the communicated feedforward acceleration had been disabled, the estimated feedforward signal $\hat{a}_i$ is used. For purposes of evaluation, the wireless information sent by the lead vehicle has been logged, here the received velocity and acceleration are assumed to equal to the actual velocity and acceleration of the lead vehicle.

Since the intended acceleration feedforward signal is unavailable, the minimal parameters $r = 11.33\ m$ and $h = 1.0\ s$ have been selected for safety purposes, for spacing policy (3.2). In the platooning experiment, the lead vehicle driven manually. The driver had been requested to initially increase and reduce the velocity slowly, followed by more severe braking and acceleration actions. Using the communicated velocity and acceleration, the performance of the controller can be further examined.

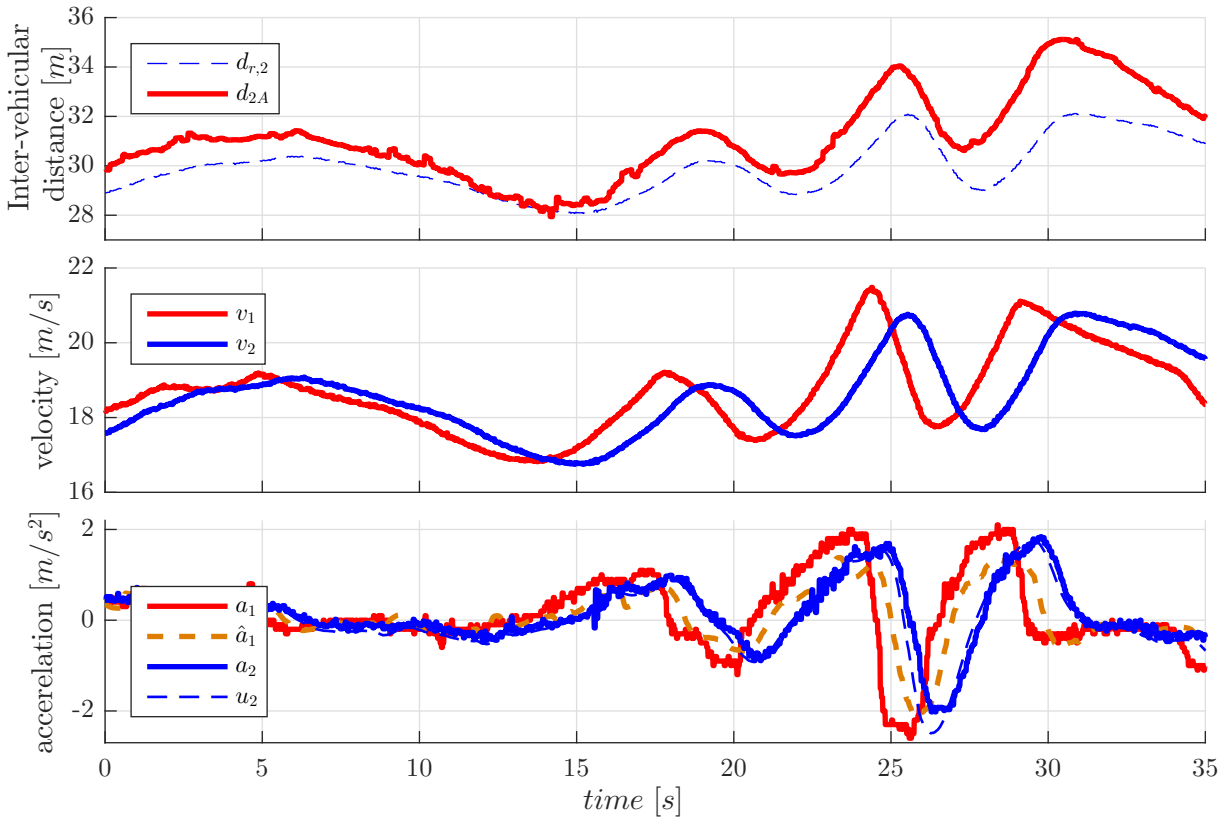

Figure 6.1: Platooning behind a vehicle with variable speed

Figure 6.1 shows the experimental result for the platooning test. Regarding the velocity, it can be seen that the amplitude of v_2 at $t \in [15\ 30]$ s is smaller than the amplitude of v_1. This will additionally be quantified using the acceleration l_2-norm $Q_1(a_i(t_k))$, as in (3.24). In accordance with the platooning performance criteria selected at Subsection 3.4.2, criteria (3.24) and (3.25) will indicate the performance of the controller.

Table 6.1: Performance for APF platooning experiment

Vehicle	$Q_1(a_i(t_k))$	$Q_2(e_{1,i}(t_k))$
1 (actual)	5.0324	-
$\hat{1}$ (estimated)	3.6023	-
2 (host)	4.2000	3.5404

In Table 6.1, the acceleration and position error norms are shown for platooning. Regarding the lead vehicle, the norm for the estimated acceleration is lower than for the actual acceleration, although this can be expected since it has been designed to provide string stabilty in combination with a linear PD controller [8, 36]. The acceleration norm has also decreased from the first to the second vehicle. Regarding the position error, it can be seen that the error is, on average, positive. Especially in response to the transient behavior from the preceding vehicle, the average error increases. With $e_{1,2A} \in [-0.24\ 3.54]$ m, the

tracking error is not large, although the difference is apparent. The average positive error can be explained by the fact that the controller is nonlinear: the response for a negative error is stronger than for a positive error of equivalent magnitude. Due to the varying behavior of the lead vehicle, in combination with measurement noise etc, a slight offset is created towards a larger gap. It should be noted that in case the lead vehicle is driving at a nearly constant speed, the offset is reduced. However, it can be concluded that the platooning experiment results are promising. Therefore, the gap closing experiment will be elaborated next.

6.2 Gap closing

One of the methods for assembling platoons is by means of gap closing control, hence by having a vehicle smoothly approach the preceding car. In this section, the gap closing experiment will be further explained. The settings $r = 11.33$ and $h = 1.0\ s$ for (3.2) have again been applied. For real-time implementation, the range of interest for the target tracking algorithm had been limited up to $d_i(t) \leq 50\ m$. This has restricted the tests for the gap closing functionality, since the MIO_A classification is only applied to objects within this range. During the test, the lead vehicle drives at a cruise speed of 60 $km/h = 16.67\ m/s$, the second vehicle starts with a lower velocity and a target cruise speed of 115 $km/h \approx 32\ m/s$. At time t_1, vehicle 1 enters the range of interest for vehicle 2, and the $APFx$ controller is activated. Hence, the APF platooning controller is only active starting from t_1, therefore the performance criteria for this maneuver will not be evaluated.

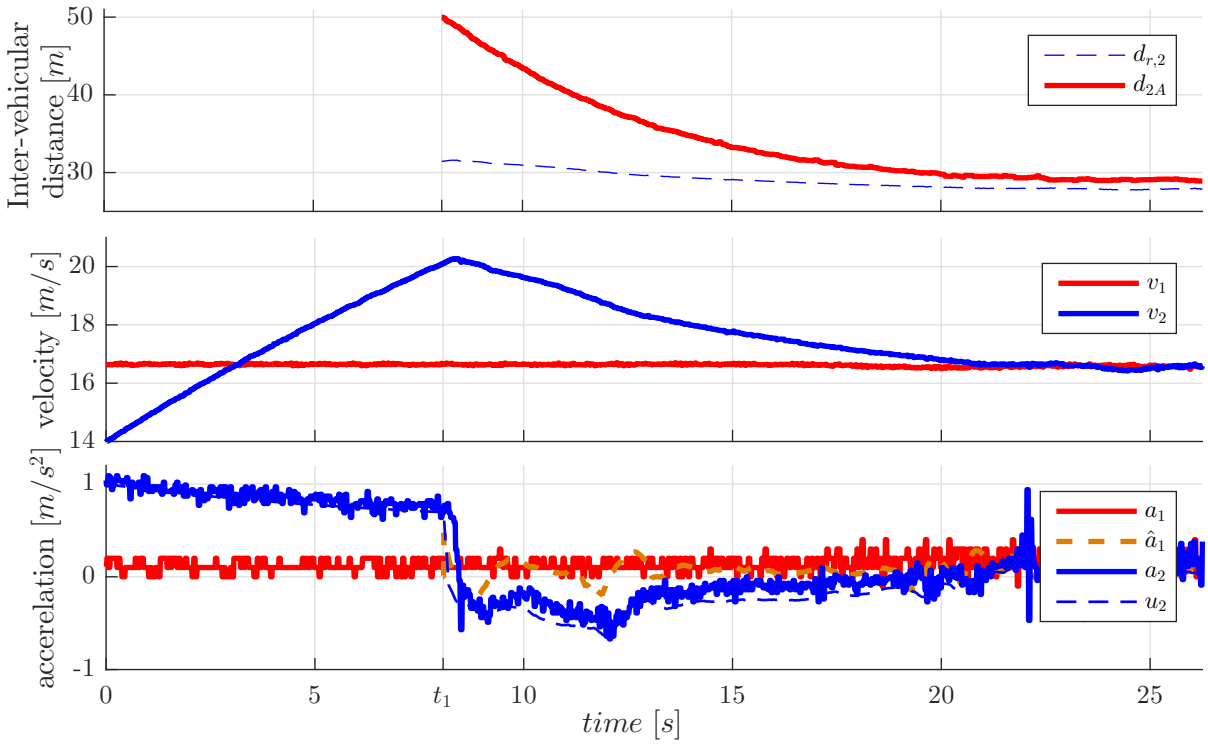

Figure 6.2: Gap closing experiment

Figure 6.2 shows the gap closing experiment, where time $t_1 = 8.07\ s$ is indicated. Shortly hereafter, the vehicle starts decelerating with $a_2(t) \approx -0.4\ m/s^2$, such that the vehicle slows down gradually, approximately from t_1 until $t = 21\ s$. Note that the jumps for $a_2(t \approx 22)$ are likely measurement errors, since no indication hereof can be found in the intended acceleration or other logged signals. The experiment therefore shows that the gap closing functionality functions properly, although the experiment specifics cannot provide a proper quantification for the performance.

6.3 Obstacle avoidance

One of the main motivations for autonomous driving is safety. Therefore, the obstacle avoidance capabilities of the *APFx* controller (3.23) will be tested. Again, equal settings have been applied with $r = 11.33\ m$ and $h = 1.0\ s$ for (3.2), along with the gracefull degradation feedforward [8, 36] estimate $\hat{a}_1$. When initially platooning with a velocity of $v_1(0) = 60\ km/h = 16.7 m/s$, the lead vehicle will start braking at $t_1 = 3\ s$, with an acceleration of $a_1(t) \approx -2.7\ m/s^2$.

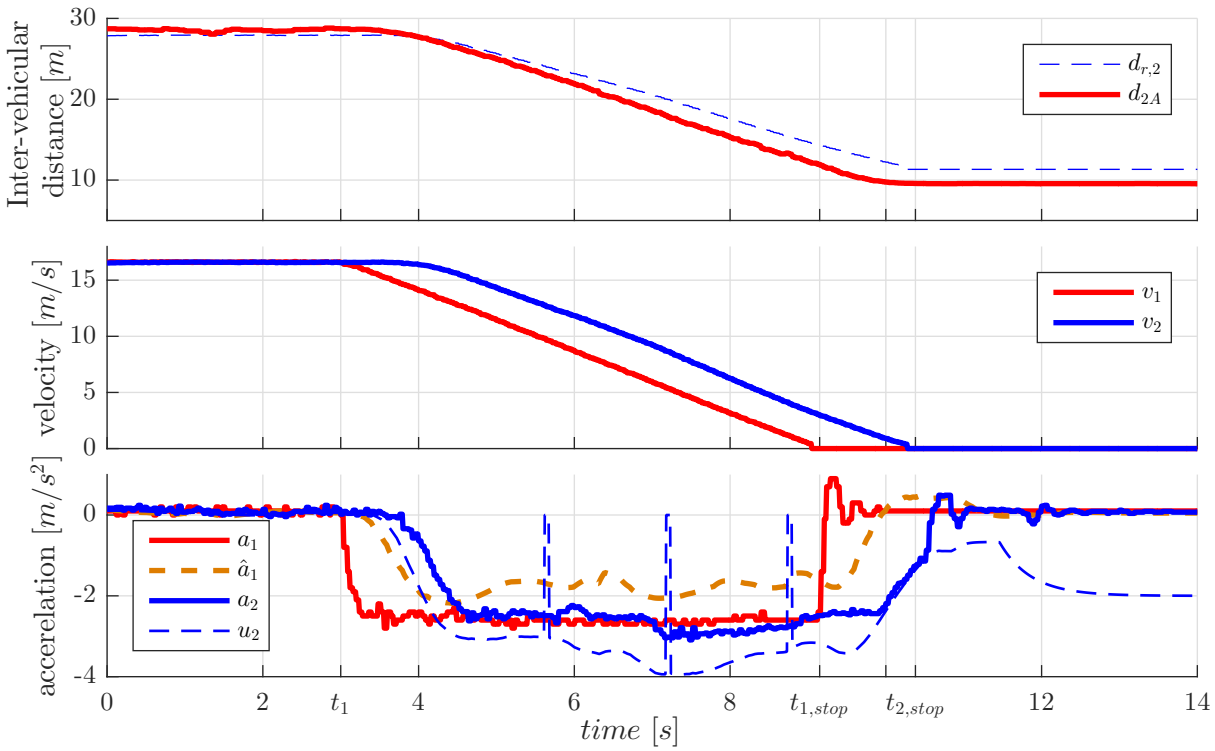

Figure 6.3: Obstacle avoidance experiment using *APFx* controller

Figure 6.3 shows the measurements performed during this test. Vehicle 1 comes to a stop at approximately $t_{1,stop} \approx 9.1\ s$. At $t_{2,stop} \approx 10.4\ s$, vehicle 2 has come to a stop with a final inter-vehicular distance of $d_{2A}(t_{2,stop}) = 9.57\ m$ and a position error or $e_{2A}(t_{2,stop}) =$

$-1.76\ m$. In the intended acceleration $u_2(t)$, some jumps to $u_2 = 0$ can be seen. Since the Prius automation system can only brake for a fixed time interval (close to 2 seconds), the braking action is periodically interrupted for a short time interval. Additionally, it can be seen that the intended acceleration is nearly consistently lower than the actual acceleration, which is probably due to an issue in the low level controller.

When comparing the actual accelerations of vehicles 1 and 2, it can be noted that the peak deceleration had only been $min(a_1(t)) = -2.8\ m/s^2$ versus $min(a_2(t)) = -3.0\ m/s^2$. When regarding the position error for this experiment, it can be seen that it is limited to an overshoot of $e_{1,2A}(t = 9.6) = -2.8\ m$. This is, considering the fact that ACC is used with $h = 1\ s$, very respectable. For comparison, let us review an experiment using the *PD* controller (3.10), with $k_p = 0.2$ and $k_d = 0.7$. The results of which are shown in Figure 6.4.

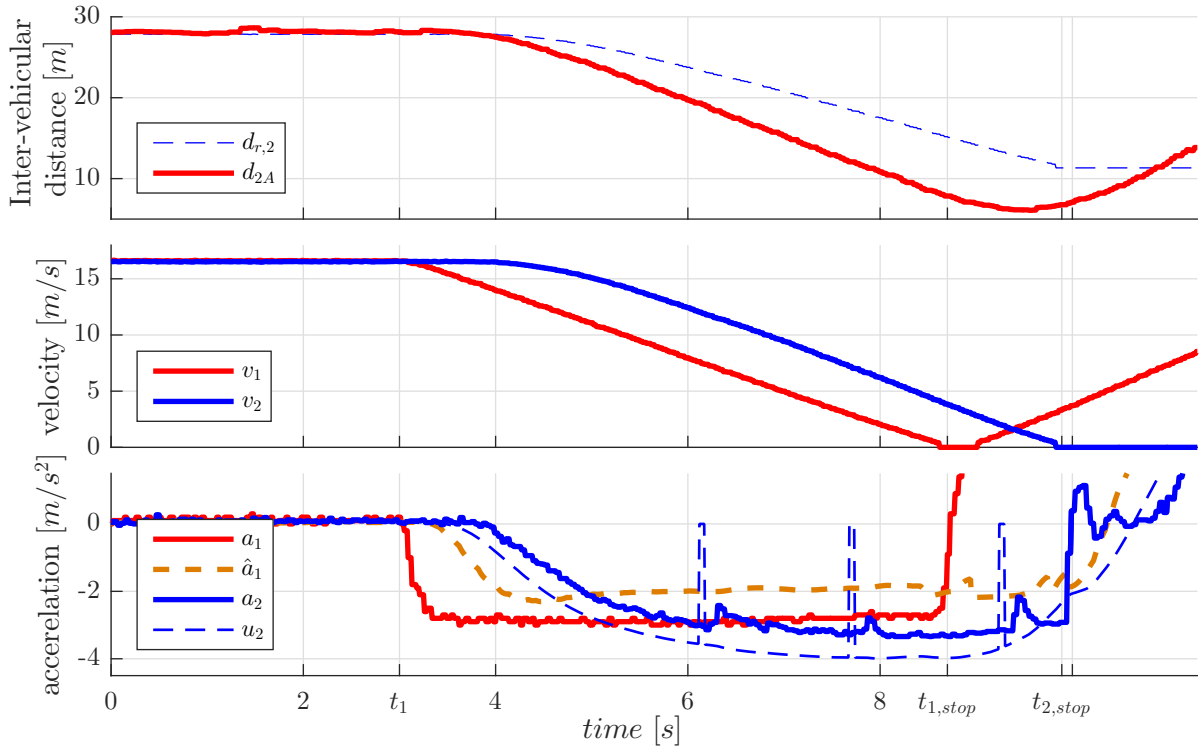

Figure 6.4: Obstacle avoidance experiment using a *PD* controller (current TNO strategy)

For this experiment, the initialization time t_1, initial velocity $v_1(0)$ and the acceleration set-point $a_1(t)$ have been chosen equal. In the experiment however, it should be noted that the lead vehicle stopped at $t_{1,stop} \approx 8.7\ s$, which is slightly quicker than in the experiment of Figure 6.3. The achieved lead vehicle deceleration had been $a_1(t) \approx -2.9\ m/s^2$, with peaks at $min(a_1(t)) = -3.0\ m/s^2$. For vehicle 2, the peak deceleration had been at $min(a_2(t)) = -3.3\ m/s^2$. However, the acceleration is introduced very slowly in comparison with respect to the acceleration response of the *APFx* controller as depicted in Figure 6.3. As a result,

the vehicle is braking much later then the lead vehicle, such that the inter-vehicular distance is reduced to only $min(d_{2A}) = 6.1\ m$. Herein, it should be noted that the lead vehicle had again started driving before vehicle 2 had come to a stop at $t_{2,stop} \approx 9.9\ s$. Therefore, the stopping distance would have been smaller otherwise. Due to the differences in both experiments, an exact comparison or conclusion cannot be drawn. However, in an attempt to still do so, the performance criteria for both experiments have been evaluated, for each vehicle within the time span $t_k \in [0\ t_{i,stop}]$.

Table 6.2: Obstacle avoidance comparison for the *APFx* and the *PD* controller

(a) Using *APFx* control method

Vehicle	$Q_1(a_i(t_k))$	$Q_2(e_{1,i}(t_k))$
1	6.3552	-
2	6.3265	2.7946

(b) Using *PD* control (TNO current)

Vehicle	$Q_1(a_i(t_k))$	$Q_2(e_{1,i}(t_k))$
1	6.6481	-
2	6.7611	7.4351

Table 6.2 shows the performance criteria for both experiments. Regarding the acceleration norms, the differences are too small for any conclusions, although the small difference between the two experiments can be noticed. When regarding the position error overshoot however, a rather significant difference can be noticed. With an overshoot $e_{1,2A}(t = 8.9) = -7.43\ m$ for the current *PD* distance controller, this vehicle has come much too close to the lead vehicle, that had additionally started driving again.

As a result of the large difference in the minimal inter-vehicular distance, it can be concluded that the *APFx* controller performs better than the linear *PD* controller, when regarding obstacle avoidance functionality.

6.4 Merging

Next to platooning, gap closing and collision avoidance, it is equally important that vehicles can perform autonomous merging maneuvers. Therefore, multiple experiments have been performed using three Priuses from the fleet of TNO. Herein, the gap making vehicle and the merging vehicle are equipped with radar, camera, GPS and wireless communication devices. Since communication between $M2$ and $M3$ is required for cooperative merging maneuvers, the communicated acceleration feedforward signal is used for control. For the lead vehicle however, the wireless communication had been malfunctioning. Therefore, the actual lead vehicle velocity is assumed to be equal to the cruise speed $v_{1,CC}$.

Since the velocity and the initial positions can be of influence for a merging maneuver, two experiments will be shown. The first experiment will have a lead vehicle cruise speed of $v_{1,CC} = 50\ km/h \approx 13.9\ m/s$, the second test is performed with $v_{1,CC} = 90\ km/h \approx 25\ m/s$. The initial positions are visible in the experiment results. Now consider the first experiment, performed with $r = 10\ m$ and $h = 1.0\ s$ for the spacing policy (3.2), and $v_{1,CC} = 50\ km/h$.

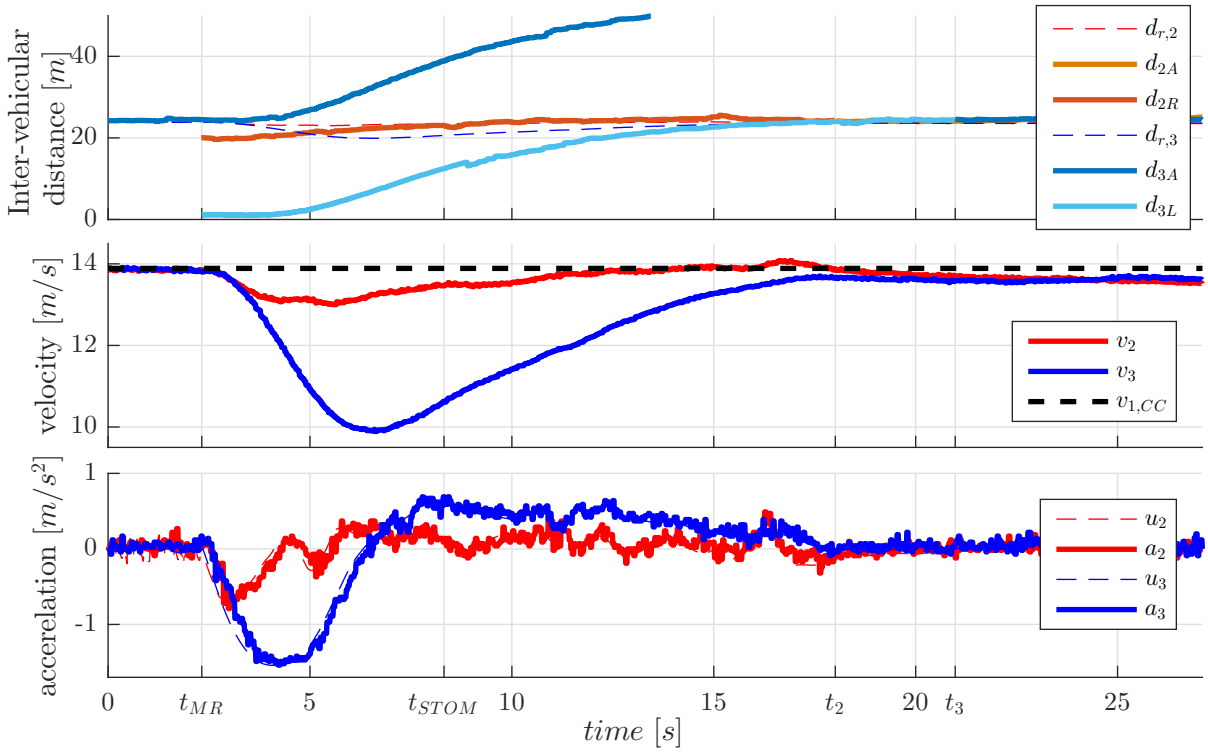

Figure 6.5: Merging experiment at 50 km/h, with $r = 10\ m$ and $h = 1\ s$

Figure 6.5 shows the first experiment, where the vehicles start in an equal configuration as the first three vehicles in Figure 5.2. At time $t_{MR} = 2.32\ s$, vehicle 2 issues a MR. At that moment, vehicle 2 is situated only a few meters in front of vehicle 3, since $d_{3L}(t_{MR} = 2.34\ m$. As a result, vehicle 2 will only need to make a slight maneuver, whereas vehicle 3 should make a gap. This can also be seen in the plots of $a_2(t)$ and $v_2(t)$, which show only small variations. With $e_{1,3L}(t_{MR}) = -22.71\ m$, vehicle 3 will need to make a relatively large gap, directly from the start. This can additionally be seen in the velocity and acceleration of vehicle 3, where the velocity $v_3(t)$ decreases from 13.8 m/s to 10 m/s during the first part of the maneuver. With the acceleration $a_2(t) \in [-1,5\ 0.7]\ m/s^2$, this maneuver is comfortably executed. At $t_{STOM} = 8.32\ s$, hence 5 s after the MR, the STOM flag is generated, allowing vehicle 2 to merge.

The merge itself has been executed manually for safety purposes. Additionally however, also much later than possible. At $t_2 = 18\ s$, vehicle 2 detects vehicle 1 as MIO_A instead of MIO_R. As a result, the maneuver is completed for vehicle 2, such that it switches to platooning. Vehicle 3 detects the merge completion at $t_3 = 20.98\ s$, and resumes platooning with respect to the new MIO_A. As a result, the merge is completed in approximately 18 seconds. It can be noted that both the acceleration and velocity is reasonably smooth throughout the experiment, also at the merge completion. Therefore, the smooth merging principle as explained in Subsection 5.2.3 is confirmed. For additional verification of the merging controller, another test is performed at $90km/h$ and a time headway of $h = 0.6\ s$ instead of $h = 1.0\ s$.

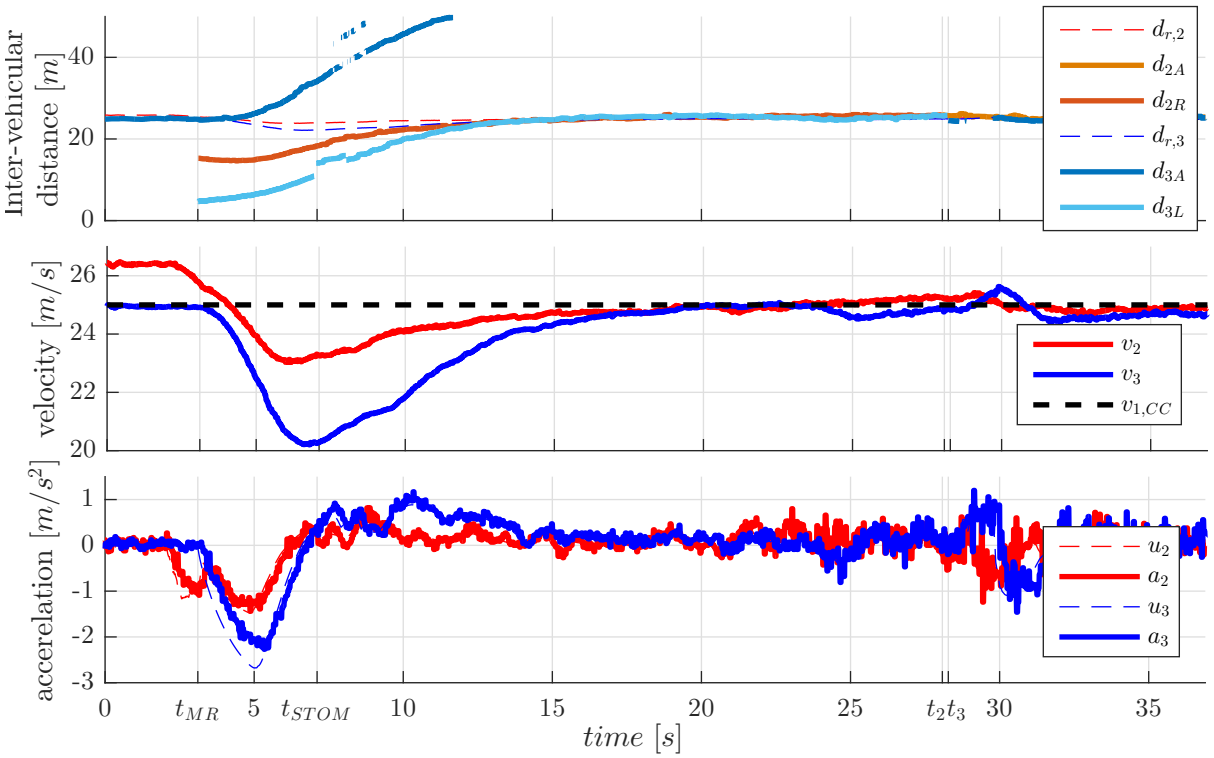

Figure 6.6: Merging experiment at 90 km/h, with $r = 10$ m and $h = 0.6$ s

Figure 6.6 shows the experiment results for the APF maneuvering test with $v_{1,CC} = 90$ km/h. In this test, vehicle 2 started close to vehicle 3, hence with $d_{3L}(t_{MR}) = 4.6$ m, such that $e_{2,R}(t_{MR}) = -10.2$ m, and $e_{3,L}(t_{MR}) = -20.3$ m. Since vehicle 2 starts braking to reduce the velocity and the magnitude of the error $e_{1,2R}(t)$, this intended deceleration level is applied as feedforward signal for vehicle 3. Combined with the feedforward, the control input results in a more significant braking level for vehicle 3 than for vehicle 2. However, for both vehicles, the acceleration remains within reasonable levels, with $a_1(t) \in [-1.4\ 0.8]$ m/s^2 and $a_2(t) \in [-2.2\ 1.1]$ m/s^2 for the complete scenario.

Since $t_{MR} = 3.11$ s and $t_{STOM} = 7.11$ s, it has taken only four seconds of maneuvering before the STOM criteria (5.7), (5.8) and (5.10) are satisfied. Note that the time t_{STOM} coincides with a jump in the estimated inter-vehicular distance, as can be seen in Figure 6.6. This jump can be explained by the available sensor information; the vehicle has camera and radar for forward perception, and only wireless communication for all-round perception, using GPS information. Before this jump, the inter-vehicular distance has been determined using wireless communication. The logging has shown that this jump coincides with vehicle 2 entering the field of view from the camera of vehicle 3, resulting in a different estimation in the inter-vehicular distance. A little later, a smaller jump is seen, this is where the radar has started detecting vehicle 2.

The effect of the sensors can be slightly seen in the acceleration plots for $a_3(t)$, where a small increase, and consequently decrease of the acceleration can be seen shortly after the

change in sensor. However, a larger acceleration variation, approximately within $\pm 1\ m/s^2$, can be seen shortly after the merge at $t_2 \approx t_3 = 28.1\ s$. First, it can be noted that this manual merge is executed much too late, since a STOM had been generated approximately 20 s earlier. This is due to an error in the supervisory controller, causing vehicle 2 to be unable to correctly process the STOM signal. The merge is executed manually at entry of a banked corner section of the test track. Shortly hereafter, the MIO detection for vehicle 3 fails; it cannot detect a MIO_A, whereas it classifies vehicle 2 as the MIO_R for the duration of approximately 1 s. As a result, the cruise control is reinstated, resulting in an temporary acceleration due to a higher velocity set-point. As the MIO_A is again detected, a deceleration is required to ensure an appropriate platooning formation. When reviewing both experiments, it can be concluded that the merge has been smoothly executed.

6.5 summary

In order to verify the capabilities and quantify performance of the presented APF controller for platooning and merging, multiple experiments have been performed. To the benefit of platooning, the gap making and obstacle avoidance functionality have been tested in the absence of communication. The experiments have shown that the controller responds as expected, the desired functionality has been confirmed. For all experiments, the APF controller has shown to be able to realize a sufficient yet smooth acceleration set-point in order to enable safe maneuvering with sufficient performance. Although highly dynamic behavior of the predecessor causes the host to temporarily increase the average position error, this is not an issue.

The APF controller has shown to perform significantly better then the current linear PD controller, especially for obstacle avoidance. Additionally, some of the implications of real-time testing have been shown, the controller has responded appropriately in each of these situations. As a result, the experiments have succeeded. The APF controller has shown to be a promising alternative for longitudinal control of autonomous vehicles. Nonetheless, additional testing or simulations might be required to provide a more extensive evaluation of the performance of the controller.

7: Conclusions and recommendations

7.1 Conclusions

Cooperative autonomous driving has the potential to significantly increase the safety and comfort of highway driving. Since the inter-vehicular distances can be decreased, the road throughput can be significantly increased, without a need to extend existing infrastructure. Due to these benefits, cooperative autonomous driving using CACC is likely to be the next step after driver assistance systems such as CC and ACC. However, by reducing the distances, a controller will be required that can take over all tasks from the driver, ensuring safety. Although research is ongoing on this topic, a comprehensive method to enable cooperative autonomous driving has not been fully developed. This thesis will contribute in the longitudinal control for safe cooperative autonomous driving on the road.

First, the design approach for platooning and CACC has been discussed in Chapter 3. After an introduction of the vehicle dynamics and a velocity dependent spacing policy, the error dynamics of a vehicle in a platoon have been presented. Hereafter, multiple control designs have been introduced and investigated using simulation and analysis. The resulting APF based controllers have additionally been compared to a linear PD controller. By evaluation of two criteria for each type of functionality, the preferred controller has been selected: a controller using a linear combination of errors as an input of an APF function. An additional string stability review has shown promising behavior in simulation, although further analysis is required.

Since safety is crucial for cooperative autonomous driving, this aspect has been investigated in Chapter 4. Herein, it is motivated that safety can be warranted in a case collision can be avoided for the worst use-case scenario: an emergency braking maneuver from the preceding vehicle. After introducing the dynamics of an emergency braking maneuver, the set of critical states could be derived. Using a state transformation, these critical states can be related to the nominal controller. As a result, an additional CA controller has been required and designed to ensure safety for small inter-vehicular distances.

For normal use-case scenarios, comfort and safety is essential. Therefore, additional requirements have been stated to ensure the CA controller is not required for nominal scenarios. For these nominal scenarios, the permitted acceleration and velocity have therefore been bounded, for the purpose of analysis. Since a vehicle is expected not to exceed these comfort bounds on the acceleration, a saturated controller is implemented. For a nominal scenario and a minimal host velocity, a domain could be determined wherein the nominal controller can ensure remaining in a safe state with respect to a preceding vehicle.

Next to platooning and maneuvering on a single lane, the merging of platoons or vehicles into a neighboring lane is considered. Herein, the vehicle requirements and the interaction protocol have been stated first. Next, the control problem is broken down into sets of three vehicles. Hereafter, an approach has been presented to solve this multi-objective control problem, without compromising safety. Using the presented approach, a smooth

acceleration set-point has been ensured, where stability is inherently provided when assuming zero feedforward.

For verification of the functionality and the real-time performance, experiments have been conducted using the fleet of Priuses from TNO. In Chapter 6, the experiments for platooning, gap closing, obstacle avoidance and merging have been elaborated. Herein, the APF control approach has shown to include the desired functionality. With respect to the current linear control implementation, the APF approach has shown to provide a significant improvement in performance and safety.

7.2 Recommendations

Although the results have been very promising, further investigation and development will be required for large scale implementation. The main recommendations for future work are:

1. String stability should be further investigated, since it is required to increase the road throughput and comfort for platooning. A piece-wise linear APF approach may provide string stability proof for small perturbations.
2. Considering safety: Effects like time delay and unequal vehicle properties are likely to affect safety. Differences in maximal braking level, perception effects and other influences should be further investigated. Additionally, safety could be warranted by considering the possibility of evasive paths.
3. When platooning or merging, a vehicle can receive multiple feedforward signals. Especially for the multi-objective scenario of merging, it can be useful to investigate the selection and processing of the received information in order to improve performance, comfort and stability.

Bibliography

[1] "EU transport in figures, statistical pocketbook," 2012, Publications Office of the European Union.

[2] A. A. Alam, A. Gattami, and K. H. Johansson, "An experimental study on the fuel reduction potential of heavy duty vehicle platooning," in *13th International IEEE Conference on Intelligent Transportation Systems (ITSC)*. IEEE, 2010, pp. 306–311.

[3] S. E. Shladover, "Automated vehicles for highway operations (automated highway systems)," *Proceedings of the Institution of Mechanical Engineers, Part I: Journal of Systems and Control Engineering*, vol. 219, no. 1, pp. 53–75, 2005.

[4] W.-H. Hucho, Ed., *Aerodynamics of road vehicles*. Society of Automotive Engineers Inc; 4 edition, 1998.

[5] A. Alam, "Fuel-efficient heavy-duty vehicle platooning," Ph.D. dissertation, KTH Royal Institute of Technology, 2014.

[6] V. Turri, B. Besselink, J. Martensson, and K. H. Johansson, "Fuel-efficient heavy-duty vehicle platooning by look-ahead control," in *53rd Annual IEEE Conference on Decision and Control (CDC)*. IEEE, 2014, pp. 654–660.

[7] J. Ploeg, B. Scheepers, E. Van Nunen, N. Van de Wouw, and H. Nijmeijer, "Design and experimental evaluation of cooperative adaptive cruise control," in *14th International IEEE Conference on Intelligent Transportation Systems (ITSC),*. IEEE, 2011, pp. 260–265.

[8] J. Ploeg, "Analysis and design of controllers for cooperative and automated driving," Ph.D. dissertation, Eindhoven University of Technology, 2014.

[9] J. Ploeg, N. Van De Wouw, and H. Nijmeijer, "Lp string stability of cascaded systems: Application to vehicle platooning," *IEEE Transactions on Control Systems Technology (CST)*, vol. 22, no. 2, pp. 786–793, 2014.

[10] H. E. Sungu, M. Inoue, and J.-i. Imura, "Nonlinear spacing policy based vehicle platoon control for local string stability and global traffic flow stability," in *IEEE European Control Conference (ECC)*, 2015, pp. 3396–3401.

[11] R. Lenain et al., "Rejection of sliding effects in car like robot control : application to farm vehicle guidance using a single RTK GPS sensor." IEEE/RSJ, 2003, intl. Conference on Intelligent Robots and Systems.

[12] V. Dolk, D. Borgers, and W. Heemels, "Dynamic event-triggered control: Tradeoffs between transmission intervals and performance," in *53rd IEEE Conference on Decision and Control (CDC)*. IEEE, 2014, pp. 2764–2769.

[13] C. Englund, J. Didoff, L. Chen, A. Voronov, E. Nunen, J. Ploeg, A. Apparicio, I. Besselink, and A. Morales Medina, "DEL140730 i-GAME D1.2 Draft report on requirements specification," European commission, 2014.

[14] E. van Nunen, J. Ploeg, A. M. Medina, and H. Nijmeijer, "Fault tolerancy in

Cooperative Adaptive Cruise Control," in *16th International IEEE Conference on Intelligent Transportation Systems (ITSC)*. IEEE, 2013, pp. 1184–1189.

[15] E. Semsar-Kazerooni, A. Morales Medina, and H. H. Bengtsson, "DEL150330 i-GAME D2.1 Interaction Protocol," European commission, 2015.

[16] A. Morales Medina and E. Semsar-Kazerooni, "DEL150401 i-GAME D2.2 Generic realtime control system," European commission, 2015.

[17] R. Olfati-Saber, "Flocking for multi-agent dynamic systems: Algorithms and theory," *IEEE Transactions on Automatic Control*, vol. 51, no. 3, pp. 401–420, 2006.

[18] B. Q. Nguyen et al., "Virtual attractive-repulsive potentials for cooperative control of second order dynamic vehicles on the Caltech MVWT," in *2005 American Control Conference*. IEEE, 2005, pp. 1084–1089.

[19] D. Kostić, S. Adinandra, J. Caarls, N. van de Wouw, and H. Nijmeijer, "Collision-free tracking control of unicycle mobile robots," in *Joint 48th IEEE Conference on Decision and Control and 28th Chinese Control Conference, (CDC/CCC)*. IEEE, 2009, pp. 5667–5672.

[20] D. Kostic, S. Adinandra, J. Caarls, and H. Nijmeijer, "Collision-free motion coordination of unicycle multi-agent systems," in *American Control Conference (ACC)*. IEEE, 2010, pp. 3186–3191.

[21] D. Kostić, S. Adinandra, J. Caarls, N. van de Wouw, and H. Nijmeijer, "Saturated control of time-varying formations and trajectory tracking for unicycle multi-agent systems," in *49th IEEE Conference on Decision and Control (CDC)*. IEEE, 2010, pp. 4054–4059.

[22] K. Elferink, "Control of ad-hoc merging manoeuvres for heavy-duty vehicle platooning," 2015, Eindhoven University of Technology & KTH Royal Institute of Technology, Internship report DC 2015.053.

[23] E. Semsar-Kazerooni, J. Verhaegh, J. Ploeg, and M. Alirezaei, "Cooperative adaptive cruise control, an artificial potential field approach," in *IEEE Intelligent Vehicles Symposium*, 2016.

[24] E. Semsar-Kazerooni, "High-level controllers for platoon maneuvers," TNO internal report, February 2015.

[25] M. T. Wolf and J. W. Burdick, "Artificial potential functions for highway driving with collision avoidance," in *2008 International IEEE Conference on Robotics and Automation (ICRA)*, 2008, pp. 3731–3736.

[26] J. C. Gerdes and E. J. Rossetter, "A unified approach to driver assistance systems based on artificial potential fields," *Journal of Dynamic Systems, Measurement, and Control*, vol. 123, no. 3, pp. 431–438, 2001.

[27] P. Vadakkepat, K. Chen Tan, and W. Ming-Liang, "Evolutionary artificial potential fields and their application in real time robot path planning," in *Evolutionary*

Computation, 2000. Proceedings of the 2000 Congress on, vol. 1. IEEE, 2000, pp. 256–263.

[28] Z.-P. Jiang, E. Lefeber, and H. Nijmeijer, "Saturated stabilization and tracking of a nonholonomic mobile robot," *Systems & Control Letters*, vol. 42, no. 5, pp. 327–332, 2001.

[29] A. Alam, A. Gattami, K. H. Johansson, and C. J. Tomlin, "Guaranteeing safety for heavy duty vehicle platooning: Safe set computations and experimental evaluations," *Control Engineering Practice*, vol. 24, pp. 33–41, 2014.

[30] G. Koudijs, "Control methods for fail-safety in cooperative automated driving," Master's thesis, Technische Universiteit Eindhoven, 2016.

[31] TNO in cooperation with Eindhoven University of Technology, Idiada, and Viktoria Swedish ICT, "i-GAME project," accessed on 2016-08-01. [Online]. Available: www.gcdc.net

[32] G. J. Naus, R. P. Vugts, J. Ploeg, M. J. van de Molengraft, and M. Steinbuch, "String-stable cacc design and experimental validation: A frequency-domain approach," *IEEE Transactions on Vehicular Technology*, vol. 59, no. 9, pp. 4268–4279, 2010.

[33] M. Alirezaei, "CACC based on Artificial Potential," August 2015, TNO internal report.

[34] S. Skogestad and I. Postlethwaite, *Multivariable feedback control: analysis and design*. Wiley New York, 2007, vol. 2.

[35] H. K. Khalil, *Nonlinear Systems*, 3rd ed. Prentice Hall, 2002, ch. 8.2.

[36] J. Ploeg, E. Semsar-Kazerooni, G. Lijster, N. van de Wouw, and H. Nijmeijer, "Graceful degradation of CACC performance subject to unreliable wireless communication," in *16th International IEEE Conference on Intelligent Transportation Systems (ITSC 2013)*. IEEE, 2013, pp. 1210–1216.

Appendix A: Comparison of APF controllers

In order to provide a more elaborate comparison of the response of the presented controllers, the control response in the plane $e_{1,i}, e_{2,i}$ is investigated. As a result, the capabilities, restrictions and design objectives can be identified. For this analysis, the feedforward $u_{i-1} = 0$ is assumed, such that the control response as a function of the error state can be examined. Hence, this analysis considers $\bar{u}_i = \bar{u}_i(e_{1,i}, e_{2,i})$.

Since gap closing and obstacle avoidance functionality is additionally desired, the states $(e_{1,i}, e_{2,i})$ will not be limited to states close to $(e_{1,i}, e_{2,i}) = (0, 0)$. As a result, a controller might result in undesirable behavior for a set of feasible combinations of states. The result can be a saturated acceleration or braking action, for scenarios in which this is unnecessary. Actually, a saturated acceleration can be considered undesirable for all scenarios. Therefore, the response of each controller will investigated over the relevant range of states $(e_{1,i}, e_{2,i})$ to investigate the capabilities and limitations of each control design.

When regarding the relevant range of states, the range of $e_{1,i} \in [-20\ 60]\ m$ and $e_{2,i} \in [-10\ 10]\ m/s$ will be investigated. When analyzing this phase plane, one should note that the assumption of $a_i = 0$ results in $e_{2,i} = \Delta v_i$, making analysis more intuitive. Hence, with $e_{2,i} \in [-10\ 10]\ m/s$, relative velocity differences of up to approximately 10 m/s will be evaluated. Within the presented range for $e_{1,i}$, the controller should respond appropriately; for large $e_{1,i}$, gap closing should ensure a smooth acceleration up to a reasonable approach velocity. For negative and small values of $e_{1,i}$, obstacle avoidance should ensure safety. When in nominal situations, hence when gap closing and platooning, the comfort acceleration limits of $\bar{u}_i \in [u_{min}\ u_{max}] = [-2\ 2]\ m/s^2$ should be respected. The limits $\bar{u}_i \in [-6, 3]\ m/s^2$ are assumed to respect the physical acceleration bounds. As a result, the control action can be evaluated for various combinations of the position error and velocity difference. Therefore, a plot of control response $\bar{u}_{i,PD}(e_{1,i}, e_{2,i})$ can be shown.

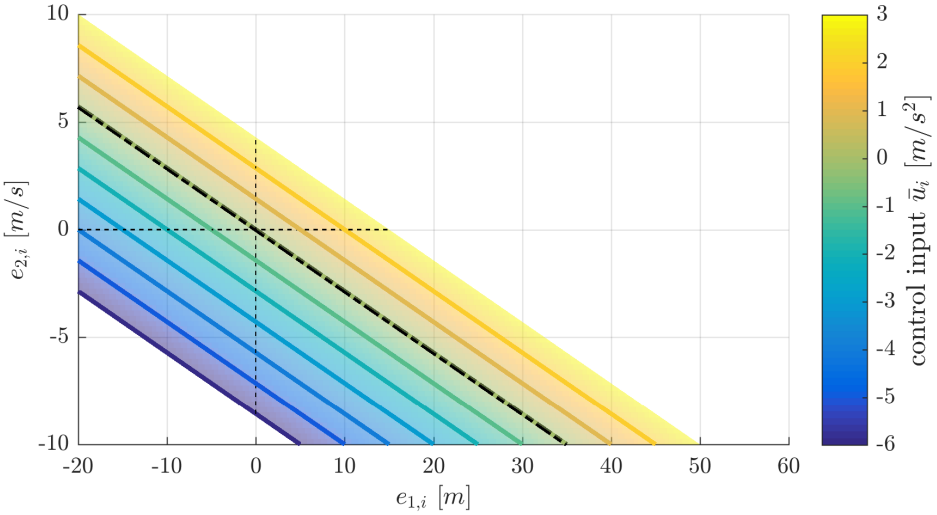

Figure A.1: Response plot of *PD* controller $\bar{u}_{i,PD}$ (3.10) in the $(e_{1,i}, e_{2,i})$ plane

Figure A.1 illustrates the control action $\bar{u}_{i,PD}(e_{1,i}, e_{2,i})$ for the *PD* controller 3.10, with $\bar{u}_i \in [-6, 3]\ m/s^2$. The lines in Figure A.1 depict the combinations of $(e_{1,i}, e_{2,i})$ wherein the control response is equal. Hence, the isoclines where $\bar{u}_i(e_{1,i}, e_{2,i}) = constant$. It can be noted that the controller is, as expected, not suitable for the large range of $(e_{1,i}, e_{2,i})$. Not only does the controller provide an insufficient braking level at critical situations, the acceleration set-point $\bar{u}_{i,PD}(e_{1,i}, e_{2,i})$ is much too large for large positive position errors. When considering the response to $e_{2,i}$, which equals Δv_i in case $a_i = 0$ is assumed, it can be seen that reasonably large approach velocities for gap closing can be expected. As a solution, one can limit the approach velocity difference. However, this is not a very desirable solution. This is similarly required for safety, which is discussed in Chapter 4. Therefore, a sketch for the approximately desired APF controller operating within the $(e_{1,i}, e_{2,i})$ domain can be posed as:

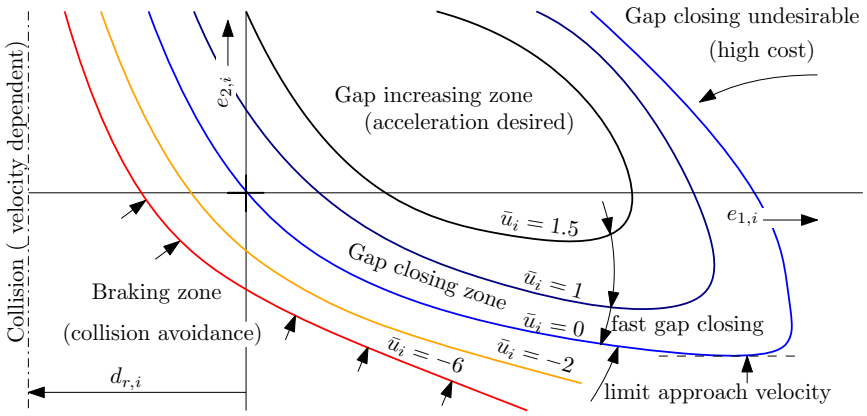

Figure A.2: Sketch of the approximately desired $\bar{u}_i(e_{1,i}, e_{2,i})$, for platooning and gap closing, with indicated design objectives

Figure A.2 shows an approximation of the desired response for an APF controller. Obviously, the specifics are vaguely noted and can be further elaborated and modeled. Consequently one can derive an APF by means of integration, yielding an APF control strategy. However, it is desirable to have a controller based upon physical properties and design choices. This will both aid in the ability for proving stability and safety, as well as enable a more diverse set of applications for the resulting control architecture. Therefore, an APF description should be found that combines these design objectives, and which will thereby likely approximate the behavior as sketched in Figure A.2. Next, the *APF1* controller will be examined.

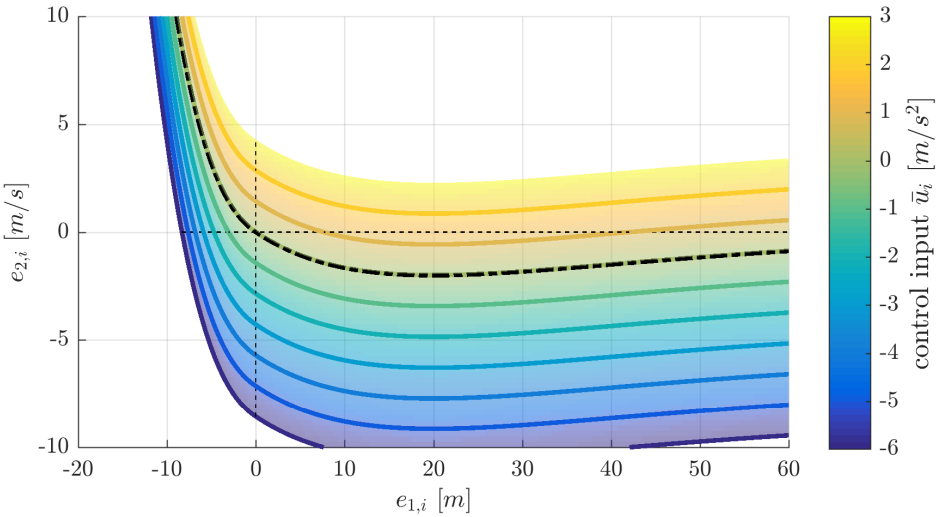

Figure A.3: Response plot of controller $\bar{u}_{i,APF1}$ (3.11) in the $(e_{1,i}, e_{2,i})$ plane

Figure A.3 shows the control response for the *APF1* controller (3.11). Although the controller does work for larger position errors, it does not work for reasonable values for $e_{2,i}$. Hence, the damping is too large, thereby the desired acceleration level can still increase to unreasonable limits. Additionally, a gap closing scenario can be expected to be rather slow. When assuming $a_i \approx 0$, $e_{2,i} \approx \Delta v_i$. Then, the controller will start braking in case the relative velocity exceeds 2.5 m/s. In an attempt to improve this, controller *APF3* has been developed.

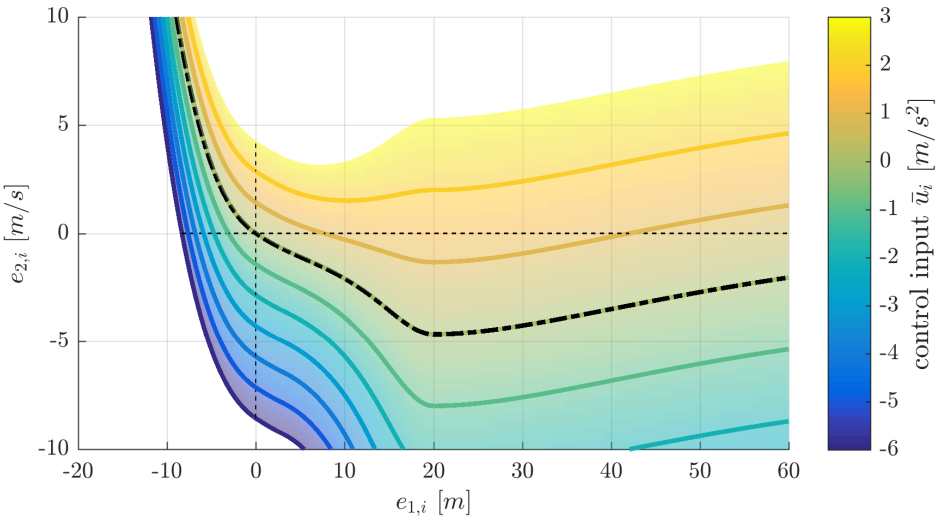

Figure A.4: Response plot of controller $\bar{u}_{i,APF3}$ (3.19) in the $(e_{1,i}, e_{2,i})$ plane

Figure A.4 shows the control response for the *APF3* controller (3.19), designed to reduce the damping at larger position errors. As can be seen however, the position dependent APF and damping result in a complicated portrait. The dotted black line, indicating isocline $\bar{u}_i = 0$, has a rather odd path. As a result, a gap closing path might be subject to unnecessary accelerations, as will be further elaborated in Section 3.4.

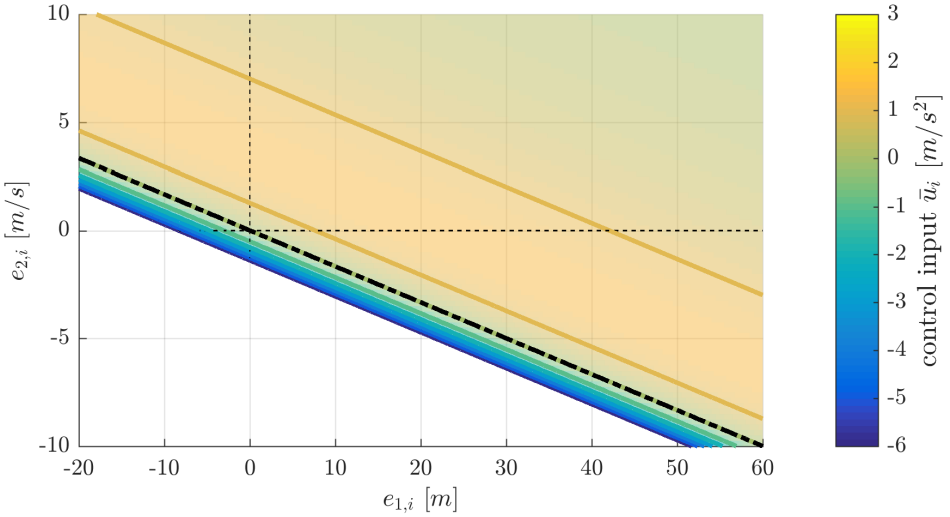

Figure A.5: Response plot of controller $\bar{u}_{i,APFx}$ (3.23) in the $(e_{1,i}, e_{2,i})$ plane

The chosen *APFx* controller (3.23) is designed using error (3.21). Therefore, all control isoclines run diagonally, in a similar fashion as the *PD* controller (3.10). However, the angle of the diagonals is different, since $c = 6$ is chosen for this example. Note, in case this angle is supposed be similar, $c = \frac{k_d}{k_p}$ must be chosen. Safety prohibits low values for c, as further elaborated in Chapter 4. It can be seen however that the approach does not introduce saturated acceleration, assuming the feed forward is non-positive.

Appendix B: Safety evaluation

In this chapter, two sections are stated as part of the safety analysis, supporting of Chapter 4. Appendix B.1 will state a two-vehicle emergency braking scenario subjected to a delay, as an addition to Subsection 4.2.1 where the effects of delay have been neglected.

In Appendix B.2, the minimal host initial velocity (4.21) is derived. Using this analysis, the safety analysis of Subsection 4.2.3 can be performed.

B.1 Two-vehicle emergency braking with delay

As a result of Subsection 4.2.1, the effect of an emergency braking maneuver performed by the preceding vehicle can be examined longitudinally. Herein, the preceding vehicle is considered to have equal characteristics as the host vehicle, hence equal dynamics parameter τ and an equal lower bound acceleration $u_{ca} = -6\ m/s^2$. For simplicity, an open loop emergency braking action is considered for both vehicles. Normally, feed forward allows a relatively short response time, ensuring safety. However, since packet loss is still a problem with wireless communication, it cannot be relied upon. Since sensors are also subjected to delay, it is assumed that a temporary packet loss is the main cause of delay. In case this occurs , the vehicle is assumed to initiate the full braking maneuver Δt seconds later than its predecessor. Consequently, the initialization time of the emergency braking maneuver is assumed to be $t_{i,0} = t_{i-1,0} + \Delta t$. Using (4.3), the distance between vehicle i and $i-1$ can be described by:

$$d_i(t) = s_{i-1}(t) - s_i(t) - L_i = \Delta_t s_{i-1}(t) - \Delta_t s_i(t) + (s_{i-1}(t_0) - s_i(t_0 + \Delta t) - L_i)\,, \quad \text{(B.1)}$$

with the simplification $t_0 = t_{i-1,0}$ for sake of readability. Using (B.1), the braking distance for both individual emergency braking maneuvers can be calculated over their respective time-span. As a result, the final stopping distance can be written as:

$$d_{i,stop} = \Delta_t s_{i-1}(t_{i-1,stop}) - \Delta_t s_i(t_{i,stop}) + d_i(t_0) - \int_{t_0}^{t_0+\Delta t} v_i(t)dt. \quad \text{(B.2)}$$

Equation (B.2) describes the final inter-vehicular distance after a two-vehicle emergency braking maneuver. Since equal dynamics are considered for both vehicles, $d_{i,stop}$ will coincide with the maneuver's smallest inter-vehicular distance in case $t_{i,stop} \geq t_{i-1,stop}$. Otherwise, $v_{i-1}(t) > v_i(t)$ holds throughout the maneuver, making collision impossible since $s_{i-1}(t_0) > s_i(t_0)$. In order to reduce complexity, the delay will be discarded in further analysis. Instead, the pursuit-evasion game approach will be considered to determine the states which describe D_m, as discussed in Subsection 4.2.2.

B.2 Evaluation of critical states in the error domain

In this section, the critical states $S = [e_{1,i}(t_0), e_{2,i}(t_0), e_{3,i}(t_0), v_i(t_0), a_{i-1}(t_0)]^T \in D_m^* \subset \mathbb{R}^5$ are evaluated with respect to the nominal controller. The objective is to find a subset the critical domain wherein $\bar{u}_i \leq u_{min}$ can be warranted by the nominal controller, as a function of $v_i(t_0)$ and other parameters. Herein, the left tops of D_m^* as in Figure 4.4 are mainly of interest, governed by $e_{1,i}(t_0) = d_{safe} - d_{r,i}(t_0)$. Using (3.2), these tops are therefore part of the domain

$$S_{crit} = \begin{cases} (d_i(t_0) = d_{safe} \mid \Delta v_i(t_0) = v_{i-1}(t_0) - v_i(t_0) = 0) & \rightarrow \quad P \in D_m, \\ (d_i(t_0) = d_{safe} \mid \Delta v_i(t_0) = v_{i-1}(t_0) - v_i(t_0) < 0) & \rightarrow \quad P \in D_c, \end{cases} \tag{B.3}$$

with $P = [d_i(t_0), v_i(t_0), \Delta v_i(t_0), a_i(t_0), a_{i-1}(t_0)]^T \in \mathcal{Y}_1 \subset \mathbb{R}^5$. Domain S_{crit} describes some of the situations where collision is of high risk or unpreventable. Preceding to a collision between vehicle i and $i-1$, vehicle i must have been in domain S_{crit}. In case of absence or inactivity of a CA controller, the normal controller should implement braking with $\bar{u}_i(t_0) \leq u_{min}$, also since the acceleration of the preceding vehicle is not accurately known. Since the dynamics of the acceleration are relatively fast with respect to the dynamics of $d_i(t)$, the acceleration dynamics are neglected. Therefore, $a_i(t_0) \approx \bar{u}_i(t_0) \approx a_{min}$ can be assumed when in domain S_{crit} of (B.3). For readability, the argument (t_0) will be omitted in the next notation. Application of the stated assumptions in the error dynamics (3.6) results in:

$$\begin{pmatrix} e_{1,i} \\ e_{2,i} \\ e_{3,i} \end{pmatrix} = \begin{pmatrix} d_i - r_i - hv_i \\ v_{i-1} - v_i - ha_i \\ a_{i-1} + (\frac{h}{\tau} - 1)a_i - \frac{h}{\tau}u_i \end{pmatrix} \approx \begin{pmatrix} d_{safe} - d_{r,i} \\ \Delta v_i - ha_{min} \\ a_{i-1} - a_{min} \end{pmatrix} \in S_{crit}. \tag{B.4}$$

Note that controller (3.23) should continue braking with $\bar{u}_i \leq u_{min}$ in S_{crit}, hence $x_{1,i}(t) \leq x_c$. Rewriting this criterion using (B.4) yields

$$\begin{aligned} x_{1,i} = e_{1,i} + ce_{2,i} &\leq x_c \\ c\,(\Delta v_i - ha_{min}) &\leq x_c - d_{safe} + d_{r,i} \end{aligned} \tag{B.5}$$

Equation (B.5) can be used to derive the limits for a combination of c, $d_{r,i}$, x_c, h and d_{safe}, in order to guarantee maximal braking in domain S_{crit} and determine $\hat{D}_m^*$. Since platooning control is mainly aimed at highway maneuvering, a minimal velocity for nominal operation $v_{min} > 0$ is not a large issue, however it can require additional work to ensure smooth and safe behavior when $0 \leq v < v_{min}$. Rewriting requirement (B.5) yields:

$$d_{r,i} = r + hv_i \geq -cha_{min} - x_c + d_{safe} + c\Delta v_i \tag{B.6}$$

$$v_i \geq -ca_{min} + \frac{1}{h}\left(d_{safe} - r - x_c + c\Delta v_i\right) \tag{B.7}$$

Equation (B.7) shows the minimal velocity for which the braking level $\bar{u}_i = a_{min}$ can continuously be applied as a function of design parameters. Note that the first term of (B.7), $-ca_{min}$, is most influential since $c \approx 5$. The danger of a high or low h however, is

dependent on the sign of $\alpha = (d_{safe} - r - x_c + c\Delta v_i)$. Consider the left tops of the lines for D_m^* in Figure 4.4, where $\Delta v_i(t_0) = 0$. Since headway times of, $h \in [0.3\ 1]\ s$ should be possible, hence if $\alpha < 0$, h_{max} should be considered, otherwise h_{min}. If we consider $a_{min} = -2\ m/s^2$, $r = 5\ m$, $h = 0.5\ s$, $x_c = -2$ and $d_{safe} = 1\ m$, then (B.7) results in $v_i \geq v_{min} = 11.4\ m/s$. For $h = h_{min} = 0.3\ s$, $v_{min} = 12.4\ m/s$ can be found.

For the presented situations, the nominal controller will be braking with $\bar{u}_i \leq u_{min}$. Hence when using the saturated control APF (4.25) for (3.23), the applied braking level will additionally remain within the comfort bounds, previous to initialization of CA. When $v_i < v_{min}$, this cannot be guaranteed and an additional controller can be required ensure a smooth acceleration profile for comfort and safety. Note however, $v_i(t) \geq 12.4\ m/s$ is a reasonable assumption for highway maneuvering. When therefore assuming $v_i t \geq v_{min}$, only D_m^* of (4.22) has to be considered for CA.

Appendix C: Stability analysis for APF-CACC

In this chapter, the equilibrium and its stability is investigated for any suitable function $\Psi()$ for APF-CACC. Such a suitable function should hold to a number of requirements. Function $\Psi()$ is continuous and has its only minimum, at $\Psi(0) = 0$.

C.1 Equilibrium

In this section, the equilibrium is examined for error function (3.21), using (3.6). Note that the potential function used for *APFx* (3.23) needs to comply to (3.13). For all states where platooning is of interest, denoted by domain $\mathbf{x}_i \in \Omega \in \mathbb{R}^3$,

$$\begin{cases} \frac{\partial \Psi_A(x_{1,i})}{\partial x_{1,i}} < 0 & x_{1,i} < 0, \qquad i \in m, \\ \frac{\partial \Psi_A(x_{1,i})}{\partial x_{1,i}} > 0 & x_{1,i} > 0, \end{cases} \tag{C.1}$$

must hold. Using (C.1), (3.12) and (3.23), it can be seen that $\bar{u}_i$ will only remain zero if $x_{1,i} = e_{1,i} + ce_{2,i} = e_{1,i} + c\dot{e}_{1,i} = 0$. Since $\dot{e}_{1,i}$ is zero, $e_{1,i}$ must equal zero. Hence, the origin $\hat{\mathbf{e}}_i = \underline{0}$ is the only equilibrium of this system. However, this does not necessarily mean that the equilibrium is attractive or stable. Therefore, further analysis must be conducted to describe the behavior and stability of the system.

C.2 Lyapunov stability analysis

In this section, the Lyapunov stability theorem [35] is used to investigate system stability for control input (3.23), which uses the error function $\mathbf{x}_i$ as in (3.21). This analysis elaborates previous work of TNO [33]. For this analysis, time delay is assumed to be negligible, thus perfect feed-forward is applied. Using this assumption, the following candidate Lyapunov function is introduced:

$$V = \Psi(x_{1,i}) + \begin{bmatrix} x_{2,i} & x_{3,i} \end{bmatrix} \underbrace{\begin{bmatrix} b_1 & b_2 \\ b_3 & b_4 \end{bmatrix}}_{\mathbf{B}} \begin{bmatrix} x_{2,i} \\ x_{3,i} \end{bmatrix}. \tag{C.2}$$

This candidate Lyapunov equation should be zero at the equilibrium point, and positive definite elsewhere. Hence, matrix $\mathbf{B}$ should be positive semi-definite. Similarly, the candidate Lyapunov function should have a derivative smaller or equal to zero. Using (3.21) and (C.3), the derivative can be derived to:

$$\dot{V} = \frac{\partial \Psi(x_{1,i})}{\partial x_{1,i}} \dot{x}_{1,i} + 2b_1 x_{2,i} \dot{x}_{2,i} + (b_2 + b_3)\dot{x}_{2,i} x_{3,i} + (b_2 + b_3) x_{2,i} \dot{x}_{3,i} + 2b_4 x_{3,i} \dot{x}_{3,i}. \tag{C.3}$$

Using (3.21), (3.8) and (3.23), the derivatives are equal to:

$$\begin{aligned}
\dot{x}_{1,i} &= x_{2,i} + cx_{3,i},\\
\dot{x}_{2,i} &= x_{3,i},\\
\dot{x}_{3,i} &= -\frac{1}{\tau}\big(x_{3,i} + \bar{u}_i - u_{i-1}\big) = -\frac{1}{\tau}\Big(x_{3,i} + \frac{\partial \Psi(x_{1,i})}{\partial x_{1,i}}\Big).
\end{aligned} \tag{C.4}$$

Substitution of (C.4) in (C.3) and rewriting yields

$$\begin{aligned}
\dot{V} = &\frac{\partial \Psi(x_{1,i})}{\partial x_{1,i}}\Big(x_{2,i} + cx_{3,i} - \frac{b_2+b_3}{\tau}x_{2,i} - \frac{2b_4}{\tau}x_{3,i}\Big)\\
&+\Big(2b_1 - \frac{b_2+b_3}{\tau}\Big)x_{2,i}x_{3,i} + \Big(b_2 + b_3 - \frac{2b_4}{\tau}\Big)x_{3,i}^2,
\end{aligned} \tag{C.5}$$

which should at least be negative semi definite. By application of this criterion on (C.5), the following conditions can be derived:

$$\begin{array}{rcl} 1 - \frac{b_2+b_3}{\tau} & = 0 \\ c - \frac{2b_4}{\tau} & = 0 \\ 2b_1 - \frac{b_2+b_3}{\tau} & = 0 \\ b_2 + b_3 - \frac{2b_4}{\tau} & < 0 \end{array} \quad \rightarrow \quad \begin{array}{rl} b_1 & = \frac{1}{2} \\ b_2 + b_3 & = \tau \\ b_4 & = \frac{c\tau}{2} \\ c & > \tau \end{array} \quad . \tag{C.6}$$

Note, since matrix $\mathbf{B}$ should be positive semi-definite, $b_1b_4 - b_2b_3 \geq 0$ should hold. Choosing $b_2 = b_3 = \frac{\tau}{2}$ yields matrix $\mathbf{B}$. Since $c > \tau$, matrix $\mathbf{B}$ is positive definite, hence $V \geq 0$, with $\dot{V} \leq 0$. Substitution of (C.6) in (C.5) yields

$$\dot{V} = (\tau - c)x_{3,i}^2, \tag{C.7}$$

which holds for all combinations of $\mathbf{x}_i$. Hence, $\dot{V}$ is negative semi definite. Therefore, LaSalle's invariance principle [35] is needed to prove global asymptotic stability of the equilibrium. Let us first define the largest domain for which $\dot{V} = 0$:

$$M = \{ \quad \mathbf{x}_i \in \mathbb{R}^3 \quad | \quad \dot{V}(\mathbf{x}_i) = 0 \quad \}, \quad 2 \leq i \leq m. \tag{C.8}$$

Within domain M of (C.8), the equilibrium as found in Appendix C.1 is the only invariant set. This can be proven since $x_{2,i}$ must be constant and $\dot{x}_{3,i} = 0$, if $x_{3,i}$ is to remain zero. Using (C.4), it can be concluded that $\frac{\partial \Psi(x_{1,i})}{\partial x_{1,i}} = 0$, and thus $x_{1,i} = e_{1,i} + ce_{2,i} = 0$. Since $e_{2,i} = \dot{e}_{1,i}$ is constant, $e_{2,i}$ and $e_{1,i}$ must be zero for the solution to remain within M. Since the only invariant set within M is the equilibrium, the equilibrium is globally asymptotically stable.

Appendix D: Simulation analysis

D.1 Lateral merging effects on longitudinal dynamics

In this project, a string of m vehicles has been considered, where all vehicles have a longitudinal distance $s_i(t)$ on a path P, and hence a velocity $v_i(t)$ and acceleration $a_i(t)$, with $i \in m$. Similarly, the set-points have been defined in a one-dimensional fashion, with $e_{1,ik}(t) = s_k - s_i - L_i - d_{r,i}$. For platooning and gap closing, this is a realistic assumption since the vehicles are supposed to drive an equal path. For merge maneuvering however, the paths are not equal for all vehicles.

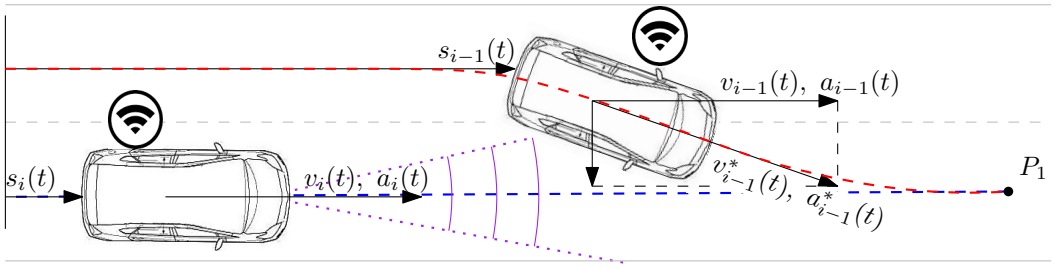

Figure D.1: Sketch of the evaluated velocity $v_{i-1}(t)$ and the real velocity $v^*_{i-1}(t)$

This is further illustrated in the sketch of (Figure D.1). There, the actual velocity $v^*_{i-1}(t)$ and the evaluated velocity $v_{i-1}(t)$, in line with path P, are given. Hence, the evaluated inter-vehicular velocity $\Delta v_i(t) = v_{i-1}(t) - v_i(t)$, which is in-line with the velocity vector of the host, is lower during a lane change. of the preceding vehicle. Similarly, the traveled distance for vehicle $i-1$ from $s_{i-1} = 0$ to point P_2, depicted with a red dashed line, will be larger than that for vehicle i, depicted with a blue line. Hence, the translation to the 1D domain reduces the velocity of the preceding vehicle if it is changing lane. This can equally be observed in the simulations, where additionally, the perception is of becomes importance. As the vehicle changes lane or is situated further forward, the vehicle comes into range of the radar. This is depicted in purple in Figure D.1. Since radar is more reliable over the previously used wifi information to determine the inter-vehicular distance and velocity, radar will have priority. As a result, the measured inter-vehicular velocity changes.

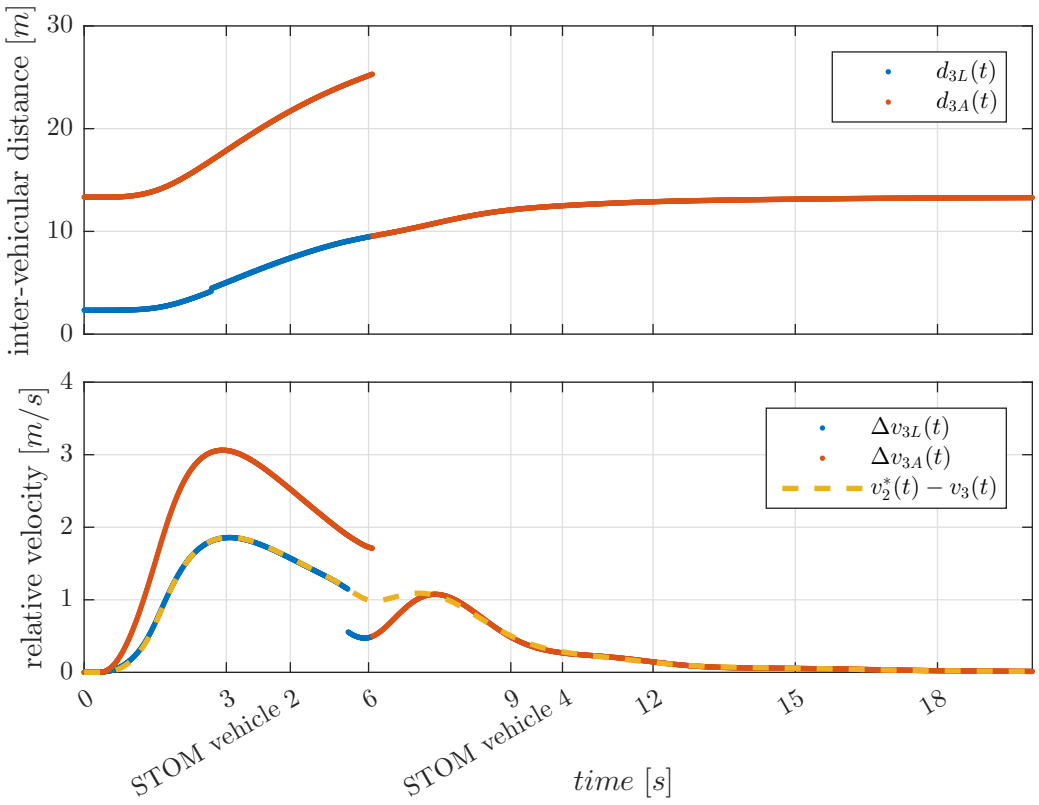

Figure D.2: Simulation, MIO perspective from vehicle 3

In Figure D.2, a part of the simulation of the APF controller as in Section 5.3 is visualized. Herein, both previously noted effects are clearly visible. A slight step can be seen in the inter-vehicular distance at $t = 4.15\ s$, where the vehicle has entered the field of view the camera. A bigger step is seen in the inter-vehicular velocity at $t = 5.57\ s$, where the radar detects the vehicle in addition to camera and wifi. Here, the change in perception along with the previously described effect of the difference in driving direction, results in a step towards a lower inter-vehicular velocity.

D.2 Merging simulation for current TNO approach

For comparison of the simulation in Section 5.3, the TNO merging approach has been additionally implemented, using equal initial conditions. Consequently, the simulation will need to be evaluated.

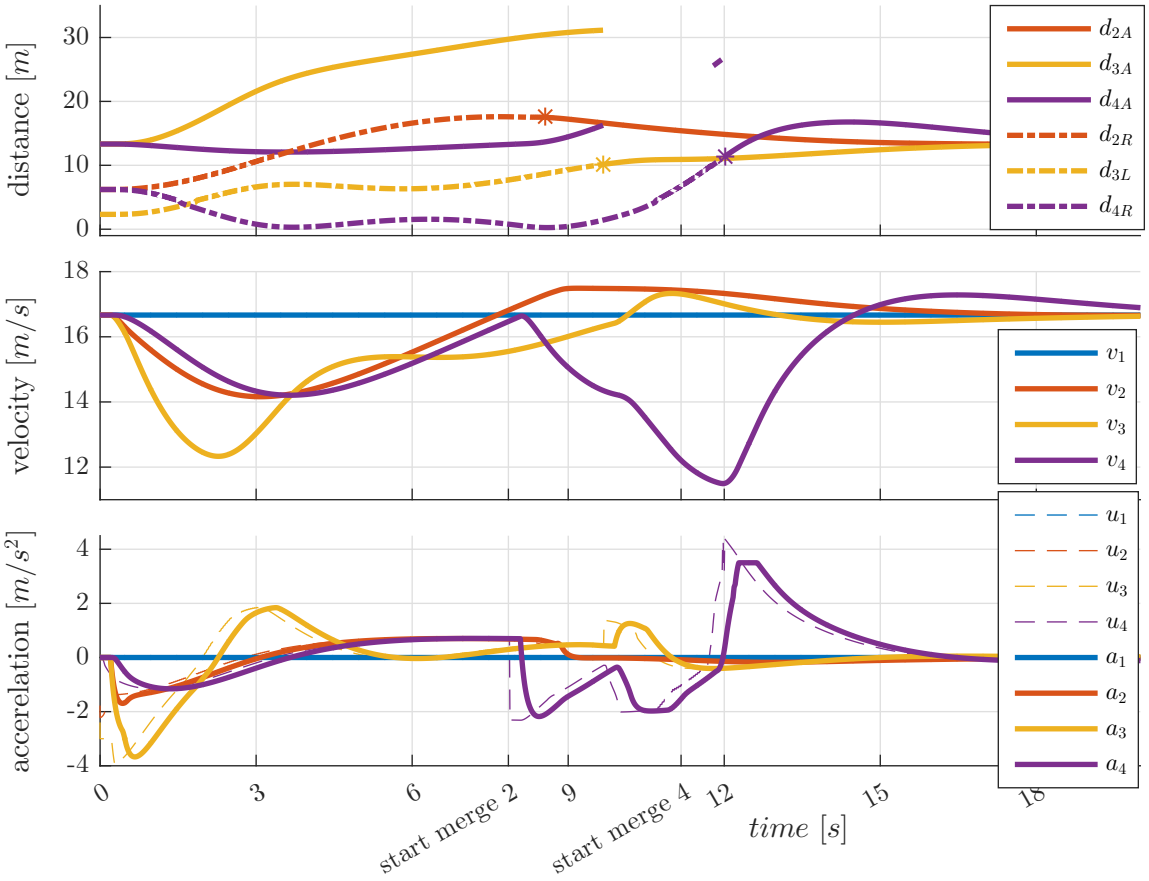

Figure D.3: Merge simulation using the TNO controller

The simulation results have been visualized in Figure D.3, where the simulation shows significant acceleration levels for vehicles 3 and 4. Where all accelerations remain within $a_i(t) \in [-2.19\ 0.98]\ m/s^2$ for the APF controller, the accelerations for the TNO controller peak to $-3.67\ m/s^2$ and $3.5\ m/s^2$ respectively. This difference in applied acceleration is similarly visible in Table 5.1. Now consider the required time for the maneuver. Vehicle 2 is allowed to merge at $t = 7.88\ s$. In comparison, this was $t = 4.83\ s$ for the APF control method, using equal STOM criteria. Hereafter, vehicle 4 had been allowed to merge at $t = 11.17\ s$, for the APF controller this was at $t = 10.09\ s$. Hence, regardless of the higher accelerations, a lower performance has been reached using the current TNO approach. This can be equally concluded from the velocity profiles, where low velocities are highly undesirable for the other vehicles in the string. When regarding the lowest velocity during the maneuver, the APF controller did not reduce the velocities as much as the APF controller. The minimal velocities for vehicles $2, 3$ and 4 when using the TNO controller were $[14.2\ 12.3\ 11.5]\ m/s$, whereas this has been $[15.4\ 13.6\ 12.75]\ m/s$ when using the APF controller. As a result, the APF controller has performed much better than the current TNO alternative.